Body temperature-controlled antiviral response and SARS-CoV-2 replication

Inaugural Dissertation

to obtain the academic degree

Doctor rerum naturalium (Dr. rer. nat)

submitted to the Department of Biology, Chemistry, Pharmacy

of Freie Universität Berlin

by

Bruna Los

2023

DECLARATION

This work was carried out in the period between September 2019 and April 2023 under the supervision of Prof. Dr. Florian Heyd at the Institute of Chemistry and Biochemistry, Freie Universität Berlin, Germany.

First reviewer: Prof. Dr. Florian Heyd
RNA Biochemistry
Institute for Chemistry and Biochemistry
Freie Universität Berlin
Takustraße 6
14195 Berlin, Germany

Second reviewer: Prof. Sutapa Chakrabarti, PhD
mRNA Metabolism
Institute for Chemistry and Biochemistry
Freie Universität Berlin
Takustraße 6
14195 Berlin, Germany

Date of defense: 12.07.2023

ACKNOWLEDGEMENTS

Firstly, I want to thank my supervisor Prof. Dr. Florian Heyd for the opportunity to work on this very interesting project, and for the continuous support and intellectual input during the entire time of this research.

I want to further extend my gratitude to:

Prof. Dr. Sutapa Chakrabarti for being the second reviewer and for the discussions and support during my Thesis Advisory Committee (TAC) meetings.

Prof. Dr. Markus Wahl for his suggestions and contributions during my TAC meetings.

Dr. Marco Preußner for all the knowledge shared with me and the assistance and input throughout my thesis.

Dr. Jakob Trimpert for performing the SARS-CoV-2 infection experiments.

The International Max Planck Research School for Biology and Computation (IMPRS-BAC) for the opportunity to be part of this Ph.D. program.

Gopika Sasikumar, with whom I shared all the challenges of the IMPRS process.

The Ph.D. coordinators: Dr. Kirsten Kelleher and Dr. Anne-Dominique Grindat, for their help and support during my time as an IMPRS student.

Felix Ostwaldt for his friendship. I really appreciated the conversations, occasional beers, the cutest penguin balloon, and work-related help. I will miss bothering you every day and stealing your precious Taq polymerase.

Ann-Kathrin Emmerichs for sharing my peculiar sense of humor and helping me with everything she could. I am very grateful to have her as a friend.

All former and current lab companions. Special thanks to Dr. Sandra Keiper for guiding me through the lab at the beginning and for her friendship, Dr. Ioana Weber and Miriam Strauch for the nice conversations and support, Mateusz Drozdz for the rides to the Institute of

Virology, and Luíza Zuvanov for helping me with my scripts, proofreading my thesis, and for bringing a bit of Brazil back to my daily lab life.

The great students, Alica Grindel, Margarida Paulo-Pedro, and Lilith Schenkmann, for helping me with my main- and side projects. I have learned a lot from supervising you.

Antje Grünwald and Bobby Viet Draegert for the technical support and Karin Hesse for the administrative support.

I want to wholeheartedly thank all my friends, who were always there to support me during all the moments of my private and academic life and for always welcoming me back as if I had never left.

With all my heart and love, I would like to thank my partner Victor Ferreira Santos, also known as “trem”. Thanks for always encouraging me and believing in me. It has been a great adventure sharing all these moments with you.

Lastly, I want to express my heartfelt gratitude to my family, particularly my mother Janete Los, for their unwavering support throughout my journey. I also want to extend my appreciation to my partner's family, who have embraced me as one of their own. I feel incredibly fortunate to have such a wonderful group of people in my life.

“In my view, all that is necessary for faith is the belief that by doing our best we shall come nearer to success and that success in our aims (the improvement of the lot of mankind, present and future) is worth attaining."

— Rosalind Franklin in a letter to Ellis Franklin, 1940.

Declaration of Independence

Herewith I certify that I have prepared and written my thesis independently and that I have not used any sources and aids other than those indicated by me. The thesis in the same or similar form has not been submitted to any examination body.

ABSTRACT

Alternative splicing (AS) is a dynamic and highly regulated process responsible for increasing the number of unique proteins encoded by a single gene, generating proteomic diversity. Additionally, AS allows cells to quickly respond to internal and external changes, such as temperature variation. The body temperature in homeothermic organisms oscillates in a circadian manner in a range of around 1-4°C. These subtle changes in core body temperature are sufficient to impact AS and gene expression by altering SR protein phosphorylation. In addition to physiological changes in body temperature, pathological changes can also occur, for example, during infection with fever. Elevated core body temperature during infection is important for pathogens clearance and the activation of the host immune cells. However, little is known about the temperature-sensing machinery that triggers changes in immune cell behavior. In this thesis, we started addressing this by performing RNA-seq with a macrophage cell line (RAW 264.7) incubated at 34°C, 37°C, and 38°C for 12h. Notably, increasing the temperature from 37°C to 38°C upregulated the expression of antiviral genes, including members of the JAK/STAT pathway. These results suggested that individual and age-dependent body temperature variations can control the expression of the antiviral genes, with higher temperatures leading to higher expression. Furthermore, we observed increased Stat2 protein and phosphorylation at higher temperatures (39°C) in RAW 264.7 cells. Inhibition of the JAK/STAT pathway prevented the temperature-controlled increase of all antiviral genes tested and reduced their basal expression at 37°C. Moreover, we showed that elevated temperature strongly increases nitric oxide production, another branch of antiviral immunity. Furthermore, we identified a temperature-dependent alternative 5' splice site in *Stat2* exon 11. The usage of the alternative 5' splice site was higher at lower temperatures (35°C and 37°C) and it leads to the inclusion of a premature termination codon (PTC), which will prevent the formation of a functional protein and lead to degradation via nonsense-mediated decay (NMD). By blocking the NMD pathway using cycloheximide (CHX), we observed an increased abundance of the PTC-containing isoform and total *Stat2* mRNA in the CHX-treated cells. To further validate the influence of the alternative 5' splice site of exon 11 in *Stat2* on the expression of antiviral genes, we used antisense oligonucleotides targeting this splice site and a CRISPR/Cas9-edited cell line lacking the alternative 5' splice site. Both approaches showed an increased expression of *Stat2* and other interferon-stimulated genes (ISGs) in the cells with reduced or depleted usage of the alternative 5' splice site. Additionally, SR proteins knockdown (KD) showed that *Srsf1* regulates the usage of this splice site. *Srsf1* KD decreased the usage of the alternative 5' splice site and led to increased expression of *Stat2* and other ISGs. Thus, our data connect body temperature and pre-mRNA processing to provide new mechanistic insight into the regulation of antiviral innate immunity. Finally, using a cell culture model we observed that higher temperature correlates with reduced SARS-CoV-2 replication. We then hypothesized that decreased body temperature with aging contributes to reduced expression of antiviral genes in older individuals, which may affect the different vulnerability of children versus seniors toward severe SARS-CoV-2 infection. In conclusion, we showed that alternative splicing coupled with NMD decreases the expression of *Stat2* at lower temperatures. The upregulation of *Stat2* at higher temperatures in conjunction with JAK1 activity induces the expression of antiviral genes, which mounts a successful antiviral response, leading to lower viral replication.

ZUSAMMENFASSUNG

Alternatives Spleißen (AS) ist ein dynamischer und hoch regulierter Prozess, der dafür sorgt, die Anzahl an Proteinen die durch ein Gen kodiert werden zu erhöhen und somit hohe Diversität im Proteom zu erschaffen. Zusätzlich erlaubt AS es der Zelle schnell auf interne und externe Veränderung zu reagieren, so zum Beispiel auf Variationen der Temperatur. Die Körpertemperatur in homoiothermen Organismen oszilliert circadian um 1 bis 4 °C. Diese subtile Veränderung der Körpertemperatur reichen aus um AS und Genexpression durch Änderung der SR Protein Phosphorylierung zu beeinflussen. Zusätzlich zu der physiologischen Änderung der Körpertemperatur, finden auch pathologische Änderungen statt, zum Beispiel bei einer Infektion mit Inflammation. Eine erhöhte Temperatur im Körper führt zur schnelleren Beseitigung von Erregern und Aktivierung des Immunsystems. Allerdings ist noch nicht viel bekannt über den Weg, wie Immunzellen durch Temperaturveränderung ihr Verhalten ändern. In dieser Arbeit haben wir mit einer Bioinformatischen Analyse begonnen, in der wir Transkriptomdaten einer Makrophagen Zelllinie (RAW 264.7) verglichen haben, die bei 34 °C, 37 °C und 38 °C für 12 Stunden inkubiert wurden. Merklich war, dass Erhöhung der Temperatur von 37 °C auf 38 °C gereicht hat, um Expression antiviraler Gene wie Teile des JAK/STAT Stoffwechselweg zu erhöhen. Diese Ergebnisse deuten darauf hin, das individuelle und altersbedingte Variationen der Körpertemperatur die Expression antiviraler Gene beeinflussen kann. Zudem konnten wir eine Erhöhung der Stat2 Proteinlevel und Phosphorylierung in RAW 264.7 Zellen bei erhöhten Temperaturen (39 °C) feststellen. Inhibierung des JAK/STAT Stoffwechselweg verhinderte den Temperatureinfluss auf antivirale Gene und reduzierte sie auf ihre basale Expressionslevel bei 37 °C. Zusätzlich konnten wir sehen, dass erhöhte Temperaturen die Stickstoffoxidproduktion erheblich erhöhten, welches wiederum ein Weg der antiviralen Immunantwort ist. Wir identifizierten eine alternative 5‘ Spleißstelle in *Stat2* Exon 11, die stark temperaturabhängig gespleißt ist. Die Nutzung der alternativen 5‘ Spleißstelle war höher in niedrigen Temperaturen (35 °C, 37 °C) und führte zum Einbau eines vorzeitigen Stopcodons (PTC), welches durch Nonsense-mediated decay (NMD) die Translation zu einem funktionalen Protein verhindert. Durch Blockieren des NMD durch Cyxloheximid (CHX) konnten wir die Präsenz der PTC-Isoform und die gesamt mRNA Menge erhöhen. Um ferner den Einfluss der alternativen 5‘ Spleißstelle von *Stat2* zu validieren, verwendeten wir Antisense-Oligonukleotide, welche diese Spleißstelle erkannten, und CRISPR/Cas9 Zelllinien, welche die alternative 5‘ Spleißstelle fehlte. Beide Ansätze zeigten eine erhöhte Expression von *Stat2* und andere Interferon-Stimulierten Gene (ISGs) in den Zellen mit reduzierter oder nicht vorhandener Verwendung der alternativen 5‘ Spleißstelle. Zusätzlich zeigte ein SR Protein Knockdown (KD), dass Srsf1 dieser Spleißseite reguliert. *Srsf1* KD führte zu einer verringerten Nutzung der alternativen 5‘ Spleißseite in *Stat2* Exon 11 und eine erhöhte Expression von *Stat2* und andere ISGs. Mit unseren Daten können wir Körpertemperatur und pre-mRNA Prozessierung miteinander in Verbindung setzen, um mechanistische Erkenntnisse zur Regulation des antiviralen angeborenen Immunsystems zu erhalten. Zum Abschluss konnten wir in einem Zellkulturmodell zeigen, dass die Verdopplungsrate von SARS-Cov-2 durch erhöhte Temperaturen erniedrigt wird. Unsere anschließende Hypothese ist, dass durch eine altersbedingte niedrige Körpertemperatur die Expression antiviraler Gene erniedrigt ist, und

somit die höhere Anfälligkeit älterer Menschen für eine SARS-CoV-2 erklärt werden kann. Abschließend konnten wir zeigen, dass alternatives Spleißen zusammen mit NMD die Expression von *Stat2* bei niedrigen Temperaturen verringert. Die Hochregulierung von *Stat2* bei erhöhten Temperaturen in Verbindung mit JAK1 Aktivität induziert die Expression antiviraler Gene, welches eine erfolgreiche antiviraler Immunantwort und eine verringerte virale Verdopplungszeit mit sich bringt.

TABLE OF CONTENTS

1. INTRODUCTION

1.1. Precursor mRNAs Splicing

In living organisms, genetic information is stored in deoxyribonucleic acid (DNA) molecules (Crick and Watson, 1953). In eukaryotic cells, genes (specific DNA sequences) that are transcribed into messenger ribonucleic acid (mRNA) in the nucleus by RNA polymerase II need to undergo several processing steps before being exported to the cytoplasm and translated into protein by the ribosomal machinery (Minchin and Lodge, 2019). The processing of the precursor mRNA (pre-mRNA) starts with the addition of a 7-methylguanosine residue (m7G) to the 5’ end (5’ capping), followed by the polyadenylation of the 3’ end (poly(A) tail). Both steps are important for mRNA stability, nuclear export, and translation initiation (Minchin and Lodge, 2019). Furthermore, pre-mRNAs are converted to mature mRNA in a process called splicing, in which noncoding sequences (introns) are removed and coding sequences (exons) are ligated together (Will and Lührmann, 2011). Nuclear splicing is catalyzed by a highly dynamic and complex molecular machine called the spliceosome. The initial task of the spliceosome involves the definition of intron-exon boundaries. Introns are flanked by short conserved sequences at the 5' splice site (ss), 3'ss, and branch-point (BP), which define the intron-exon boundaries and are recognized by the spliceosome machinery. Introns are excised from the pre-mRNA by two consecutive SN2-type transesterification reactions. In the first reaction, the 2' hydroxyl group of the BP nucleotide (adenosine) carries out a nucleophilic attack on the phosphate of the 5’ss. This results in cleavage at this site and ligation of the 5’ end of the intron to the BP adenosine, generating a 2’–5’ phosphodiester bond and formation of the intron lariat. In the second reaction, the 3’ hydroxyl group of the 5’ exon attacks the phosphodiester bond of the 3’ss, resulting in the ligation of the 5’ and 3’ exons and the release of the intron lariat (**Figure 1.1.**) (Will and Lührmann, 2011).

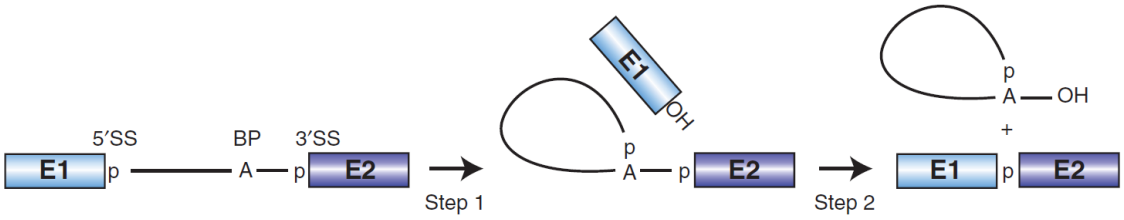

Figure 1.1. Two-step mechanism of pre-mRNA splicing.

The scheme represents the two transesterification steps that lead to the cleavage of the intron, the ligation of the two adjacent exons, and the release of the intron lariat. Exons and introns are depicted as boxes and lines, respectively. The splicing sites 5ss and 3ss, and the branch point (BP) adenosine are also shown (Adapted from Will and Lührmann, 2011).

Most eukaryotes have two unique spliceosomes: the U2-dependent (major) spliceosome, which catalyzes the removal of introns with the GT-AG splice sites, and the less abundant U12-dependent (minor) spliceosome, which catalyzes the removal of introns with non-consensus AT-AC splice sites, distinct BP and polypyrimidine tract (PPT) sequences (Jackson, 1991; Patel and Steitz, 2003; Will and Lührmann, 2011; Turunen et al., 2013).

The U2-dependent spliceosome is assembled in a stepwise manner. First, the U1 small nuclear ribonucleoprotein (snRNP) is recruited to the 5' ss, the splicing factor 1 (SF1) interacts with the BP, and the U2 auxiliary factor (U2AF) interacts with the PPT and the 3'ss, forming the E complex. Subsequently, the U2 snRNP associates with the BP, forming the A complex. Further, the U4/U6.U5 tri-snRNP is recruited, which results in the formation of the pre-catalytic B complex. After major conformational and compositional rearrangements that lead to the destabilization of U1 and U4 snRNPs, the B complex is activated. Catalytic activation by Prp2, a DEAH-box RNA helicase, forms the B* complex. The B* complex is responsible for the first transesterification reaction of pre-mRNA splicing, resulting in the formation of the C complex. The C complex catalyzes the second transesterification reaction. After additional conformational remodeling, the spliceosome dissociates, releasing the snRNPs, which will be used in additional rounds of splicing. The mRNA is also released and the intron lariat is degraded (**Figure 1.2.**) (Wahl, Will and Lührmann, 2009; Will and Lührmann, 2011).

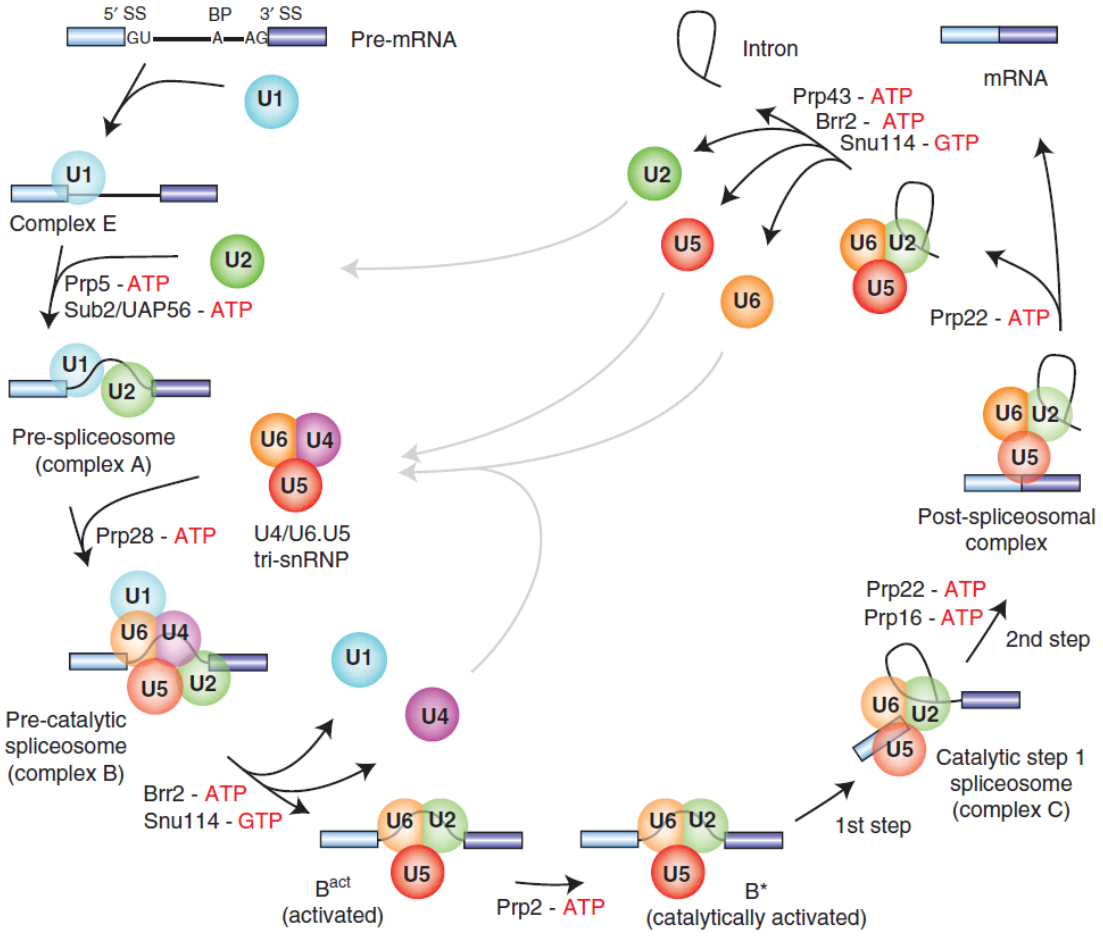

Figure 1.2. The U2-dependent spliceosome cycle.
Schematic representation of the assembly of the spliceosome. The snRNPs are illustrated as colored circles. Exons and introns are depicted as boxes and lines, respectively. The composition of the complexes E, A, B, B^{act}, B*, and C, as well as the conserved ATPases and GTPases important for catalyzing conformational changes in each stage, are shown (Adapted from Will and Lührmann, 2011).

1.2. mRNA Alternative Splicing

Although some exons, called constitutive exons, are present in every mRNA produced from a determined pre-mRNA, many exons are alternatively spliced. Alternative splicing (AS) is responsible for increasing the number of unique proteins encoded by a single gene, generating proteomic diversity and potentially contributing to the evolution of multicellular eukaryotes (Maniatis and Tasic, 2002; Nilsen and Graveley, 2010). Approximately, 95% of human multi-exon genes are alternatively spliced (Pan et al., 2008; Wang et al., 2008; Merkin et al., 2012). There are different types of AS: inclusion or skipping of cassette exons, usage of an alternative 5' or 3' splice site, intron retention, mutually

exclusive splicing of alternative exons, and usage of the alternative promoter or poly(A) sites (**Figure 1.3.**).

AS-mediated changes can influence gene expression levels by modifying mRNA stability, translational activity, and subcellular localization (McGlincy and Smith, 2008; Mockenhaupt and Makeyev, 2015) In addition, AS can result in the formation of mRNA isoforms containing premature termination codons (PTCs), which are normally degraded through the nonsense-mediated decay (NMD) pathway, leading to the down-regulation of mRNA levels (McGlincy and Smith, 2008). Furthermore, a recent study reported that around 64% of in-frame AS isoforms of highly expressed genes are translated (Sinitcyn *et al.*, 2023). Proteins translated from alternatively spliced mRNAs may have different functions, such as altered enzymatic activity, interaction properties, binding affinity, protein stability, or cellular localization (Kelemen *et al.*, 2013; Rogalska, Vivori and Valcárcel, 2022).

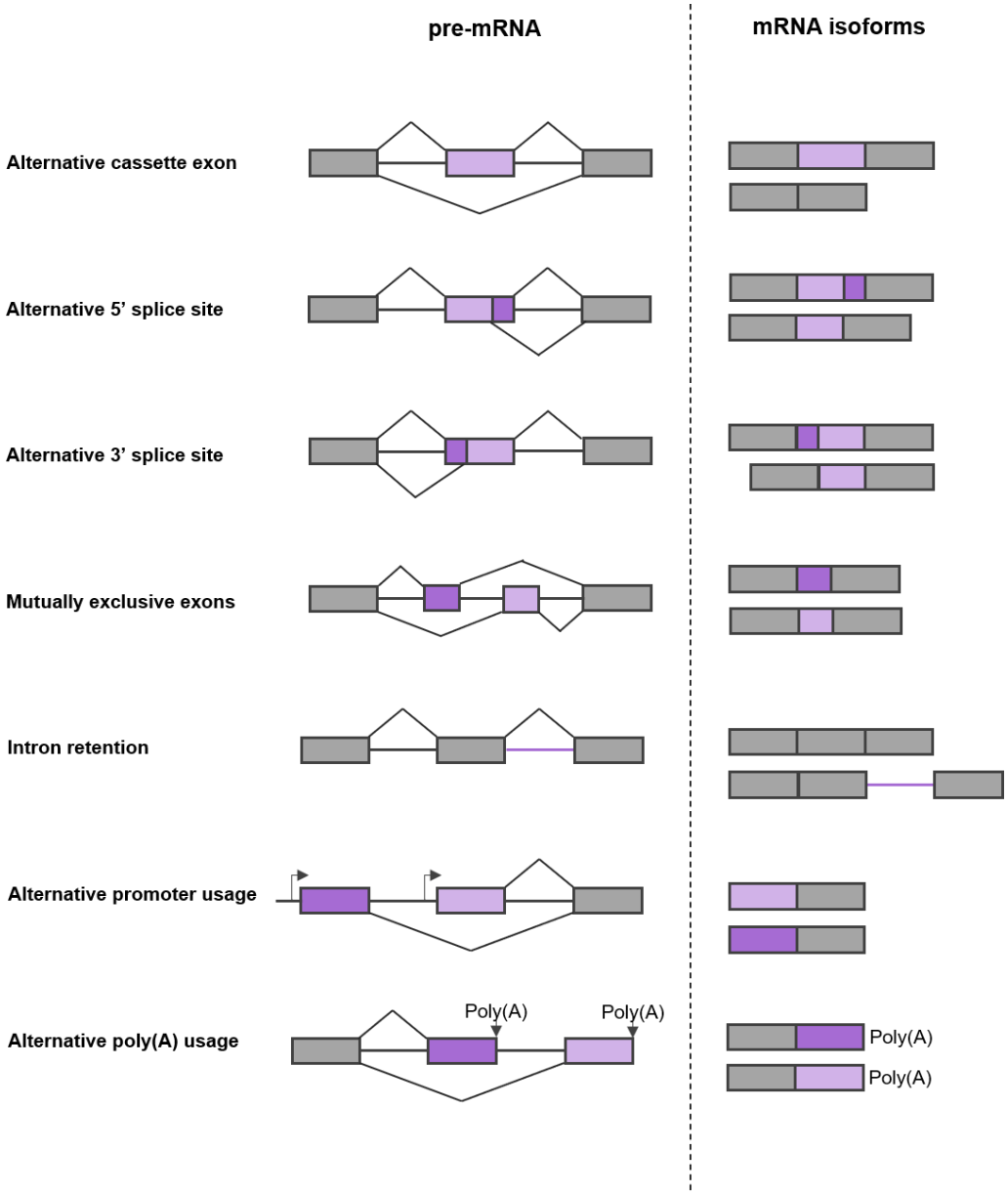

Figure 1.3. Different types of alternative splicing.
Different types of alternative splicing. The scheme is illustrating the pre-mRNA on the left and the alternatively spliced isoforms on the right. Constitutive exons are depicted as gray boxes, alternative exons or regions as purple boxes or lines, and introns as lines.

1.3. Nonsense-mediated decay pathway

NMD is an mRNA surveillance mechanism that prevents the synthesis of truncated proteins by degrading mRNAs that undergo aberrant termination. In eukaryotes, both active mRNA translation and NMD-specific *trans*-acting factors are necessary for NMD. The *trans*-acting factors encoded by the following genes: *UPF1*, *UPF2*, *and UPF3*, form a trimeric complex that composes the core of the NMD machinery (McGlincy and Smith, 2008; Brogna and Wen, 2009). The trimeric complex is the first NMD factor to bind to prematurely

terminating ribosomes, and links premature translation termination to mRNA degradation (Brogna and Wen, 2009). Additional factors, such as the SMG1, SMG5, SMG6, and SMG7 proteins, are also involved in NMD. SMG1 is responsible for the phosphorylation of UPF1. Phosphorylation of UPF1 is necessary for its interactions with mRNA-decay-inducing factors, such as SMG5 and SMG7 (Brogna and Wen, 2009).

Pre-mRNA splicing is an important regulator of NMD. Simultaneously to intron splicing, the exon junction complex (EJC) is deposited by spliceosomes onto the coding sequence of the mRNA, 20–24 nt upstream of the exon-exon junction (Le Hir *et al.*, 2000). The EJCs are responsible for recruiting several factors involved in splicing, transport, translation, and NMD. EJCs remain bound to the mRNA during transport to the cytoplasm, and their removal happens during the first round of translation (Le Hir, Saulière and Wang, 2016). However, in NMD targets the PTC is located upstream of the EJC. A typical target has a PTC located more than 50-55 nt upstream of the last exon-exon junction (Lykke-Andersen and Jensen, 2015). Therefore, translation termination can occur in PTC-containing transcripts, while one or more EJCs are still attached to the mRNA (Hoek *et al.*, 2019). The EJC stimulates NMD due to its association with UPF3 and UPF2, which will later form the UPF1-UPF2-UPF3 trimeric complex (Lykke-Andersen and Jensen, 2015). During translation termination, the ribosome stalled on a PTC recruits UPF1 via its interaction with the termination factors eRF1/3 and SMG1. This interaction between UPF1, eRF1/3, and SMG1 forms the SURF complex (Kashima *et al.*, 2006). The SURF complex forms a bridge between the ribosome and the downstream EJC associated with UPF3 and UPF2. The UPF2 bound to the EJC interacts with the UPF1 and triggers the phosphorylation of UPF1 by SMG1 (Chamieh *et al.*, 2008). Subsequently, this interaction promotes the dissociation of eRF1/3. The complex formed by the phosphorylated UPF1, SMG1, EJC, UPF2, and UPF3 triggers the degradation of the mRNA (Lykke-Andersen and Jensen, 2015). The degradation can occur through different mechanisms. One of these mechanisms is mediated by the endonuclease SMG6, which interacts with UPF1 and endonucleolytic cleavages the mRNA (Eberle *et al.*, 2009). This process is then followed by an exonucleolytic decay of the cleavage fragments. Another mechanism is mediated by the SMG5/7 complex, which interacts with the phosphorylated UPF1. The SMG5/7 complex recruits the CCR4-NOT deadenylation complex, and triggers mRNA deadenylation, decapping, and exonucleolytic decay (Loh, Jonas and Izaurralde, 2013; Chakrabarti *et al.*, 2014; Boehm *et al.*, 2021).

1.4. Regulation of splicing

The decision of which exon is removed or included is regulated by *trans*-acting factors which bind to *cis*-regulatory elements, also known as splicing regulatory elements. The *cis*-regulatory elements are present within exons or introns and have one or more RNA-binding domains and protein-protein interaction domains. There are four types of *cis*-regulatory elements: exonic splicing enhancers (ESE), exonic splicing silencers (ESS), intronic splicing enhancers (ISE), and intronic splicing silencers (ISS) (Chen & Manley, 2009). The most studied *trans*-regulatory elements are members of the serine/arginine (SR)-rich proteins and heterogeneous nuclear ribonucleoproteins (hnRNP) families (Nilsen and Graveley, 2010).

SR proteins usually facilitate splice site recognition by binding to an ESE and recruiting U1 to the 5'ss and U2AF and U2 to the 3'ss. SR proteins also play an important role in regulating mRNA nuclear export, NMD, and translation (Zhang and Krainer, 2004; Chen and Manley, 2009; Busch and Hertel, 2012). Contrary to SR proteins, hnRNPs generally repress splicing by binding to ESS or ISS regions, interfering with the recognition of splice sites by the spliceosome (Nilsen and Graveley, 2010; Fu and Ares, 2014). For example, hnRNP 1 binds to the polypyrimidine tract and blocks the binding of U2AF to regulated exons (Singh, Valcárcel, and Green, 1995).

The expression of RNA-binding proteins (RBPs) can be auto-regulated and cross-regulated. For example, SR proteins and hnRNPs regulate their mRNA abundance by generating transcripts containing PTCs, which will be degraded via the NMD pathway (Müller-Mcnicoll *et al.*, 2019). Furthermore, these proteins can often influence the binding and function of each other cooperatively or competitively (Fu and Ares, 2014). hnRNP C has been shown to compete with the splicing factor U2AF65 at cryptic splice sites, preventing the inclusion of suppressed Alu-containing exons that could disrupt the transcript function (Zarnack *et al.*, 2013). Additionally, post-translational modifications of RBPs were shown to affect splicing. For example, phosphorylation of RBPs can alter their intracellular localization and ability to interact with other proteins or mRNA substrates, leading to changes in splice site selection (Chen and Manley, 2009). RNA secondary structures and the speed of transcription elongation can also influence splicing by modulating the accessibility to *cis*-regulatory elements or by affecting splicing site selection (de la Mata and Kornblihtt, 2006; Naftelberg et al., 2015; Georgakopoulos-Soares, Parada and Hemberg, 2022).

RBPs have different expression levels in different cell and tissue types, therefore, the regulation of AS is cell-, tissue-, and developmental stage-specific. The dysregulation of AS contributes to several diseases, such as neuronal disorders, cancer, and hypercholesterolemia (Tazi, Bakkour and Stamm, 2009).

1.5. Body temperature changes gene expression and alternative splicing in mammals

Endothermic organisms have evolved an elaborate thermoregulatory system that can maintain a relatively stable body temperature (Refinetti, 2020). In mammals, the thermoregulatory response is controlled by neurons in the preoptic area of the hypothalamus through inducing, for example, behavioral adaptation, heat dissipation, and thermogenesis (Boulant, 2000). The mammalian core body temperature is not directly affected by changes in the ambient temperature but can oscillate daily, monthly, and seasonally depending on endogenous rhythms or behavioral patterns (Refinetti, 2020). Rhythmic changes in core body temperature are observed daily with the circadian clock, monthly with the female hormone cycle, and seasonally in animals that hibernate (Ruf and Geiser, 2015; Hall *et al.*, 2016; Preußner *et al.*, 2017). Behavioral patterns that can alter body temperature are, for example, exercise and diet. Behavioral mechanisms allow the organism to escape from extreme environmental conditions that could lead to tissue damage, morbidity, or mortality (Wetsel, 2011).

The circadian clock in mammals is organized hierarchically. The central clock is located in the brain's hypothalamic suprachiasmatic nucleus (SCN) and receives direct light input from the eye (Takahashi, 2017). In response, the SCN produces output signals, such as neuronal signals, hormone rhythms, oscillating body temperatures, and the control of feeding-fasting cycles, that synchronize all peripheral clocks throughout the body and the environment (Gerber *et al.*, 2015). In addition, several other physiological systems are under circadian control, including the cardiovascular, digestive, and endocrine systems; and metabolic and immune functions (Man, Loudon and Chawla, 2016).

The molecular clock machinery consists of several transcription-translation feedback loops that activate and inhibit one another in 24 hours. The core clock genes include the transcription factors (TFs): CLOCK and BMAL1 (activators), and PER1, PER2, CRY1, and CRY2 (repressors) (Takahashi, 2017).

Additionally, it has been shown that 5-20% of all expressed genes undergo circadian oscillations at the mRNA level (Zhang *et al.*, 2014). Furthermore, other regulatory mechanisms, such as splicing, transcription termination, polyadenylation, nuclear export, miRNA regulation, translation, and RNA degradation, were shown to be essential in controlling the circadian clock (Lim and Allada, 2013; Kojima and Green, 2015). For example, previous work from our group described a rhythmic and light-inducible splicing switch that changes the reading frame of the mouse *U2af26* mRNA. This *U2af26* isoform lacking exons 6 and 7 promotes the destabilization of PER1 and defects in circadian mRNA expression in peripheral clocks (Preußner *et al.*, 2014).

Moreover, to respond to temperature changes, the organism needs to have sensors that can detect thermal changes in the environment (Wetsel, 2011). Previous studies have identified a family of thermo-sensitive receptors, transient receptor potential (TRP) ion channels, in the skin and primary sensory neurons (Wetsel, 2011; Song *et al.*, 2016). For example, the ion channel TRPM2 in hypothalamic neurons has been shown to limit fever response and prevent overheating (Song *et al.*, 2016). Recent work from our group described a second family of thermo-sensors, the Cdc2-like kinases (CLKs) (Preußner *et al.*, 2017; Haltenhof *et al.*, 2020). CLKs are responsible for regulating splicing through altering SR protein phosphorylation. The activation segment of CLKs undergoes temperature-controlled structural rearrangements to control kinase activity in the body temperature range (36 and 38°C for mice and humans). CLKs activity is higher at lower temperatures, leading to higher SR protein phosphorylation (**Figure 1.4.**) (Haltenhof *et al.*, 2020). This rhythmic SR protein phosphorylation controls global changes in AS and gene expression (GE), and a temperature change of 1°C is sufficient to induce a splicing switch in a large group of genes (Preußner *et al.*, 2017; Haltenhof *et al.*, 2020). However, functional implications of body temperature-controlled AS and GE remain to be elucidated.

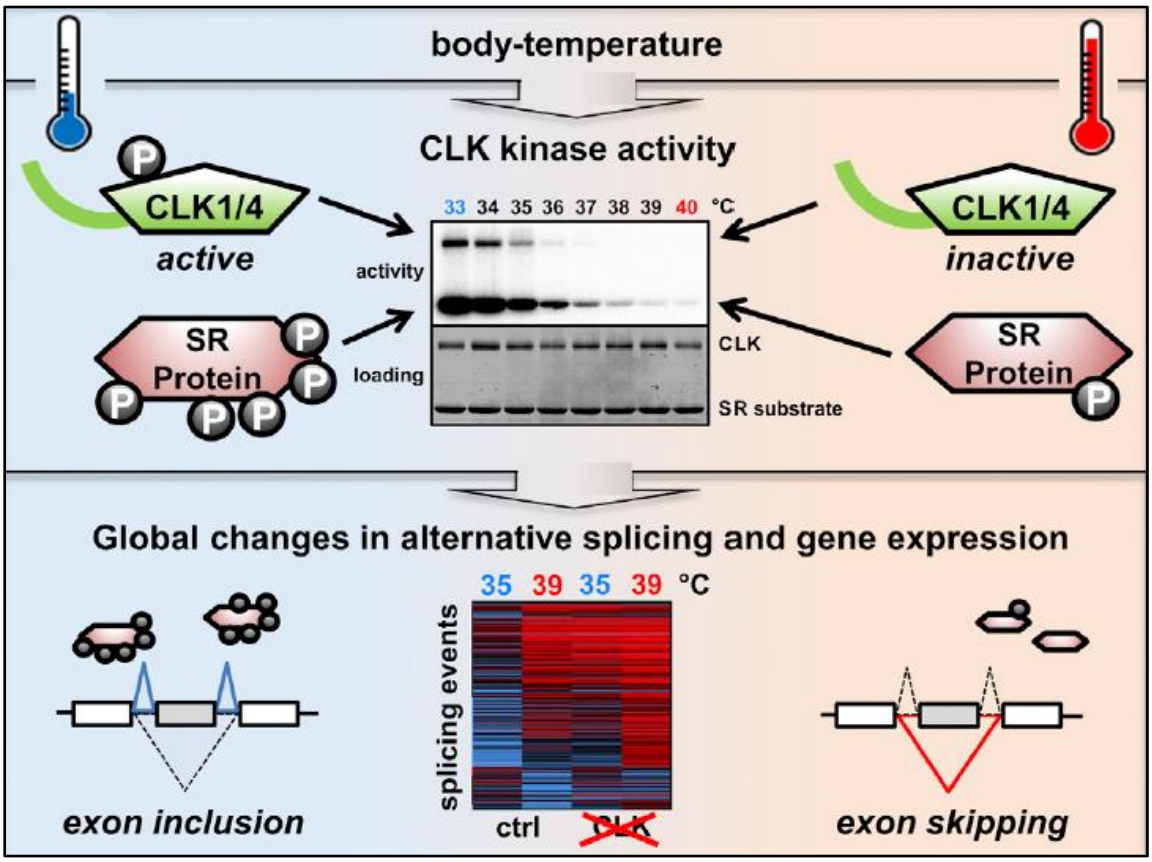

Figure 1.4. Body temperature controls the activity of CLKs.
Schematic representation of CLKs activity at different temperatures. CLKs are more active at lower temperatures, leading to higher SR protein phosphorylation. As a consequence of this rhythmic SR

protein phosphorylation, more exon inclusion is observed at lower temperatures, and more exon skipping is observed at higher temperatures. Consistently, CLK inhibition reduces exon inclusion at lower temperatures (Adapted from Haltenhof *et al.*, 2020).

1.6. Viral infection and changes in body temperature

Several aspects of immune function are under circadian control, including leukocyte trafficking, innate and adaptative response activation, and host-pathogen interactions (Man, Loudon and Chawla, 2016). In support of this, studies have shown that virus infection and the subsequent host immune responses are time-of-day dependent (Edgar *et al.*, 2016; Diallo *et al.*, 2021; Wang *et al.*, 2022). For instance, WT mice infected during the morning (resting phase) with herpes virus showed 10-fold higher viral replication than mice infected during the evening (active phase) (Edgar *et al.*, 2016).

In addition to physiological alterations in core body temperature, pathological changes can also occur, for example, during infection with fever. Fever is responsible for elevating the core body temperature to 1-4°C, which is associated with improved survival and the resolution of many infections (Evans, Repasky and Fisher, 2015). Fever is induced and maintained during infection by a tightly coordinated interplay between the innate immune system and the central and peripheral nervous systems (Evans, Repasky and Fisher, 2015).

The innate immune cells secrete prostaglandin E2 (PGE2) and pyrogenic cytokines responsible for inducing fever. The pyrogenic cytokines, especially interleukin 6 (IL-6), cause the hypothalamus to produce more PGE2, which raises the thermoregulatory setpoint and increases the core body temperature (Vardam *et al.*, 2007; Evans, Repasky and Fisher, 2015).

Fever acts as a systemic alert system that promotes immune surveillance during infection. Several studies have shown the importance of febrile temperatures in reducing the replication of pathogens; while increasing the proliferation, migration, and phagocytic activity of host immune cells (Osawa and Muschel, 1964; Ostberg *et al.*, 2001; Hatzfeld-Charbonnier *et al.*, 2007; Knippertz *et al.*, 2011). Consistently diminishing or preventing fever during infection increases mortality in several organisms, including humans (Earn, Andrews and Bolker, 2014; Evans, Repasky and Fisher, 2015).

Febrile temperatures (38-41°C) can also induce the transcription of heat shock proteins (HSP) (Evans, Repasky and Fisher, 2015). For example, IL-6 together with the signal transducer and activator of transcription (STAT) 3 signaling triggers the production of the heat-shock protein (HSP) 90 (Sato *et al.*, 2003). Additionally, HSP controls the production of chemokines, cytokines, and the release of nitric oxide (NO) by immune cells

(e.g. monocytes, macrophages, and dendritic cells), thus being a potent activator of the immune response (Tsan and Gao, 2004).

1.6.1. Severe acute respiratory syndrome coronavirus 2 infection

The coronavirus disease 2019 (COVID-19) is caused by severe acute respiratory syndrome coronavirus 2 (SARS-CoV-2). SARS-CoV-2 is a positive-sense, single-stranded RNA virus, with a genome of around 30 kb (Lu *et al.*, 2020). The open reading frames (ORFs), ORF1a and ORF1b, are translated from the positive-strand RNA and produce continuous polypeptides. These polypeptides are cleaved into 16 nonstructural proteins (NSPs) (Finkel *et al.*, 2021). The other functional ORFs encode four conserved structural proteins: spike (S), envelope (E), membrane (M), and nucleocapsid (N) (Hu *et al.*, 2021).

According to the World Health Organization (WHO), the COVID-19 pandemic is responsible for more than 760 million infections and more than 6 million deaths worldwide (https://covid19.who.int/). The clinical presentation of COVID-19 can range from asymptomatic or mild to severe disease that can progress to acute respiratory distress syndrome (Huang *et al.*, 2020). The severity of the COVID-19 disease has been associated with age and comorbidities, including obesity, diabetes, immunosuppression, and cardiovascular diseases (Martin-Sancho *et al.*, 2021).

In addition, the innate immune response to SARS-CoV-2 infection was also reported to be critical in determining the disease outcome (Hadjadj *et al.*, 2020). The innate immune response is the first line of defense against invading pathogens and is essential to control the early phase of infection (Park and Iwasaki, 2020; Schultze and Aschenbrenner, 2021). Consistently, impaired type I interferon (IFN-I) response was observed in severe and critically ill COVID-19 patients (Arunachalam *et al.*, 2020; Hadjadj *et al.*, 2020). Also, silencing or reduction of the circadian regulator Bmal1 induced the expression of interferon-stimulated genes (ISG) and limited the replication of SARS-CoV-2 in Calu-3 cells (Zhuang *et al.*, 2021). These findings suggest that a more efficient IFN-I-mediated cellular response in the early phase contributes to the control of SARS-CoV-2 infection and a milder course of the disease (Martin-Sancho *et al.*, 2021).

The main cellular entry point for SARS-CoV-2 is the surface receptor angiotensin-converting enzyme 2 (ACE2) (Hoffmann *et al.*, 2020). The SARS-CoV-2 S protein mediates the viral entry into target cells. The S protein binds to ACE2 for viral attachment. Subsequently, the coronavirus enters the endosome and fuses the viral envelope with the host lysosomal membrane (Shang *et al.*, 2020). The fusion is triggered by the proteolytically cleaved S protein by the serine protease TMPRSS2 (Hoffmann *et al.*, 2020).

1.6.2. Type I interferon-mediated signaling

Immune sensing of viral infection, including coronavirus, begins with the binding of viral RNA to pathogen recognition receptors (PRRs), such as the RNA helicases retinoic acid-inducible gene I (RIG-I, also known as DDX58) and melanoma differentiation-associated gene 5 (MDA5) (McNab *et al.*, 2015; Sa Ribero *et al.*, 2020). The cytosolic RNA sensors RIG-I and MDA5 trigger the adaptor mitochondrial antiviral signaling protein (MAVS) to activate the TANK-binding kinase 1 (TBK1) and the inhibitor of nuclear factor κB kinase-ε (IKKε). The kinases TBK1 and IKKε are responsible for the phosphorylation of the interferon regulatory factor (IRF) 3 and IRF-7. IRF-3 and IRF-7 lead to the transcription of IFN-I genes, which mediates the early innate immune response to viral infections (McNab *et al.*, 2015). Subsequently, secreted IFN-I binds to a heterodimeric transmembrane receptor composed of the interferon alpha and beta receptor subunit 1 and 2 (IFNAR1 and IFNAR2), which leads to the activation of the Janus kinase 1 (JAK1) and tyrosine kinase 2 (TYK2). The JAK1/TYK2 phosphorylates STAT1 and STAT2. Phosphorylated STAT1 and STAT2 associate with IRF9 to form a complex called IFN-α-Stimulated Gene Factor 3 (ISGF3). The ISGF3 translocates to the nucleus to bind to interferon-stimulated response elements (ISREs; consensus sequence TTTCNNTTTC) in ISG promoters, leading to ISG transcription (**Figure 1.5.**) (Ivashkiv and Donlin, 2014; McNab *et al.*, 2015; Schultze and Aschenbrenner, 2021). The ISRE-driven ISGs are responsible for establishing an antiviral state, which includes the degradation of viral nucleic acids and the inhibition of viral transcription, translation, and replication (Ivashkiv and Donlin, 2014). For example, the interferon-induced 2'-5'-oligoadenylate synthetases (OAS) family limits viral infection by activating the latent ribonuclease (RNase L), which degrades viral RNAs and suppresses viral replication (Eskildsen *et al.*, 2003). Another family of proteins responsible for reducing viral replication is the interferon-induced proteins with tetratricopeptide repeats (IFIT) (Yan and Chen, 2012).

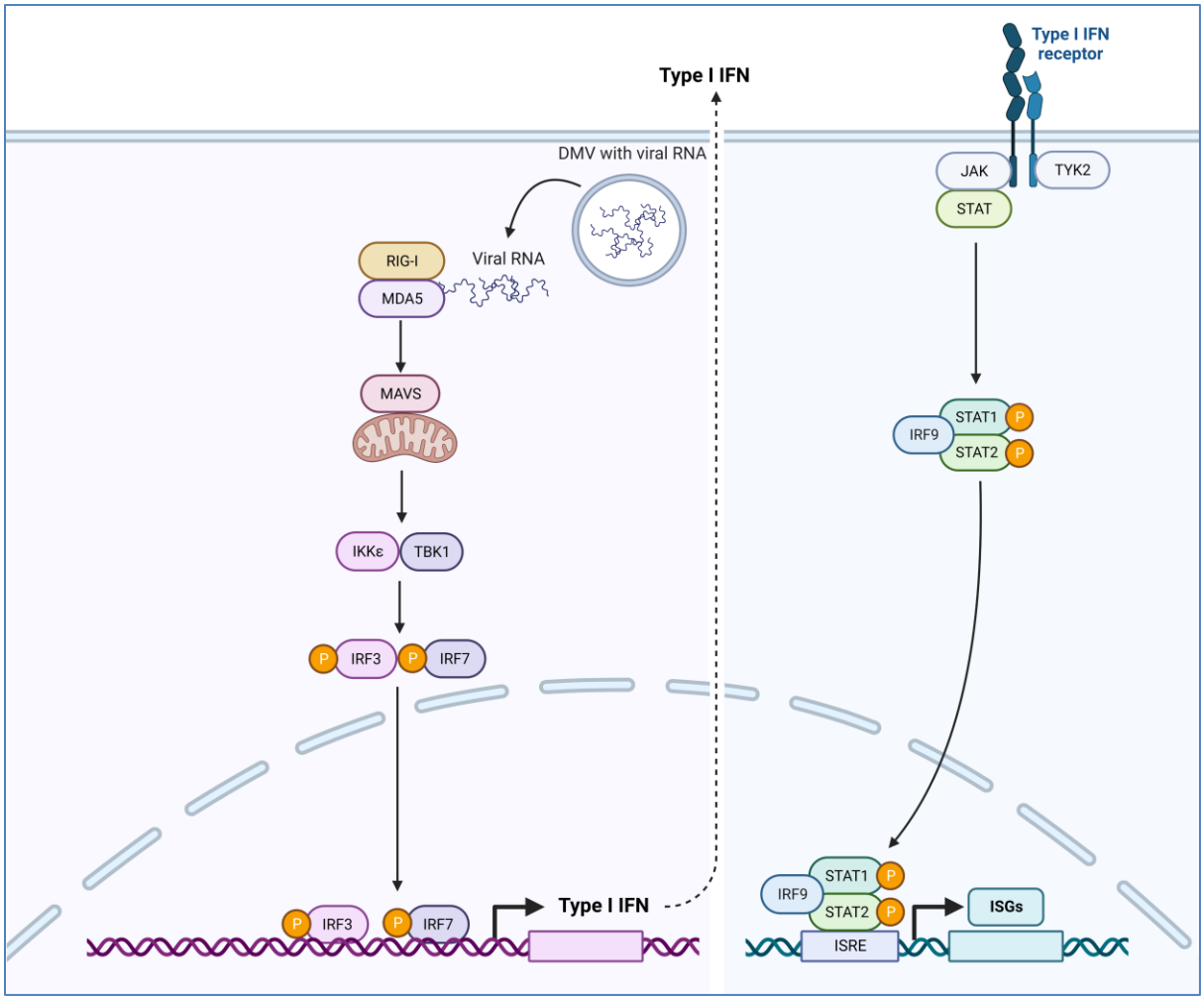

Figure 1.5. Type IFN-I-mediated signaling.
Recognition of viral RNA by RIG-I and MDA5 leads to the induction of IFN-I gene expression. The binding of Type I IFN to their receptor can induce several downstream signaling pathways, such as the JAK-STAT pathway, that will induce the expression of ISGs. Created with BioRender.com.

Interestingly, some ISGs are involved in the regulation of cell metabolism, intracellular RNA degradation, translation arrest, and cell death. Further, the IFN-I response is responsible for recruiting and activating several immune cells (Sa Ribero *et al.*, 2020). Although a robust IFN-I response is necessary to mount a successful antiviral response, this pathway must be tightly regulated as overactivation or prolonged response can harm the host and lead to pathological consequences (Sa Ribero *et al.*, 2020). Therefore, as a negative feedback loop, IFN-I induces the expression of the suppressor of cytokine signaling (SOCS) 1, SOCS3, and ubiquitin specific peptidase 18 (USP18) to limit the duration of the IFN-I response (Ivashkiv and Donlin, 2014). Additionally, alternative splicing of key members of the antiviral cascade has been reported to regulate host immunity during viral infection. Two isoforms of RIG-I are usually expressed upon viral infection, the FL and one with a short deletion in its N-terminal caspase recruitment domain (CARD). This deletion impairs the

binding of TRIM25, and therefore, the CARD ubiquitination, a requirement for RIG-I activation. The short isoform acts as a negative regulator of the antiviral response by suppressing the RIG-I -mediated IFN-I production (Gack *et al.*, 2008). Two isoforms of IKKε have also been identified to act in a dominant negative manner. The two isoforms form a dimer with the FL IKKε and inhibit the IKKε-induced IRF3 signaling (Koop *et al.*, 2011).

Although the host evolved a complex mechanism to regulate the IFN-I response, viruses have also developed many strategies to interfere and evade host regulators of this response. Thus, the host response to the virus is not uniform (García-Sastre, 2017). Consistently, studies have reported a heterogenous IFN-I response in COVID-19 patients and in *in vitro* infection models. For instance, ISGs were shown to be upregulated in infected human epithelial cell line Calu-3 (Wyler *et al.*, 2021), while another study points to a moderate ISG response during infection (Blanco-Melo *et al.*, 2020). SARS-CoV-2 was also reported to encode at least ten proteins that allow the virus to escape or counteract the induction of the IFN response (Sa Ribero *et al.*, 2020). One of these proteins is the Nsp1, which binds to the host 40S ribosomal subunits inhibiting the host mRNA translation, including the antiviral response (Thoms *et al.*, 2020). Another SARS-CoV-2 protein: Ns16 binds to the mRNA recognition domains of U1 and U2 and globally suppresses host mRNA splicing (Banerjee *et al.*, 2020). Additionally, comorbidities and host genetic factors can negatively affect IFN production during an infection (Hadjadj *et al.*, 2020). For example, the absence of STAT1 in humans and mice increased their susceptibility to virus infections (Durbin *et al.*, 1996; Dupuis *et al.*, 2003). Nevertheless, SARS-CoV-2 seems to be sensitive to IFN treatment, and several ISGs were shown to restrict SARS-CoV-2 infection in human lung cells (Lokugamage *et al.*, 2020; Martin-Sancho *et al.*, 2021). In addition, inhibition of the JAK/STAT pathway by Ruxolitinib increased SARS-CoV-2 replication in Calu-3 cells (Felgenhauer *et al.*, 2020).

1.7. Objectives

Body temperature is an omnipresent factor responsible for controlling many biological processes, including gene expression and alternative splicing. Furthermore, elevated body temperature during fever is known to confer survival advantages to several organisms. Cellular components of the immune system are responsible for inducing fever while acting as thermo-sensors. However, the molecular mechanisms by which variations in core body temperature controls the efficiency of the innate immune response following virus infection, such as SARS-CoV-2, are still not fully understood. Additionally, most studies addressing the

molecular mechanisms controlling fever have used temperatures greater than or equal to 39°C (Lane *et al.*, 2018; Herder *et al.*, 2021), leaving the sub-pathological temperature range unexplored. Therefore, the main questions in the present study are:

I. What temperature-sensing machinery triggers changes in immune cell behavior?

II. How does the healthy human core body temperature variation contribute to gene expression control programs and cellular functionality?

We used a combination of classical biochemical, cell biology, and RNA sequencing approaches to address these questions. We used cell culture-based experiments with different stimuli and inhibition to analyze antiviral gene expression patterns and alternative splicing at different temperatures and to determine virus infection. CRISPR/Cas9 methodology and antisense oligonucleotides were also used to further access the impact of alternative splicing on the expression of antiviral genes.

2. MATERIAL AND METHODS

2.1. Buffers

Buffers and solutions were prepared with deionized water and, if necessary, autoclaved. Buffers with heat-labile components were filter-sterilized (0.22 µm). The pH was adjusted using 5 M NaOH, 3 M KCl, 5 M KOH, or 32% HCl.

10x PCR Buffer

200 mM Tris pH 8.3
500 mM KCl
5 mM $MgCl_2$
0.1% Gelatine

Extraction Buffer

Stock	Final concentration
1% Gelatine	0.08%
10x PCR Buffer	1x
10% Tween	0.4%
10% NP-40	0.4%

50x TAE Buffer

2 M Tris Base
5.7% Glacial acetic acid
400 mM EDTA pH 8.0

10x Taq Buffer

0.5 M KCl
0.1 M Tris pH 8.3
15 mM $MgCl_2$
0.01% Gelatine

CTX Buffer

10 mM HEPES–NaOH, pH 7.9
1.5 mM $MgCl_2$
10 mM KCl

NX Buffer

20 mM	HEPES–NaOH, pH 7.9
1.5 mM	MgCl2
420 mM	KCl
0.2 mM	EDTA
25% (v/v)	Glycerol

5x Hybridization Buffer

1.5 M	NaCl
50 mM	Tris pH 7.5
10 mM	EDTA

1.25x RT mix

12.5 mM	DTT
12.5 mM	Tris pH 8.0
7.5 mM	$MgCl_2$

2x Formamide loading dye

80%	Formamide
1 mM	EDTA
0.05% (w/v)	Bromphenol blue
0.05% (w/v)	Xylene cyanol

5x TBE Buffer

1.8 M	Tris Base
1.8 M	Boric acid
400 mM	EDTA

2x RIPA

20 mM	Tris-HCl pH 8.0
200 mM	NaCl
4 mM	EDTA
2%	NP-40
10 mg/mL	Sodium Deoxycholate

2x SDS Loading Dye

0.125 M	Tris-HCl, pH 6.8
4%	SDS
10%	β-mercaptoethanol
20%	Glycerol
0.2%	Bromphenol blue

SDS-PAGE running buffer

25 mM	Tris-HCl, pH 6.8
192 mM	Glycine
1% (w/v)	SDS
21.2% (w/v)	Glycerol
0.12% (w/v)	Bromphenol blue

Transfer Buffer

500 mM	Tris-HCl, pH7.5
400 mM	Glycine
0.1% (w/v)	SDS

1x LS TBST

50 mM	Tris-HCl, pH 7.5
150 mM	NaCl
0.1%	Tween-20

1x HS TBST

50 mM	Tris-HCl, pH7.5
400 mM	NaCl
0.1%	Tween-20

2.2. RNA-sequencing and data analysis

This part was performed by: Marco Preußner and Didrik Olofsson (AG Heyd).

For RNA-sequencing (RNA-seq), RAW 264.7 cells were seeded on 10-cm dishes and grown for ~48 hours at 37°C until ~75% confluence. Subsequently, cells were incubated at 34, 37, and 38°C for 12 h. Total RNA was extracted as described in section 2.6. RNA-seq libraries were prepared from total RNA by poly(A) selection using the TruSeq mRNA library preparation kit (Illumina, USA), according to the manufacturer's protocol. RNA-seq was carried out on an Illumina HiSeq 2500 system (Illumina, USA), using V4 sequencing chemistry, generating around 50M 150 bp paired-end reads per sample. Reads were then aligned to the mouse genome (GRCm38) with gene annotation (GENCODE M21) using STAR (version 2.7.5b) on default settings. Gene counting was performed with featureCounts (version 1.6.4), and the resulting count matrix was used as input for DESeq2 (version 1.28.1). Differential gene expression (DGE) analysis was performed by DESeq2 with fitType = “local”. Log2 fold change (FC) shrinkage was performed using the adaptive shrinkage algorithm to reduce the effect of low expression levels on FC. Significantly differential genes were identified by filtering on Benjamini-Hochberg adjusted *P*-value (*P*adj) ≤ 0.001 and absolute log2FC ≥ 0.8 (or ≤ -0.8). For heatmaps, mean normalized expression counts were calculated for each condition and normalized to the sum of all three temperatures. Gene ontology (GO) term enrichment was performed using PANTHER GO for biological processes (http://geneontology.org/), comparing differentially expressed genes with all expressed genes in RAW 264.7 cells. Only GO enrichments with a false discovery rate (FDR) < $1x10^{-5}$ were shown. Data analysis was performed using Python 3.7.11 with scientific libraries pandas, NumPy, matplotlib, and seaborn. Volcano plots were generated using R v. 4.2.1. with libraries tidyverse, ggrepel, dplyr, and ggplot2.

2.3. Cell culture

RAW 264.7, HeLa, Caco-2, Calu-3, 3T3, and N2a cells were maintained in DMEM High Glucose (Biowest, France), supplemented with 10% (v/v) fetal bovine serum (FBS) and 1% (v/v) penicillin/streptomycin (Invitrogen, USA). Jurkat (JSL1) cells were maintained in RPMI 1640 (Biowest, France) supplemented with 10% (v/v) FBS, and 1% (v/v) penicillin/streptomycin. Cell cultures were kept in a humidified atmosphere at 37°C under 5% CO_2. For cell culture maintenance, adherent cells were dissociated from the T75 flask using 2 mL of the dissociation reagent trypsin or a cell scraper for RAW 264.7 cells. Suspension cultures were collected and centrifuged for 4 min at 100 g. Afterward, cells were

resuspended in a fresh medium. The cells were tested for *Mycoplasma* sp. contamination monthly using a PCR-based assay.

2.3.1. Primary cell culture

Bone marrow-derived primary macrophages were isolated from C57BL/6 wild-type mice using FACS-sorting (BD FACSMelody™ Cell Sorter, BD Biosciences, USA). Bone marrow cells were pipetted through a 70 µm cell strainer, centrifuged at 500 g and 4°C for 5 min, lysed in 1 mL of red blood cells lysis buffer, and incubated for 10 min at room temperature. Cells were then centrifuged at 500 g and 4°C for 5 min and resuspended in 100 µl of 1x PBS. The following antibodies were used for reverse staining: CD4-FITC (1:20, Miltenyi Biotec, Germany), CD8-FITC (1:20, Miltenyi Biotec, Germany), and CD3-FITC (1:20, Miltenyi Biotec, Germany). Sorted cells were seeded in 12-well plates ($0.5x10^6$ cells per well) and maintained in DMEM medium supplemented with 10% (v/v) FBS, 1% (v/v) penicillin/streptomycin, and L- Glutamine in a humidified atmosphere at 37°C under 5% CO_2.

2.3.2. Temperature experiments

For temperature experiments, cells were seeded in 6- or 12-well plates and allowed to adhere at 37°C. Subsequently, cells were shifted to CO_2 incubators set to 34, 35, 36.5, 37, 37.5, 38, or 39°C. Cells were incubated at the respective temperature for 12 or 16 h unless otherwise stated.

2.3.3. Stimulation and inhibition treatments

Cells were stimulated with 0.1 µg/mL of lipopolysaccharides (LPS), 1 ng/mL of phorbol myristate acetate (PMA), and 100U/mL of IFN-I (**Table 2.1.**). LPS stimulation was performed in sorted primary mouse bone marrow-derived macrophages. These cells were incubated at 37 or 39°C for 16 h in the absence or presence of LPS. PMA stimulation was performed in Jurkat cells. Jurkat cells were incubated at 37 or 39°C for 12 h, and then for 16 h ± PMA. IFN-I stimulation was performed in 3T3, Caco-2, and Calu-3 cells. Cells were incubated at 37 or 39°C for 12 h, and then for 4 h ± IFN-I.

Inhibitors were used at the following concentrations: 5 µg/mL of actinomycin D (ActD), 40 µg/mL of cycloheximide (CHX), 50 µM of TG003, and 10 µM Ruxolitinib (**Table 2.2.**). Dimethyl sulfoxide (DMSO) was used as a control. For transcription inhibition, ActD was used. RAW 264.7 cells were seeded in 6-well plates and allowed to adhere at 37°C. Cells were then incubated for 12 h at 37°C or 39°C for 12 h. After 12 h, cells were treated with

ActD for an additional 2 and 4 h at the respective temperatures. For NMD/translation inhibition, CHX was used. RAW 264.7 or HeLa cells were seeded in 6-well plates and allowed to adhere at 37°C. Cells were then incubated for 8 h at 37 or 39°C. After 8 h, cells were treated with CHX for an additional 4 h at the respective temperatures. For inhibition of the kinases: CLK1/4 and JAK1/2, TG003 and Ruxolitinib were used, respectively. RAW 264.7 cells were seeded in 12-well plates and allowed to adhere at 37°C. Subsequently, cells were treated with TG003 or Ruxolitinib and incubated for 6 h at 37°C. After 6 h, cells were shifted to 39°C or kept at 37°C for 12 h. After all treatments, cells were harvested, and RNA extraction was performed (see section 2.6).

Table 2.1. Stimulators.

Name	**Abbreviation**	**Supplier**
Lipopolysaccharide Solution 500× eBio-science™, #00-4976	LPS	Invitrogen, Thermo Fisher Scientific, USA
Universal Type I Interferon #11200-1	IFN-I	R&D Systems, USA
Phorbol myristate acetate	PMA	Sigma-Aldrich, USA

Table 2.2. Inhibitors.

Name		**Concentration**	**Supplier**
Actinomycin D (ActD)	Transcription inhibitor	5 µg/mL	Sigma-Aldrich, USA
Cycloheximide (CHX)	NMD/translation inhibitor	40 µg/mL	Carl Roth, Germany
TG003	CLK1/4 inhibitor	50 µM	Cayman Chemical Company, USA
Ruxolitinib	JAK1/2 inhibitor	10 µM	Cayman Chemical Company, USA

2.3.4. Transfection in mammalian cells

2.3.4.1. Antisense oligonucleotides

We designed a 2‘-O-(2-Methoxyethyl)-oligoribonucleotides antisense oligonucleotide (2′MOE-ASO) flanking the alternative 5’ splice site in exon 11 of *Stat2* (**Table 2.3**). The methoxyethyl attached at the 2’-O-position protects the oligo from nuclease degradation. This ASO chemistry also increases mRNA affinity and prevents immune responses, and therefore, can be used as a potential therapeutic agent (*e.g.* SPINRAZA® - Nusinersen) (Hua *et al.*, 2010; Lim *et al.*, 2020). N2a and 3T3 cells were reverse transfected with 200 µM/mL of the 2'-MOE-ASO using Lipofectamine 2000 (Invitrogen, Thermo Fisher Scientific, USA) at a 1:1 ratio following the manufacturer’s protocol. Briefly, the ASO-Lipofectamine complex was prepared as follows: the ASO was diluted in 100 µL of Opti-MEM - Reduced Serum Media (Gibco, Thermo Fisher Scientific, USA), and the Lipofectamine was diluted in 100 µl Opti-MEM. Both dilutions were incubated at room temperature (~21°C) for 5 minutes. Afterwards, the dilutions were combined and incubated for 20 minutes at room temperature (~21°C). During incubation, N2a and 3T3 cells were harvested, counted, and diluted in DMEM medium without antibiotics. After 20 minutes, the ASO-Lipofectamine complex was added to each well, and then 1 mL of diluted cells were added on top of each complex. As a control, cells were transfected with a scrambled ASO. N2a cells were maintained in a CO_2 incubator for 48 h. 3T3 cells were incubated at 37°C for 32 h, then incubated for an additional 16 h at 37 or 39°C. Forty-eight hours post-transfection, the RNA was extracted, and RT-PCR and RT-qPCR were performed as described in sections 2.6 and 2.7.

Table 2.3. Sequence of the ASOs.

Name	**Target sequence (5’ → 3’)**	**Supplier**
ASO1	TGGGTACCTGTGCTTCTA	Microsynth, Switzerland
ASO2	TGAAGTGGGTACCTGTGC	Microsynth, Switzerland

2.3.4.2. Small interfering RNA against SR proteins

N2a cells were reverse transfected with a pool of four small interfering RNAs (siRNAs) (20 μM/mL) against SR proteins (**Table 2.4**) using Lipofectamine 2000 at a 1:1 ratio following the manufacturer's protocol (as described in section 2.2.4.1).

Table 2.4. Sequence of the siRNAs against SR proteins.

Name	**Target sequence (5' → 3')**
Srsf1	GGAAAGAAGAUAUGACGUA
	GUUUAGAUCUCACGAGGGA
	GGUAAAAGGAGCAAAGCGA
	AGGUUUAGGUGGGUAGUAA
Srsf2	GGGAGCAGUUUCUUCCUAA
	AAGCGAGAGUCCAAGUCUA
	UGAGGCGCGUCUUCGAGAA
	GCCCGAAGAUCCAAGUCCA
Srsf3	GAAAGGCACCUGAGAAUAU
	CCAGAUGAGAUUUAGGUAU
	CUAGCAUAAUUGUGUAGUA
	CUAGAAGGUUCCAACAUGA
Srsf4	GUACAUGUUGGUAGCCGUA
	GAGAGGCGAAGGAGCGUGA
	GUCAAAGGAGCGCGAACAU
	CCUGACAAGAGCCGCAGUA
Srsf5	AAGAACAGAAAUCGACUUA
	GCACAUCGACCUAAACUAA
	CCUCUUAUGGUGACUUAAA
	GGACGAUACUCCGACCGUU
Srsf6	GCAGAAAUAUUAGGCUUAU
	GAAGCAGGUCUAAGGAUAA
	CAGUAGAUCUCGAAGUAUC
	GAAAAUCUGUCUAGUCGUU
Srsf7	UCGCUAUAGCCGACGAAGA
	CGACCAAGAAGCAGCCGAU

	GGAUGCAGUUCGAGGAUUG
	GGGCCUGUAUUCAAAGUUU
Srsf9	GAAGAAACGGUUACGAUUA
	UGGAAUAUGCUCUGCGUAA
	ACGUACAGAAGGACGGAAU
	CCUGAAAGAUCACAUGCGA
Srsf10	CGAUAUAGACGCUCUCGAA
	AAUUUGAGGAUGUUCGUGA
	GAAGAUUUACGUCGGGAAU
	CUUCACGAUAUGACGAUUA
Srsf11	AAACAGGUGACUCGGGAUU
	CCAUGAAGAGAGUGCGUGA
	AGUCAGACACCUCUAGUAA
	GGGAUGAUCACCACGAAGA
Srsf12	GCAAAACAUUUAAGGUCGA
	CUGAAAGAGUCUCGGCACA
	GAUCGAAGACACAGACAAC
	CUUCAAGGCCCGUAGAAAU
siAllstar (control)	UUCUCCGAACGUGUCACGU

2.3.5. Generation of CRISPR/Cas9 edited N2a cells

For CRISPR/Cas9-mediated deletion of the alternative 5' splice site in exon 11 of *Stat2*, single guide RNAs (sgRNAs) were designed using the Benchling tool (**Table 2.5.**) and cloned into the pSpCas9(BB)-2A-GFP (px458) plasmid (Addgene, USA). Before cloning, the sgRNAs were phosphorylated and annealed (see the reaction in **Table 2.6.**) in the S1000 Thermal Cycler (Bio-Rad, USA) using the following parameters: 37°C for 30 min, 95°C for 5 min, and then ramped down to 25°C at 5°C/min. The px458 was digested for 1 h at 37°C (**Table 2.7.**) and purified using the NucleoSpin® Gel and PCR Clean-up Kit (Macherey-Nagel, Germany) accordingly to the manufacturer's protocol. The phosphorylated and annealed oligo duplex was ligated to the BpiI digested px458 (see the reaction in **Table 2.8.**) for 1 h at room temperature (~21°C). The ligated product was transformed into chemically competent Top10 *Escherichia coli* (*E. coli*). For that, the entire ligation was incubated with 50 µL of Top10 *E. coli* on ice for 20 min. Heat shock was performed at 43°C for 90 sec, followed

by a 2 min incubation on ice. Afterward, 1 mL of LB was added to the cells, which were incubated in a thermomixer at 37°C and 600 rpm for 1 hour. Cells were plated on LB plates containing 100 µg/mL ampicillin. Plasmids were isolated using the NucleoBond® Xtra Midi (Macherey-Nagel, Germany) as described in the manufacturer's protocol. The sequence was verified by Sanger sequencing (Microsynth Seqlab, Germany). Finally, N2a cells were reverse transfected with a combination of two sgRNAs (1 µg/sgRNA) using 10 µl of Lipofectamine 2000 following the manufacturer's protocol (as described in section 2.2.4.1). The px458 empty vector was used as a control. Forty-eight hours post-transfection, GFP-positive single cells were sorted in 96-well plates using the BD FACSMelody™ Cell Sorter (BD Biosciences, USA). Sorted single cells were maintained in DMEM medium supplemented with 10% (v/v) FBS, and 1% (v/v) penicillin/streptomycin in a humidified atmosphere at 37°C under 5% CO_2. DNA and RNA from expanded clones were extracted and analyzed by PCR or RT-PCR (as described in sections 2.4-2.7).

Table 2.5. Forward sequence of the sgRNAs.

Name	**Target sequence (5' → 3')**	**Supplier**
sgRNA1	TAAAACAGCCAACAGGCAC	Eurofins, Germany
sgRNA2	GCCAACAGGCACAGGCTGG	Eurofins, Germany
sgRNA3	CAGGTACCCACTTCACGGC	Eurofins, Germany
sgRNA4	AGGCTAGTTTCATTGTCC	Eurofins, Germany

Table 2.6. Oligos phosphorylation and annealing.

Component	**Final concentration**	**Supplier**
sgRNA forward (100 µM)	10 µM	Eurofins, Germany
sgRNA reverse (100 µM)	10 µM	Eurofins, Germany
10x T4 Ligase Buffer	1x	Thermo Fisher Scientific, USA
T4 PNK (10 U/µL)	5 U	Thermo Fisher Scientific, USA

Table 2.7. px458 digestion.

Component	Final concentration	Supplier
px458 (1 µg/µL)	1 µg	Addgene, USA
FastDigest BpiI (1 µL/1 µg DNA)	1 µL	Thermo Fisher Scientific, USA
10x FastDigest Buffer	1x	Thermo Fisher Scientific, USA
FastAP (1 U/µL)	1 U	Thermo Fisher Scientific, USA

Table 2.8. Ligation.

Component	Final concentration	Supplier
BpiI digested px458	50 ng	-
Oligo duplex (1:200 dilution)	0.1 µM	-
10x T4 Ligase Buffer	1x	Thermo Fisher Scientific, USA
T4 Ligase (5 U/µL)	5 U	Thermo Fisher Scientific, USA

2.4. DNA extraction

For DNA extraction, cells were collected and transferred to 1.5 mL tubes, followed by centrifugation for 5 min at 4700 g and 4°C. Cell pellet was resuspended in 200 µL of extraction buffer containing Proteinase K, and incubated at 56°C for 4h or overnight (~16h). Afterwards, samples were incubated at 95°C for 15 min to inactive the Proteinase K. The DNA was used as a template for PCR.

2.5. Polymerase chain reaction and electrophoresis

Polymerase chain reaction (PCR) was performed as described in **Tables 2.9**-**10**. The PCR products were analyzed by agarose gel electrophoresis. Agarose gels contained 1x TAE Buffer and 2% agarose. Gels were stained with ethidium bromide (0.5 mg/mL) for visualization of the DNA fragments. The PCR products were mixed with 2x orange gel loading dye and separated by electrophoresis at 150 V for 40 min. The Quick-Load® 1kb Plus DNA Ladder (New England Biolabs Inc., USA) was used to evaluate the size of the DNA fragments. The bands were visualized with UV light using the UVsolo touch system (Analytik Jena, Germany).

Table 2.9. PCR master mix.

Component	**Final concentration**
10x Taq Buffer	1x
10 mM dNTPs	200 µM
$MgCl_2$	1.5 mM
10 µM Forward primer	0.5 µM
10 µM Reverse primer	0.5 µM
Taq Polymerase (5U/µL)	2.5 U
DNA	variable

Table 2.10. PCR reaction.

Stage	**Temperature [°C]**	**Cycles**	**Time [min]**
Denaturing	95	1	5:00
Denaturing	95	35	0:30
Annealing	primer specific		0:30
Extending	72		2:00
Extending	72	1	7:00
Hold	4	1	∞

2.6. RNA extraction

Total RNA was extracted using RNA Tri-Flüssig (Bio&SELL, Germany) as described in the user manual, followed by DNase digest to remove DNA contamination. Cells were resuspended in 1 mL of RNA Tri-Flüssig. Subsequently, 200 µl of Trichloromethane/Chloroform (Carl Roth, Germany) were added to the samples, followed by 10 min incubation at room temperature (~21°C). Samples were centrifugated at 17 000 g and 4°C for 10 min. The aqueous layer was then transferred to a fresh 1.5 mL tube containing 600 µl of ice-cold isopropanol. Samples were centrifugated at 17 000 g and 4°C for 10-30 min. The pellet was washed with 1 mL of 70% ethanol and centrifugated at 17 000 g and 4°C for 3 min. The supernatant was removed, and samples were centrifugated at 17 000 g and 4°C for 1 min, and then the remaining liquid was removed completely. The pellet was resuspended in 16 µl MiliQ water. For DNAse digestion, samples were incubated with 2

µl 10x DNase Buffer and 2 µl DNase for 20 min at 37°C. Further, 180 µl MiliQ water and 200 µl of ROTI®Aqua-P/C/I (Carl Roth, Germany) were added to the samples. Samples were centrifugated at 17 000 g and 4°C for 15 min. The aqueous layer was then transferred to a fresh 1.5 mL tube containing 1 µl of glycogen, 20 µl 3M sodium acetate, and 500 µl of 100% ethanol. Samples were centrifugated at 17 000 g and 4°C for 10 min. Finally, samples were washed with 1 mL of 70% ethanol as described above. The pellet was resuspended in 12 µl of MilliQ water. The RNA concentration was determined using NanoDrop spectrophotometer (at wavelengths of 260 nm and 280 nm) according to the manufacturer's instructions. The RNA was diluted to 500 ng/µl or the lowest concentration.

2.6.1. Chromatin-associated RNA

For chromatin-associated RNA extraction, cells were resuspended in 100 µl of cold CTX buffer, and incubated on ice for 5 min. Furthermore, 100 µl of cold CTX buffer supplemented with 0.2% (v/v) NP-40 was added to the samples, followed by incubation on ice for 5 min. Nuclei were pellet by centrifugation at 4100 g for 3 min at 4°C. The nuclear fraction was resuspended in 40 µl of NX buffer. The chromatin-associated RNA was then isolated using RNA Tri-Flüssig as described in section 2.6.

2.7. Reverse transcription polymerase chain reaction

Total RNA was used to synthesize cDNA via reverse transcription polymerase chain reaction (RT-PCR). For that gene-specific primers were annealed to template RNA (as described in **Tables 2.11-12**). Further, the RT reaction was prepared and combined with the annealed RNA (as described in **Tables 2.13-14**). The synthesized cDNA was used as a template for radioactive RT-PCR or reserve transcription quantitative real-time PCR (RT-qPCR). See **Table 2.19** for primer sequences.

Table 2.11. Hybridization reaction.

Component	Final concentration
RNA (500 ng/µl)	1 µg
5x Hybridization Buffer	1x
Reverse primer mix (10 µM)	0.1 µM/µl

Table 2.12. Thermocycler program for hybridization.

Temperature [°C]	Cycle	Time [sec]
90 … 70	1	20
69 … 51		30
50 … 44		40
43		∞

Table 2.13. RT reaction.

Component	Final concentration
RT annealing mix (Table 2.11)	
1.25x RT mix (+dNTPs)	1x
MmuLV reverse transcriptase (100 ng/µl)	1 ng/µl

Table 2.14. Thermocycler program for RT.

Temperature [°C]	Cycles	Time [min]
43	1	30
94		5
4		∞

2.7.1. Radioactive RT-PCR and denaturing polyacrylamide gel electrophoresis

Radioactive RT-PCR with a [^{32}P]-labeled forward primer was performed to analyze alternative splicing events. The PCR master mix as well as the temperature profile are described in **Tables 2-15.16**.

Table 2.15. Radioactive RT-PCR master mix.

Component	**Final concentration**
10x Taq Buffer	1x
Forward primer (2.5 ng/µl)	2.5 ng
Reverse primer (5 ng/µl)	5 ng
[^{32}P]-labeled forward primer	2.5 ng
Taq Polymerase (5U/µL)	2.5 U
Template	variable

Table 2.16. Radioactive RT-PCR reaction.

Stage	**Temperature [°C]**	**Cycles**	**Time [min]**
Denaturing	95	1	3:00
Denaturing	95	25-30	0:30
Annealing	Primer-specific (usually 60)		0:30
Extending	72		0:45
Extending	72	1	7:00
Hold	4	1	∞

PCR products were dissolved in 2x formamide loading dye and incubated for 5 min at 95°C. PCR products were then separated by denaturing polyacrylamide (PAGE) gels in the presence of 7 M urea (**Table 2.17**). The electrophoresis was performed in 0.5x TBE Buffer at 30 mA. The products were visualized with the phosphorimager Typhoon 9200 (GE Healthcare, USA) and quantified with ImageQuantTL software (Cytiva, Germany). The [^{32}P]-labeled pBR322 DNA-MspI Digest (New England Biolabs Inc., USA) was used to evaluate the size of the products. Quantifications are given as mean values of several technical and biological replicates, error bars represent standard deviation, and *P*-values were calculated using Student's unpaired *t*-test. Significance is indicated by asterisks (*$P < 0.05$; **$P < 0.01$; ***$P < 0.001$; ****$P < 0.0001$). See **Table 2.19** for primer sequences.

Table 2.17. PAGE gel composition.

Stock concentration	Final concentration
7 M Urea/0.5x TBE	50%
10% Acrylamide/7 M Urea/0.5x TBE	50%
10% APS	0.1%
TEMED	0.01%

2.7.2. RT-qPCR

For RT-qPCR, up to 6 gene-specific primers were combined in one RT reaction using 1 µg of purified RNA (see section 2.7). qPCR was performed in a 96-well format using the Biozym Blue S'Green qPCR Kit (**Table 2.18**) and a Line-Gene 9600 Plus Real-time PCR System (Bioer Technology Co., China). qPCRs were performed in duplicates, mean C_T values from target genes were normalized to the mean of *Hprt* C_T values (mice cell lines) or *GAPDH* C_T values (human cell lines); (ΔC_T) and $\Delta(\Delta C_T)$s were calculated for different conditions. Quantifications are given as mean values, error bars represent standard deviation, and *P*-values were calculated using Student's unpaired *t*-test. Significance is indicated by asterisks (*$P < 0.05$; **$P < 0.01$; ***$P < 0.001$; ****$P < 0.0001$). See **Table 2.19** for primer sequences.

Table 2.18. qPCR master mix.

Component	Final concentration	Supplier
2x qPCR S'Green BlueMix	1x	Biozym, Germany
10 µM Forward primer	250 nM	Eurofins, Germany
10 µM Reverse primer	250 nM	Eurofins, Germany
Template	variable	-

Table 2.19. Primers sequences.

Name	Target sequence (5' → 3')	Used for:
Mus musculus primers		
mStat2_E11_F	CTGGTGAGACTCCAGGAAGG	CRISPR/Cas9 cloning genotyping or Splicing PCR
mStat2_I11_R2	CTCACAGCGACATGGCATGG	CRISPR/Cas9 cloning genotyping
mStat2_E13_R	AAGAAGCCGAAGTCCCAAAT	Splicing PCR
mStat2_qF	GAAGATGAAGCTGCAGACGG	RT-qPCR
mStat2_intron_qF	TAACTCCGGTCTTCCTCCCAG	RT-qPCR
mStat2_qR	TTGGGCTGAGCATGTTGAAC	RT-qPCR
mDdx58_qF	CGACAAGGAAAACTGGCCAA	RT-qPCR
mDdx58_intron_qF	AGAAACCCTGCCTCGACCAC	RT-qPCR
mDdx58_qR	CTCCGCTCCATCATCCTCAT	RT-qPCR
mTrim25_qF	CGGAAAATTCGACACCATCT	RT-qPCR
mTrim25_intron_qF	CCCTGGCTTTCCTCCAATCAC	RT-qPCR
mTrim25_qR	CTTAGGGATGTAGACTGGTT	RT-qPCR
mMavs_qF	AGAGCAACTCCTCCAGACCA	RT-qPCR
mMavs_qR	AACGGTTGGAGACACAGGTC	RT-qPCR
mIrf7_qF	TGATCCGCATAAGGTGTACG	RT-qPCR
mIrf7_qR	GCATCACTAGAAAGCAGAGG	RT-qPCR
mIfit3_qF	CAGCAGCACAGAAACAGATC	RT-qPCR
mIfit3_qR	CTGGACATACTTCCTTCCCT	RT-qPCR
mOasl2_qF	TAAAGGTTCAGTCCCGGAAG	RT-qPCR
mOasl2_qR	CAGGGTAGCCCTTACTTCTT	RT-qPCR
mOas3_qF	TAATCCTGCTGGTCAAACAC	RT-qPCR
mOas3_qR	GGTACTTGCTGTGTTGGATC	RT-qPCR
mNos2_qF	GGAATCTTGGAGCGAGTTGT	RT-qPCR
mNos2_qR	CCTCTTGTCTTTGACCCAGTAG	RT-qPCR
mHprt_qF	CAACGGGGGACATAAAAGTTATTGGTGGA	RT-qPCR
mHprt_qR	TGCAACCTTAACCATTTTGGGGCTGT	RT-qPCR
Homo sapiens primers		

hSTAT2_E15_fwd	TGCACATCATCAGCTTCACG	Splicing PCR
hSTAT2_E18_rev	TTAGTGAAGTCAGCCCAGGA	Splicing PCR
hSTAT2_qF2	GAAGCAGGAGCTGAAAACGG	RT-qPCR
hSTAT2_qR2	TTGGGCTGAGCAAATTGAAC	RT-qPCR
hDDX58_qF	GCGTCAGTGATAGCAACAGTC	RT-qPCR
hDDX58_qR	GTCGCTAATCCGTGATTCCAC	RT-qPCR
hTRIM25_qF	GAGGAGATTGAACAGAGCCTGAC	RT-qPCR
hTRIM25_qR	CTGGCTTTGTTGAGATTCCTCG	RT-qPCR
hOAS1_qF	GAGAAGGCAGCTCACGAAAC	RT-qPCR
hOAS1_qR	CCTCCAACCCTTTGGGTCTC	RT-qPCR
hGAPDH_qF	CTTCGCTCTCTGCTCCTCCTGTTCG	RT-qPCR
hGAPDH_qR	ACCAGGCGCCCAATACGACCAAAT	RT-qPCR

2.8. Western blotting

Whole-cell lysates were prepared in RIPA lysis buffer containing proteinase inhibitors. Protein concentration was measured using the BCA protein assay (Thermo Fisher Scientific, USA). Protein samples were mixed with 2x SDS loading dye and denatured for 5 min at 95°C. Equal amounts of denatured protein were separated on 10% SDS-PAGE (**Table 2.20.**). The PageRuler™ Prestained Protein Ladder (Thermo Fisher Scientific, USA) was used to estimate the sizes of the proteins. The SDS-PAGE gel was run in 1x SDS running buffer at 100-180 V and then transferred onto a nitrocellulose membrane (Amersham, GE Healthcare, USA). The electrotransfer was performed using the Mini Trans-Blot® Cell and Criterion™ Blotter (Bio-Rad, USA) at 100 V for 1 h. The membrane was then incubated in 2% BSA-LS TBST or 5% non-fat dry milk-LS TBST at room temperature (~21°C) for 1h and subsequently with primary antibody overnight at 4°C. The following primary antibodies were used (**Table 2.21.**): rabbit anti-phospho-Stat2 (Tyr690), 1:1000; rabbit anti-phospho-Stat3 (Tyr705), 1:1000; mouse anti-RIG-I, 1:1000, rabbit anti-Stat2 (mouse specific), 1:1000. The blot was washed 3x for 10 min using HS TBST. Further, antibody recognition was detected with the secondary antibody linked to horseradish peroxidase at room temperature (~21°C) for 1h. hnRNP-L bands were used as a loading control. The immunoreactive bands were visualized with Pierce™ ECL Western Blotting Substrate (Thermo Fisher Scientific, USA) using the Amersham Imager 600 (GE Healthcare, USA). The bands were quantified using ImageQuantTL software.

Table 2.20. Composition of SDS gels.

Component	Stock concentration	Stacking gel	Separating gel
Acrylamide	30%	4%	10%
Tris-HCl, pH 6.8	1M	125 mM	-
Tris-HCl, pH 8.8	1M	-	375 mM
SDS	10% (w/v)	0.1%	0.1%
APS	20% (w/w)	0.1%	0.14%
TEMED	100%	0.1%	0.07%

Table 2.21. WB antibodies.

Antibody	Supplier
rabbit anti-phospho-Stat2 (Tyr690), #4441	Cell Signaling Technology, USA
rabbit anti-phospho-Stat3 (Tyr705), #9131	Cell Signaling Technology, USA
rabbit anti-Stat2 (mouse specific), #4597	Cell Signaling Technology, USA
mouse anti-RIG-I, #sc-376845	Santa Cruz Biotechnology, USA
mouse anti-hnRNP-L, #sc-32317	Santa Cruz Biotechnology, USA
anti-mouse IgG HRP, #7076s	Cell Signaling Technology, USA
anti-rabbit IgG HRP, #7074s	Cell Signaling Technology, USA

2.9. Nitric Oxide Assay

RAW 264.7 or primary macrophages were incubated with 1.25 or 2.25 µg/mL of LPS at 37°C or 39°C for 16h to induce endogenous nitric oxide (NO) formation. For measuring intracellular NO levels, the Nitric Oxide Assay Kit (flow cytometry - orange, #ab219933, Abcam, UK) was used according to the manufacturer's protocol. The analysis was performed using the BD FACSMelody™.

2.10. SARS-CoV-2 infection and quantification

This experiment was performed by: Kathrin Eschke, Ricardo Martin Vidal, Azza Abdelgawad and Jakob Trimpert from the Institut für Virologie at Freie Universität Berlin.

SARS-CoV-2 virus stocks were prepared from passage 3 of an early 2020 SARS-CoV-2 B.1 outbreak isolate (BetaCoV/Germany/BavPat1/2020) on Vero E6 cells. All work related to authentic SARS-CoV-2 was performed under appropriate BSL-3 safety conditions (Freie Universität Berlin, Institut für Virologie). Virus was propagated on Calu-3 cells and Caco-2 cells. Titrations were performed on VeroE6 cells in minimal essential medium (MEM; PAN Biotech, Aidenbach, Germany) supplemented with 10% fetal bovine serum (PAN Biotech, Aidenbach, Germany), 100 IU/mL penicillin G and 100 µg/mL streptomycin (Carl Roth, Karlsruhe, Germany). For temperature-controlled SARS-CoV-2 infection experiments, Calu-3 cells and Caco-2 cells were grown to 80% confluence on 6-well plates and maintained at 37°C or 39°C for 16h before infection. SARS-CoV-2 infection was performed by adding virus stock at a multiplicity of infection (MOI) of 0.01 to cell monolayers and subsequent incubation at 37°C for 90 min. Virus inoculum was then removed, cells were washed with 1x PBS, and fresh cell culture medium was added before cells were returned to 37°C and harvested at 24 h post-infection and 48 h post-infection. All cell culture experiments were performed in 12 biological replicates for each cell line and condition. To determine virus titers as plaque-forming units (pfu), cells grown in 12-well plates were infected with 100 µl of serial 10-fold dilutions of the virus. After 75 minutes of incubation, the viral inoculum was removed, and cells were overlaid with 2x EMEM containing 1.5% microcrystalline cellulose and carboxymethyl cellulose sodium Vivapur MCG (JRS Pharma). Forty-eight hours after infection, cells were fixed with 4% formalin. The wells were stained with 1 mL of a 0.75% aqueous methylene blue solution, washed with 1x PBS to remove residual stain and plaques were counted in an appropriate dilution to calculate virus titers in the inoculum.

3. RESULTS

Most of the data and figures in the results part were published at Bruna Los, Marco Preußner, Kathrin Eschke, Ricardo Martin Vidal, Azza Abdelgawad, Didrik Olofsson, Sandra Keiper, Margarida Paulo-Pedro, Alica Grindel, Stefan Meinke, Jakob Trimpert, Florian Heyd. Body temperature variation controls pre-mRNA processing and transcription of antiviral genes and SARS-CoV-2 replication. Nucleic Acids Res. 2022 Jun 17;50(12):6769-6785.doi: 10.1093/nar/gkac513.

3.1. A subtle temperature increase induces the expression of antiviral response genes

To evaluate the impact of core body temperature changes on the expression of genes related to the innate immune system, we performed RNA-seq using the mouse macrophage cell line RAW 264.7. RAW 264.7 cells were incubated for 12 h at the following temperatures: 34, 37, or 38°C (**Figure 3.1. A**). The strongest inverse correlation between temperature and gene expression was observed for the cold-induced RNA binding protein 3 (*Rbm3*). Rbm3 was around 10-fold increased at 34°C when compared to 38°C, and almost 3-fold increased at 37°C when compared to 38°C, confirming that the temperature treatment was effective, even for the small change between 37 and 38°C (**Figure 3.1. B**). Therefore, we could use this dataset to look for global changes in temperature. We identified 132 genes differentially expressed between 37 and 38°C, while only 45 were differentially expressed between 34 and 37°C (**Figure 3.1. C**). Interestingly, there was only a small overlap when cells were transferred from 37°C (normothermia) to 34°C (hypothermia) or 38°C (mild fever), suggesting specific responses depending on the temperature (**Figure 3.1. C**). Notably, increasing the temperature from 37°C to 38°C upregulates the expression of genes associated with antiviral defense. These genes did not show a change in expression between 34°C and 37°C, suggesting a specific activation of innate immunity and antiviral pathways at elevated temperatures (**Figure 3.1. D**). This was also confirmed by GO term analysis showing a strong and highly significant enrichment of processes such as ‘response to virus’, ‘defense response to virus’, ‘innate immune response’, amongst others (**Figure 3.1. E**). The same GO term enrichments were found when comparing genes differentially expressed between 34 and 38°C (**Figure 3.2. A-C**). However, these GO terms were less significantly enriched than when comparing differences between 37 and 38°C (**Figure 3.1. C**), supporting our hypothesis that these genes are specifically induced by a one-degree increase in temperature. In addition, genes that were differentially expressed between 34 and 37°C did not show similar enrichments (**Figure 3.2. A-C**). We then had a closer look at

the genes associated with the GO term “response to virus”. We found 174 genes expressed in RAW 264.7 cells that were associated with this GO term. More than 25% of them were induced at 38°C when compared to 37°C, while only a few genes showed higher expression at 34°C when compared to 37°C (**Figure 3.2. D**).

To validate our RNA-seq data findings, RAW 264.7 cells were incubated at 35, 37, 38, and 39°C for 12 h and gene expression analysis was carried out by RT-qPCR. For the validation, genes associated with defense against RNA viruses, including SARS-CoV-2, were selected (**Figure 3. 3.**). In **Figure 3.3.**, the antiviral pathway is depicted together with the RT-qPCR data. Remarkably, all target genes showed a similar gene expression pattern to that seen in the RNA-seq data. The most significant differences in gene expression happened between 37°C and 38°C. Increasing the temperature to 39°C or decreasing it to 35°C did not substantially impact the expression of these temperature-controlled antiviral genes (**Figure 3. 3.**), suggesting that this regulation happens within the normothermic range. To test this hypothesis, RAW 264.7 cells were incubated at 36.5, 37, 37.5 and 38°C for 12 h and gene expression analysis was carried out by RT-qPCR. Notably, the expression of *Stat2*, *Ddx58* (RIG-I), and *Irf7* was significantly higher when increasing the temperature from 36.5 to 37.5°C, while *Trim25* displayed a similar trend (**Figure 3.4.).** These results suggest that individual and age-dependent body temperature variations can control the expression of the antiviral genes, with higher temperatures leading to higher expression. Although our data showed that an increase from 36.5 to 37.5/38°C could already induce the expression of antiviral genes, in the following experiments we compared 37 and 39°C to accommodate a 0.5°C degree error margin of the incubators used for the experiments.

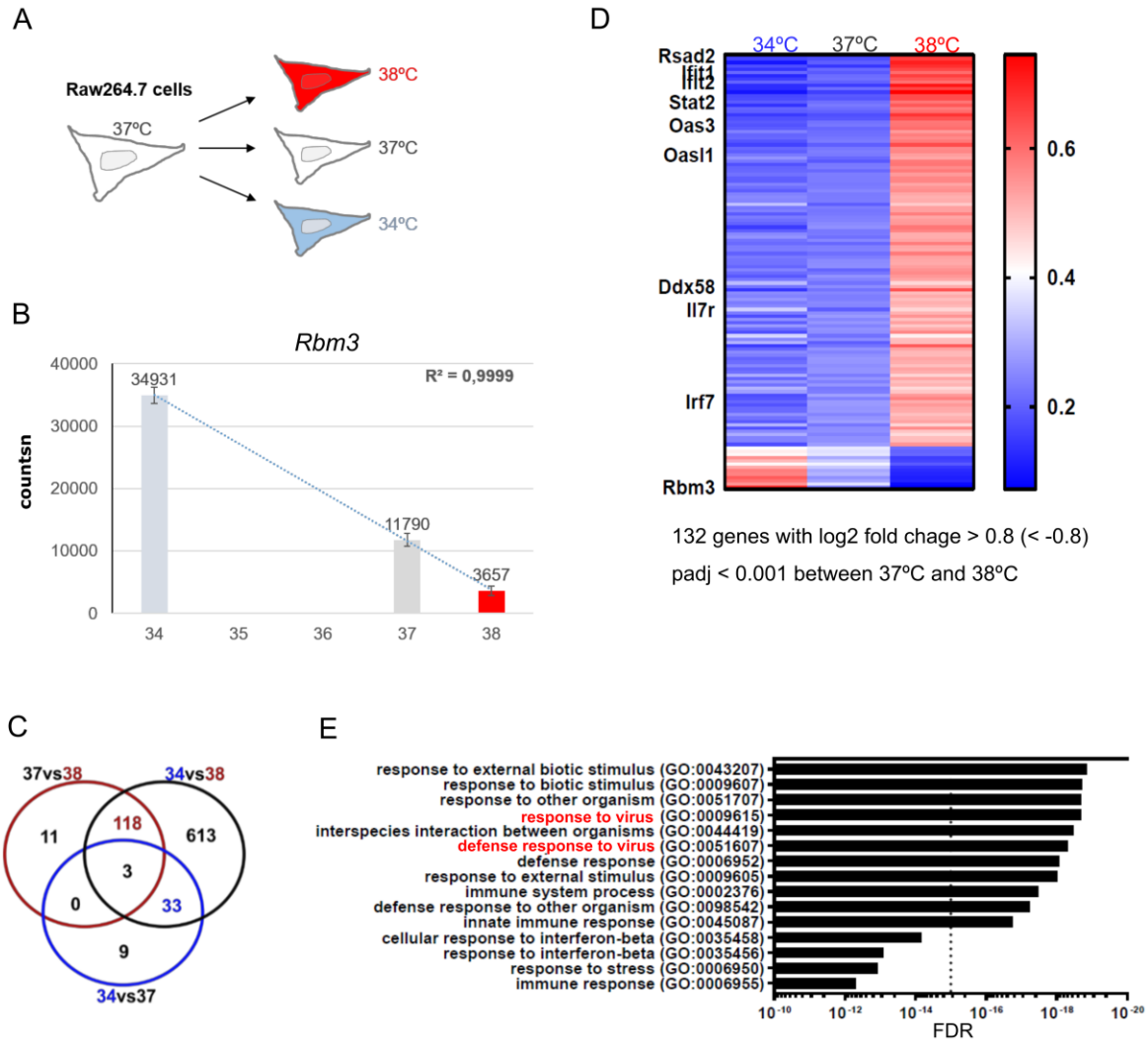

Figure 3.1. Antiviral genes are upregulated at elevated temperatures (38°C) in RAW 264.7 cells.
(A) Schematic representation of the experimental design. RAW 264.7 cells were maintained at 37°C, then incubated for 12h at the indicated temperatures. RNA-seq was performed in triplicates for 34 and 38°C, and in quadruplicates for 37°C. **(B)** The RNA-binding protein 3 (*Rbm3*), a known cold-induced gene, is upregulated at 34°C in RAW 264.7 cells. The dotted line represents a linear regression fit of temperature and *Rbm3* expression. **(C)** Venn diagram showing differentially expressed genes between 34 vs 37°C (blue circle), 34 vs 38°C (black circle), and 37 vs 38°C (red circle). Genes were considered differentially expressed if $P^{adj} \leq 0.001$ and absolute log2FC ≥ 0.8 (or ≤ -0.8) between two temperatures. **(D)** Heatmap showing temperature-dependent changes in gene expression between 37 and 38°C. **(E)** The strongest enriched GO terms of genes upregulated at 38°C when compared to 37°C (FDR < $1x10^{-5}$). The GO terms related to virus were highlighted in red. A list of all genes expressed in RAW 264.7 cells was used as a background. The RNA-seq data analysis was performed by Marco Preußner and Didrik Olofsson. Adapted from Los *et al.*, 2022.

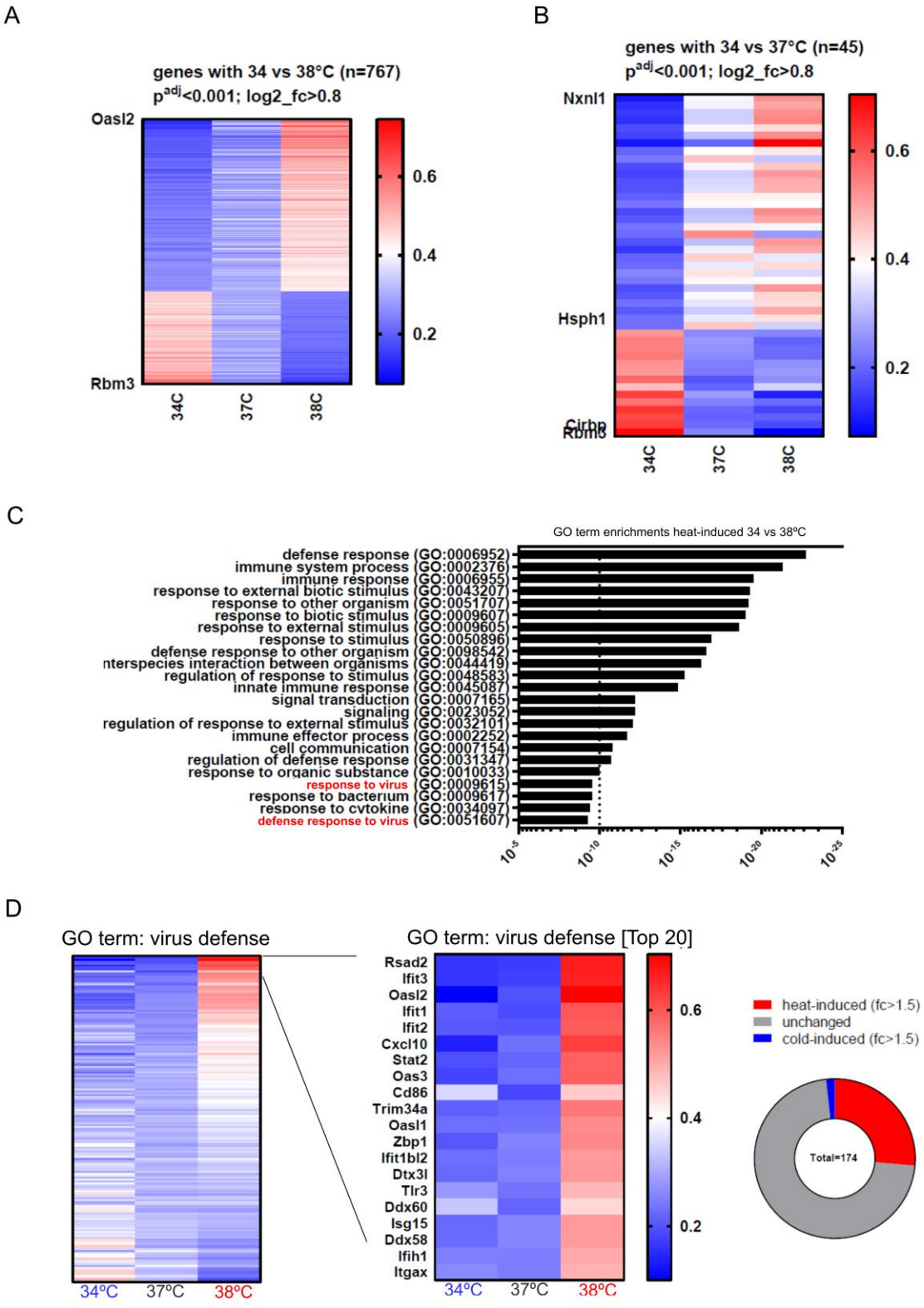

Figure 3.2. Changes in gene expression comparing 34°C and 37-38°C.
(A) Heatmap as in Figure 3.1. showing differentially expressed genes between 34 and 38°C (n=767, sorted by change 34°C to 38°C). **(B)** Heatmap showing differentially expressed genes between 34 and 37°C (n=45, sorted by change 34°C to 37°C). **(C)** The strongest enriched GO terms of genes upregulated at 38°C when compared to 34°C (FDR < $1x10^{-5}$). The GO terms related to virus were highlighted in red. No GO enrichment was found when comparing 34 vs 37°C. **(D)** Heatmap showing

all 174 genes related to the GO term “defense response to virus”. Genes were sorted by changing 37 to 38°C (left). The 20 strongest heat-induced genes are shown in the middle. The donut chart (right) is showing the percentage of genes that are heat-, cold-induced, or unchanged. More than 25% of genes (n = 46) are heat-induced (FC 37°C / 38°C > 1.5), and only 1.7% of genes (n = 3) are cold-induced (FC 34°C / 37°C > 1.5). The RNA-seq data analysis was performed by Marco Preußner and Didrik Olofsson. Adapted from Los *et al.*, 2022.

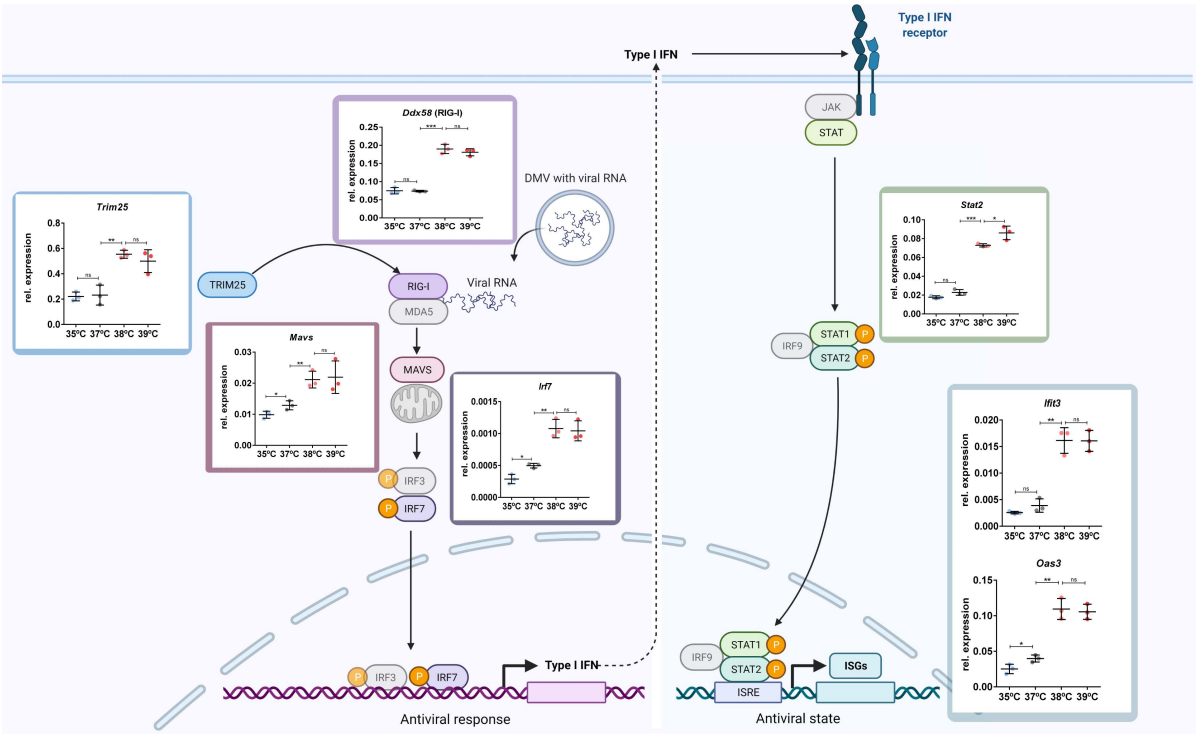

Figure 3.3. Antiviral-related genes are upregulated at 38°C.
Schematic representation of the IFN-I-mediated signaling as in Figure 1.5. Created with BioRender.com. Graphics are showing the validation of the RNA-seq data (Figures 3.1. and 3.2.) via RT-qPCR. RAW 264.7 cells were incubated at the indicated temperature for 12h and gene expression was analyzed. C_T values from target genes were normalized to the mean of *Hprt* C_T values (n = 3, mean ± SD). Genes shown in color were upregulated at 38°C in the RNA-seq data (Figures 3.1. and 3. 2.). Genes shown in gray were not changed. Statistical significance was determined by unpaired *t*-tests and is indicated by asterisks, *P < 0.05; ** P < 0.01; *** P < 0.001; ns = not significant. The experiment was performed by Sandra Keiper. Adapted from Los *et al.*, 2022.

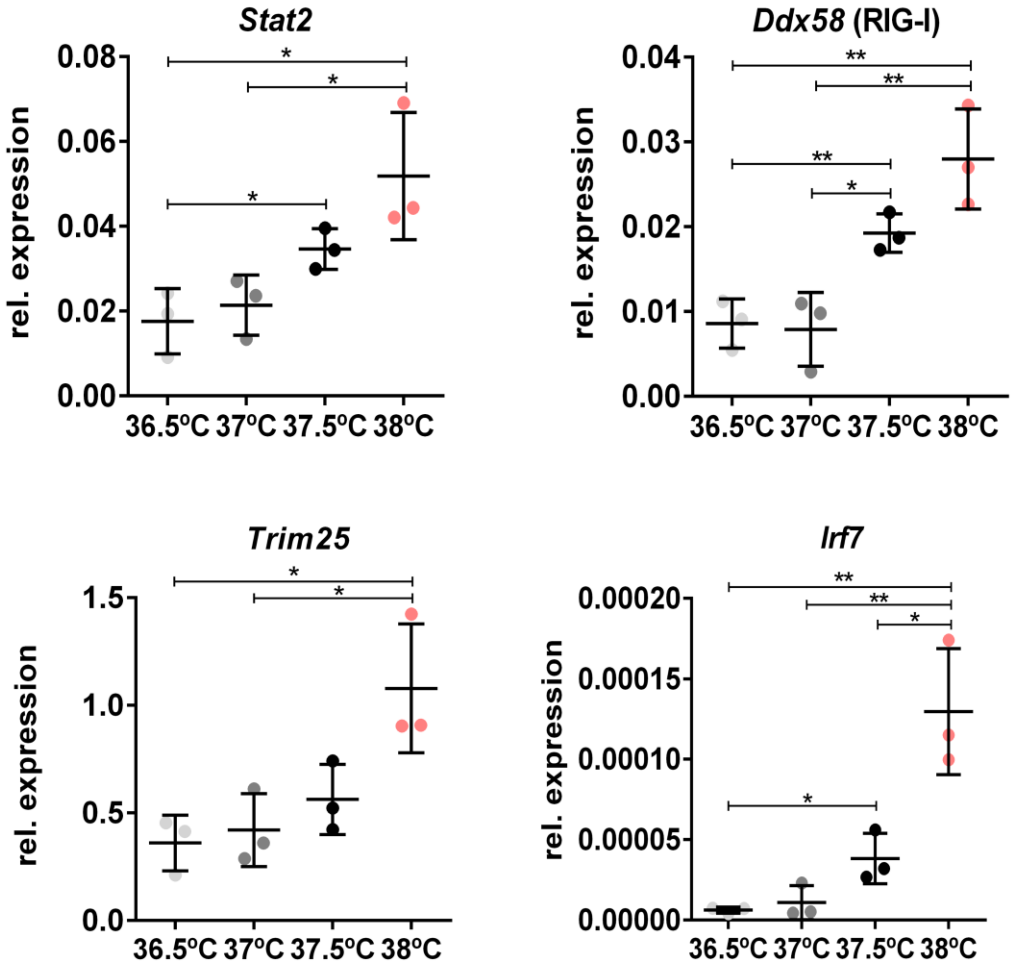

Figure 3.4. Antiviral-related genes are upregulated in the sub-pathological temperature range.

RAW 264.7 cells were incubated at the indicated temperature for 12 h and gene expression was analyzed by RT-qPCR. C_T values from target genes were normalized to the mean of *Hprt* C_T values (n = 3, mean ± SD). Adapted from Los *et al.*, 2022.

3.2. JAK-STAT pathway is responsible for inducing the expression of antiviral genes at elevated temperature

The major pathway activated by IFNs, which leads to the expression of ISGs is the JAK-STAT pathway. Therefore, we investigated a potential activation of the JAK/STAT pathway at elevated temperatures by using Phospho-STAT antibodies. We observed a significant increase in the phosphorylation of both Stat2 and Stat3 in RAW 264.7 cells incubated at

39°C compared to 37°C, indicating more activation at higher temperatures (**Figure 3.5. A, Figure S1**). Interestingly

, Stat2 phosphorylation at 39°C was similar to the phosphorylation obtained by stimulating RAW 264.7 with LPS (**Figure 3.5. A**). This result suggests that higher temperatures may prime macrophages for antiviral response. Additionally, an increase in RIG-I (Ddx58) and Stat2 protein levels at 39°C was also observed, indicating that the changes observed for mRNAs are translated to the protein level (**Figure 3.5. B-C**). Further, we addressed the impact of the JAK-STAT pathway in the temperature-controlled expression of antiviral genes using the JAK1/2 inhibitor Ruxolitinib at 37°C and 39°C. Ruxolitinib completely prevented the temperature-controlled increase in all antiviral genes tested and reduced their basal expression at 37°C (**Figure 3.5. D**). The reduced gene expression upon Ruxolitinib treatment was not only observed for ISGs, but also upstream mediators of the IFN-I pathway, such as *Ddx58* (RIG-I), *Trim25*, and *Irf7*, suggesting that they are also under the control of the JAK-STAT pathway.

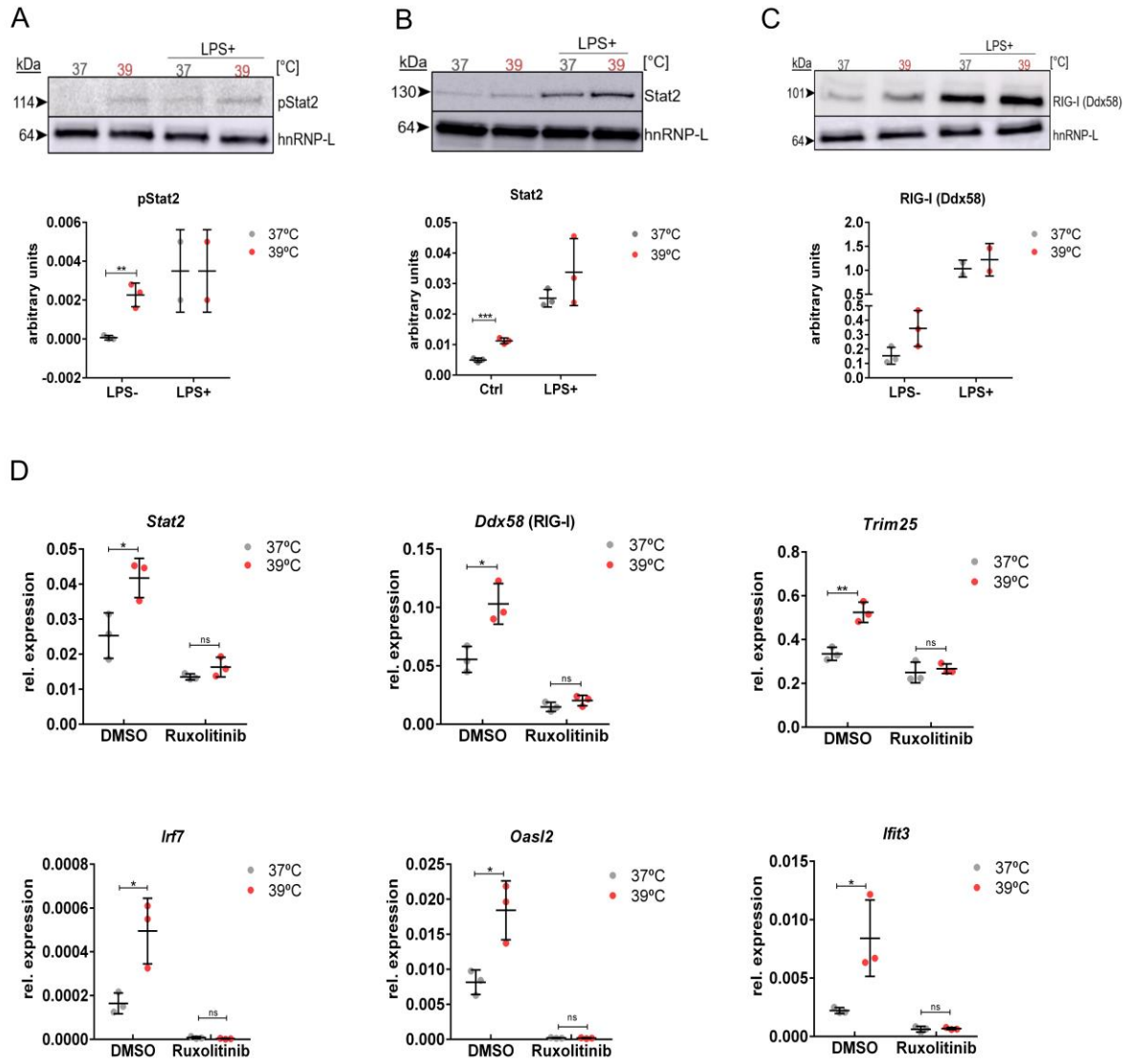

Figure 3.5. JAK-STAT signaling is required for the temperature-controlled increase of antiviral genes.

(A) RAW 264.7 cells were incubated at the indicated temperature for 12 h and phosphorylation of Stat2 was analyzed by Western blot. As positive control cells were incubated for 16h with LPS (2.25 µg/mL) (n=2, mean ± SD). A representative image of a blot and the quantification relative to hnRNP L are shown. **(B)** Western blot as in (A) showing elevated Stat2 protein levels at 39°C. A representative image of a blot and quantification relative to hnRNP L are shown (n=3, mean ± SD). **(C)** Western blot as in (B) showing elevated RIG-I (Ddx58) protein levels at 39°C. A representative image of a blot and quantification relative to hnRNP L is shown. **(D)** Inhibition of the JAK/STAT pathway via Ruxolitinib abolishes temperature-induced increased expression of anti-viral genes and reduces their basal expression. RAW 264.7 cells were incubated at the indicated temperature for 6 h ± Ruxolitinib for 6 h at 37°C, and then at the indicated temperature for 12h. DMSO was used as a control. Gene expression was analyzed using RT-qPCR. C_T values from target genes were normalized to the mean of *Hprt* C_T values. (n = 3, mean ± SD). Statistical significance was determined by unpaired *t*-tests and is indicated by asterisks, * $P < 0.05$; ** $P < 0.01$; *** $P < 0.001$; ns = not significant. Adapted from Los *et al.*, 2022.

3.2. Elevated temperature increases antiviral genes and NO production in macrophages

The INFs and the JAK-STAT pathway are also responsible for inducing the production of nitric oxide (NO), another antiviral defense mechanism. In our RNA-seq data, we found that the nitric oxide synthase 2 (*Nos2*) was upregulated at 38°C when compared to 37°C. This increase was further validated using RT-qPCR (**Figure 3.6. A**). In addition, we observed that the effect of temperature on the expression of *Nos2* was even stronger in RAW 264.7 cells pre-incubated at different temperatures and then treated with LPS (**Figure 3.6. A**). To test if elevated temperatures would lead to more NO production, RAW 264.7 cells were incubated with 1.25 or 2.25 µg/mL of LPS at 37°C or 39°C for 16h to induce endogenous NO formation. We could confirm a significant increase in the number of NO-producing cells and in the amount of produced NO in RAW 264.7 cells incubated at 39°C (**Figure 3.6. B-C**). Furthermore, we addressed the impact of temperature on the expression of antiviral genes and NO production in primary mouse macrophages. For this purpose, we sorted primary mouse macrophages from bone marrow and incubated them at different temperatures for 16h in the presence or absence of LPS. Primary macrophages did not show differential expression of antiviral genes when only incubated at different temperatures (except *Ifit3*). However, a substantial increase in the expression of antiviral genes at a higher temperature was observed in cells stimulated with LPS (**Figure 3.6. D**). This is in line with a previous report suggesting that RAW 264.7 cells are chronically activated (Lee *et al.*, 2012) and points to a model in which temperature and an additional stimulus act together for full activation of the antiviral pathway. Consistent with that, we observed a similar pattern in Jurkat cells. Jurkat cells showed a temperature-controlled expression of antiviral genes only in the activated state (**Figure 3.7.**). This data suggests a general mechanism conserved across cell types and species that uses temperature to prime cells for stronger activation of antiviral-related pathways. Additionally, we could also confirm a small but significant increase in the number of NO-producing cells and in the amount of produced NO in LPS-stimulated primary mouse macrophages incubated at 39°C (**Figure 3.6. E-F**). Altogether these data showed that elevated temperature increases two branches of antiviral immunity, the IFN-I response, and the production of NO.

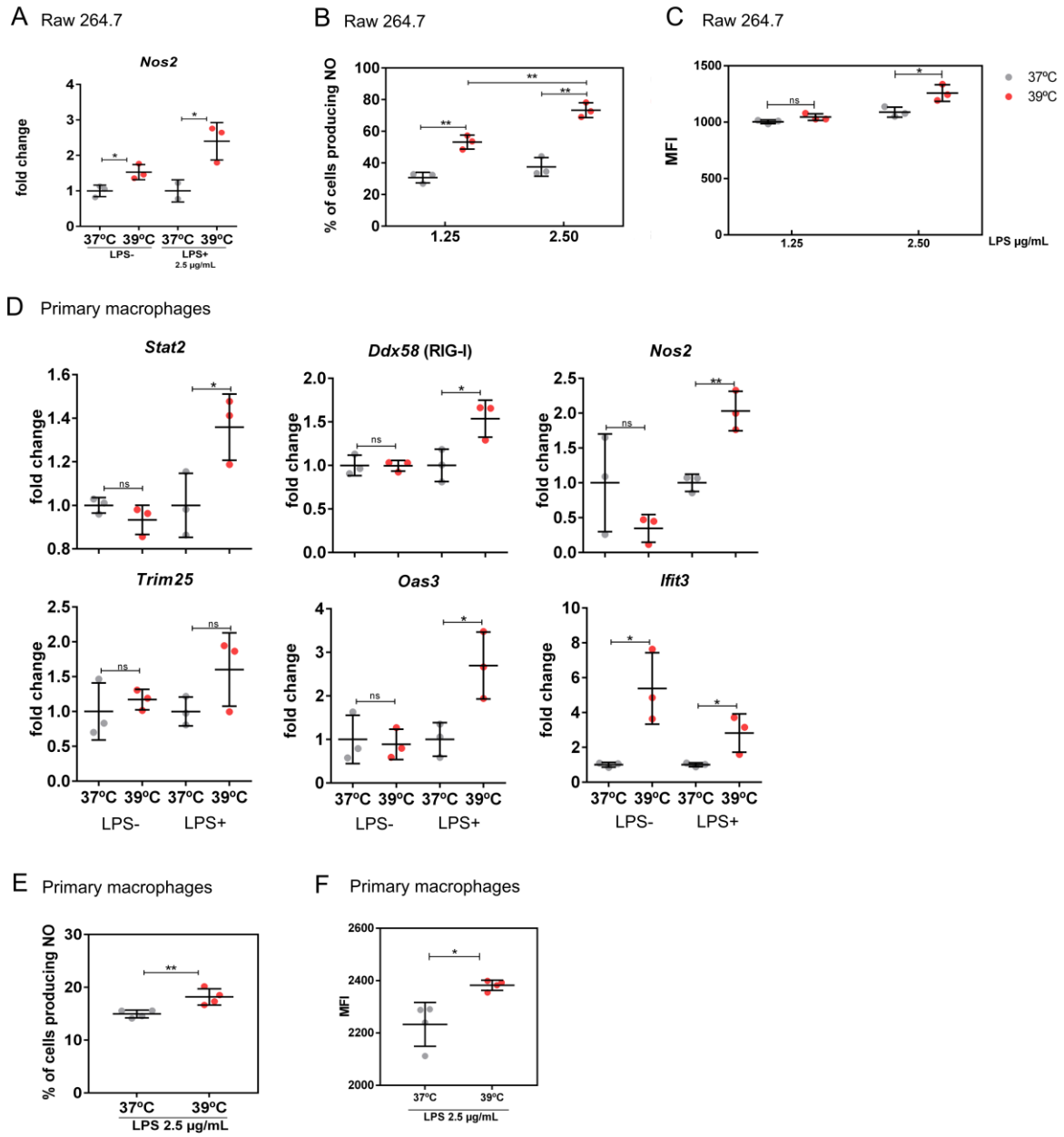

Figure 3.6. Elevated temperature induces NO production and upregulates the expression of antiviral genes in RAW 264.7 cells and primary mouse macrophages.
(A) Nitric Oxide Synthase 2 (*Nos2*) expression is upregulated at 39°C in RAW 264.7 cells. Gene expression was analyzed using RT-qPCR. mRNAs are normalized to 37°C of the respective treatment (n = 3, mean ± SD). RAW 264.7 cells were incubated at the indicated temperature for 12h ± LPS. **(B)** RAW 264.7 cells were incubated with 1.25 or 2.25 µg/mL of LPS at 37°C or 39°C for 16 h to induce endogenous NO formation. NO producing cells were detected by flow cytometry. Graphics are showing the percentage of NO-producing cells (n = 3, mean ± SD). **(C)** Quantitation of mean fluorescence intensity of NO production from (B). **(D)** Antiviral gene expression in primary mouse macrophages. Primary mouse macrophages were incubated at the indicated temperatures for 16 h ± LPS (0.1 µg/mL). Gene expression was analyzed using RT-qPCR. mRNAs are normalized to 37°C of the respective treatment (n = 3, mean ± SD). **(E)** NO production in primary mouse macrophages was analyzed as in (B) (n = 3, mean ± SD). **(F)** Mean fluorescence intensity of NO production from (D).

Statistical significance was determined by unpaired t-tests and is indicated by asterisks, * $P < 0.05$; ** $P < 0.01$; *** $P < 0.001$; ns = not significant. Adapted from Los *et al.*, 2022.

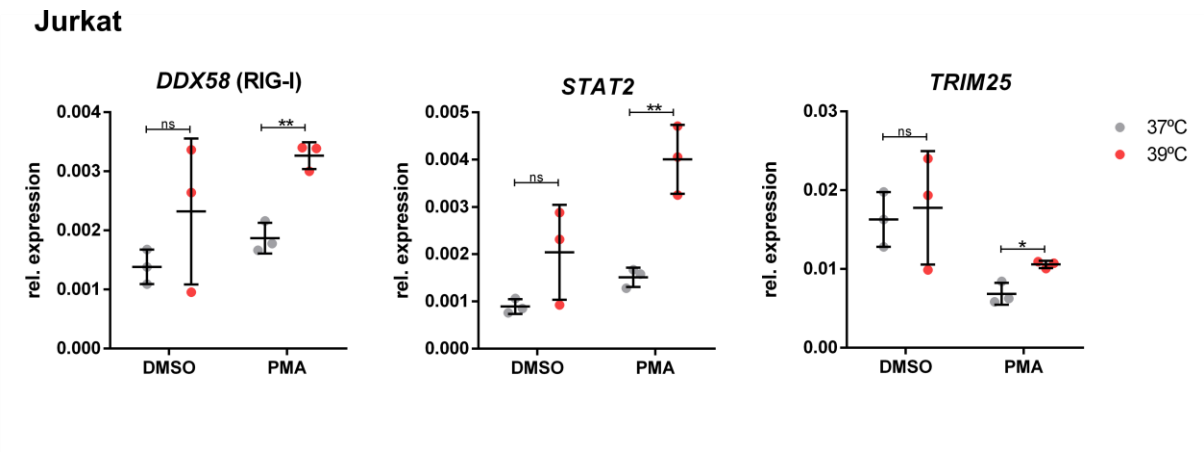

Figure 3.7. Upregulation of antiviral genes in Jurkat cells at warmer temperatures.
Jurkat cells were incubated at the indicated temperatures for 12h, then ± PMA (1 ng/mL) for 16h. DMSO was used as a control. Gene expression was analyzed using RT-qPCR. C_T values from target genes were normalized to the mean of GAPDH C_T values (n = 3, mean ± SD). Adapted from Los et al., 2022.

3.3. Mechanistic basis for increased expression of antiviral genes at higher temperature

To start addressing the mechanistic basis for increased expression of antiviral genes at elevated temperatures, we investigated the kinetics of gene expression. We observed a significant increase in the expression of antiviral genes only after 12 h at 39°C (**Figure 3.8. A**). We then tested if and how fast the increased expression at elevated temperatures was reversible. When cells were switched back from 39°C to 37°C, the expression of antiviral genes gradually decreased and reached their basal level after around 12 h (**Figure 3.8. B**). Each target gene showed slightly different kinetics, which probably reflects differences in mRNA turnover. These data showed that antiviral genes have a delayed response to elevated temperature, which is reversible upon restoration of lower temperature. Furthermore, we investigated changes in mRNA stability and *de novo* transcription as mechanisms that could be responsible for the temperature-controlled change in antiviral gene expression. To determine the mRNA stability of antiviral genes, we treated RAW 264.7 cells at 37°C and 39°C with ActD and quantified the remaining mRNA after 2h and 4h. We did not observe altered mRNA stability when comparing cells at 37°C and 39°C, suggesting that regulated mRNA stability is not the cause of temperature-controlled expression of antiviral genes (**Figure 3.8. C**). As an approximation of *de novo* transcription, we analyzed

the expression of antiviral genes in chromatin-associated, intron-containing RNA. Our results showed a trend toward increased expression after 8 h and 12 h at 39°C, resembling the kinetics of accumulation of the respective mRNAs (**Figure 3.8. D**), suggesting that increased expression of antiviral genes at elevated temperature is mediated, at least partially, through increased *de novo* transcription.

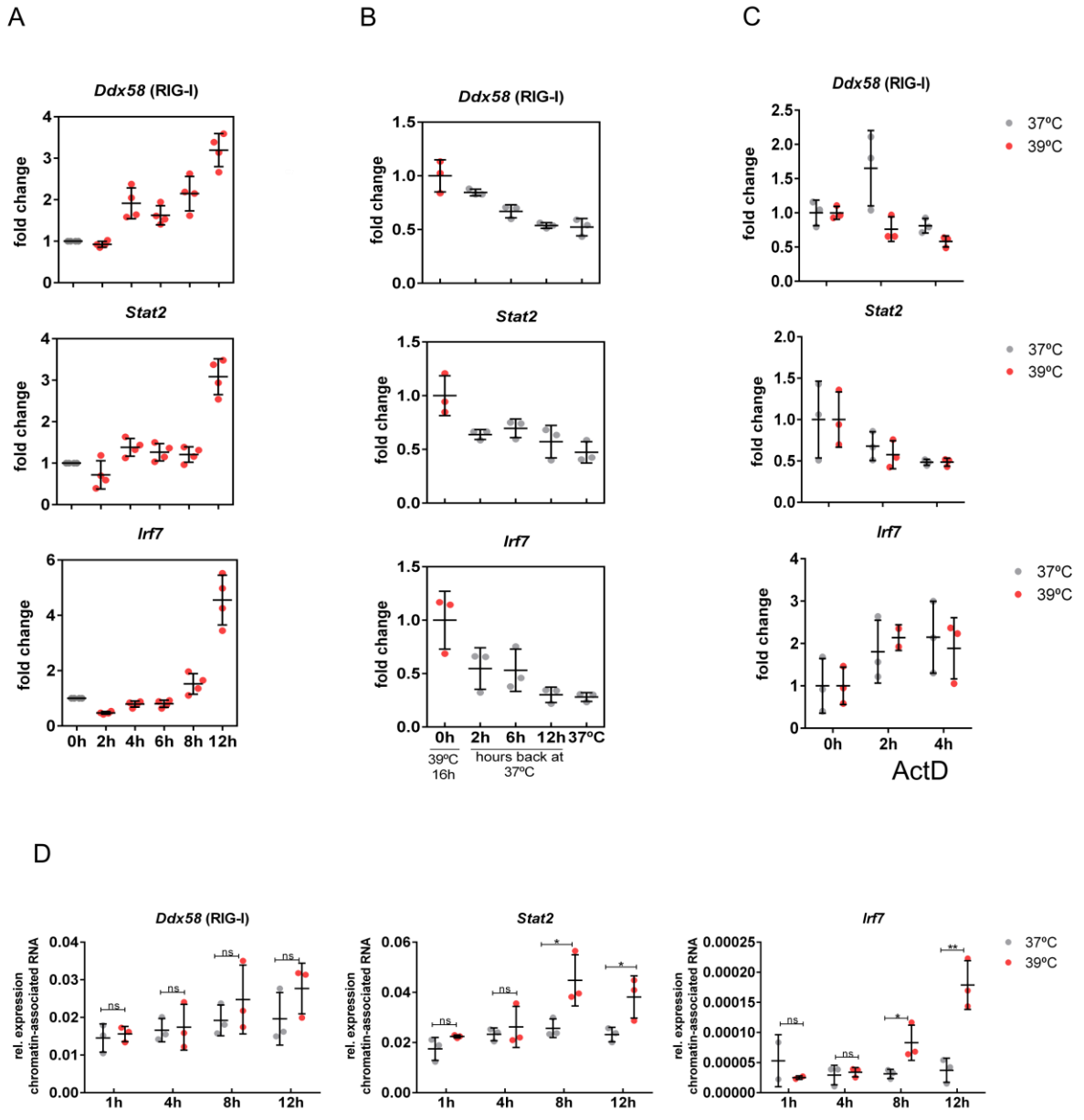

Figure 3.8. Mechanisms regulating the expression of antiviral genes at elevated temperatures.

(A) Time course gene expression analysis in RAW 264.7 cells. RAW 264.7 cells were incubated at 39°C for the indicated time. Gene expression was analyzed using RT-qPCR. mRNAs are normalized to 37°C (n = 4, mean ± SD). **(B)** The temperature-induced increase in antiviral gene expression is reversible. RAW 264.7 cells were incubated at 39°C for 16h, then shift to 37°C for the indicated time.

Gene expression was analyzed using RT-qPCR. mRNAs are normalized to 39°C (n = 3, mean ± SD). **(C)** RNA stability of antiviral genes. RAW 264.7 cells were incubated at the indicated temperature for 12 h, then treated with ActD for 2 h and 4 h. mRNAs are normalized to t=0 of the respective temperature (n = 4, mean ± SD). **(D)** *De novo* transcription of antiviral genes at elevated temperatures. RAW 264.7 cells were incubated at 37°C or 39°C for the indicated time. Chromatin-associated RNA was purified and analyzed by RT-qPCR. This experiment was performed with the forward primer binding to an intronic region (except for *Irf7*, whereas the forward primer binds in an exonic region). C_T values from target genes were normalized to the mean of *Hprt* C_T values (n = 3, mean ± SD). Statistical significance was determined by unpaired t-tests and is indicated by asterisks **P* < 0.05, ***P* < 0.01, ns = not significant. The experiments in A and C were performed by Sandra Keiper. Adapted from Los *et al.*, 2022.

3.4. Temperature-controlled *Stat2* alternative splicing

To have a closer look into the mechanism behind the increased expression of antiviral genes at a higher temperature, we look for differences in AS of members of the JAK/STAT pathway, as we saw that this pathway was responsible for regulating the temperature-dependent expression of the antiviral genes. We identified in our RNA-seq data a non-annotated temperature-dependent alternative 5' splice site in *Stat2* exon 11. Usage of the alternative 5' splice site was higher at lower temperatures (34°C and 37°C) and leads to a frameshift and the inclusion of a PTC, which usually prevents the formation of a functional protein and leads to degradation by NMD (**Figure 3.9. A**). NMD, and other mRNA surveillance pathways, including no-go decay and non-stop decay, are coupled to translation (Shoemaker and Green, 2012). We then treated cells with CHX, a translation elongation inhibitor, and performed Radioactive Splicing PCR and RT-qPCR. CHX treatment leads to the stabilization of NMD-targeted mRNAs (Hurt, Robertson and Burge, 2013). Consistently, we observed an increase in the abundance of the PTC-containing isoform and total *Stat2* mRNA in the CHX-treated cells (**Figure 3.9. B-C**). This shows that alternative splicing coupled to NMD is the main mechanism regulating temperature-dependent *Stat2* expression. Consistently, we found that the PTC-containing isoform and total *Stat2* mRNA levels were increased in mouse hepatocytes treated with CHX in a temperature-dependent manner (**Figure 3.10. A-B**). Additionally, *Stat2* mRNA levels were increased at higher temperatures in MEFs (**Figure 3.10. C**), thus validating our findings in two independent RNA-seq datasets. Furthermore, we identified several NMD-inducing *STAT2* splicing isoforms and temperature-controlled *STAT2* expression in HeLa cells (**Figure 3.10. D-E**). These data suggest that the temperature-controlled alternative splicing coupled to NMD in *STAT2* is conserved across species. Previous work from our lab showed that CLKs act as thermo-sensors translating changes in the core body temperature range into changes in alternative splicing and gene expression (Preußner *et al.*, 2017; Haltenhof *et al.*, 2020).

Here, we observed that the expression of antiviral genes, including *Stat2*, is higher in the presence of the CLK inhibitor (TG003) at 37°C. The observed increase in the presence of TG003 is similar to the increase in expression in DMSO samples at 39°C (**Figure 3.11.**), which is consistent with the fact that CLKs are less active at higher temperatures and that inhibition of CLKs at 37°C mimics the effect of warmer temperature (Haltenhof *et al.*, 2020). However, as the expression of antiviral genes in TG003-treated cells is further increased at 39°C, additional mechanisms are probably involved in this regulation.

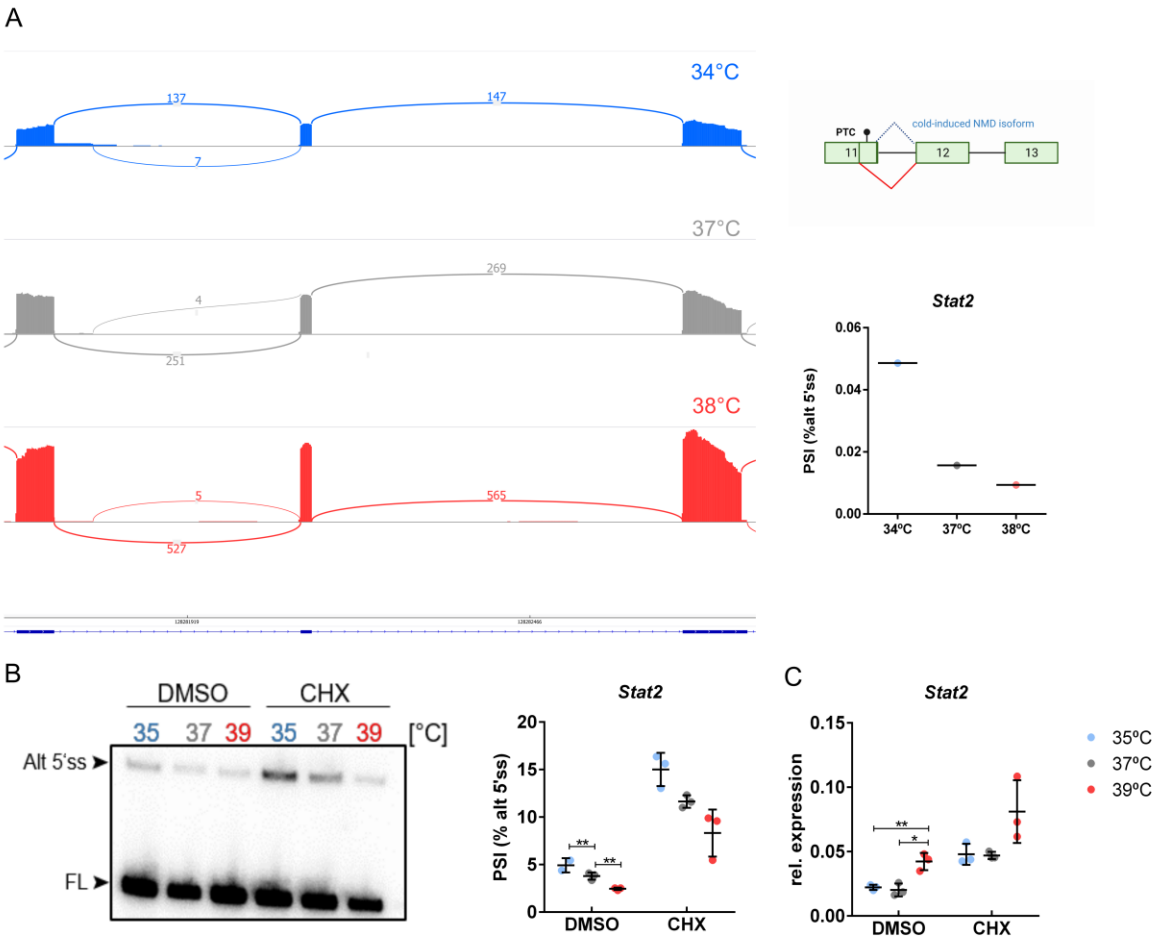

Figure 3.9. *Stat2* alternative splicing coupled to NMD in RAW 264.7 cells.
(A) Sashimi plot showing an alternative NMD-inducing 5' splice site in *Stat2* exon 11 in RAW264.7 cells (left). The usage of the alternative 5' splice site is more frequent at 34°C and is reduced at 38°C. Reads from the sashimi plot are quantified (right, bottom). Schematic representation of the NMD-inducing 5' splice site in *Stat2* exon 11 (right, top). Created with BioRender.com. **(B)** Representative image of a denaturing urea-PAGE gel showing the alternative NMD-inducing 5' splice site in *Stat2* (left). FL = full length. Alt 5'ss = alternative 5' splice site. Quantification of the radioactive splice-sensitive PCR shown in percent spliced in (PSI) (right, n = 3, mean ± SD). RAW 264.7 cells were incubated at the indicated temperature for 8h, then treated with ± CHX for 4 h. DMSO was used as a control. **(C)** *Stat2* mRNA expression analysis by RT-qPCR. Samples as in (B) were used. C_T values of *Stat2* were normalized to the mean of *Hprt* C_T values (n = 3, mean ± SD). Statistical significance was

determined by unpaired t-tests and is indicated by asterisks *$p < 0.05$, **$p < 0.01$, ns = not significant. Adapted from Los *et al.*, 2022.

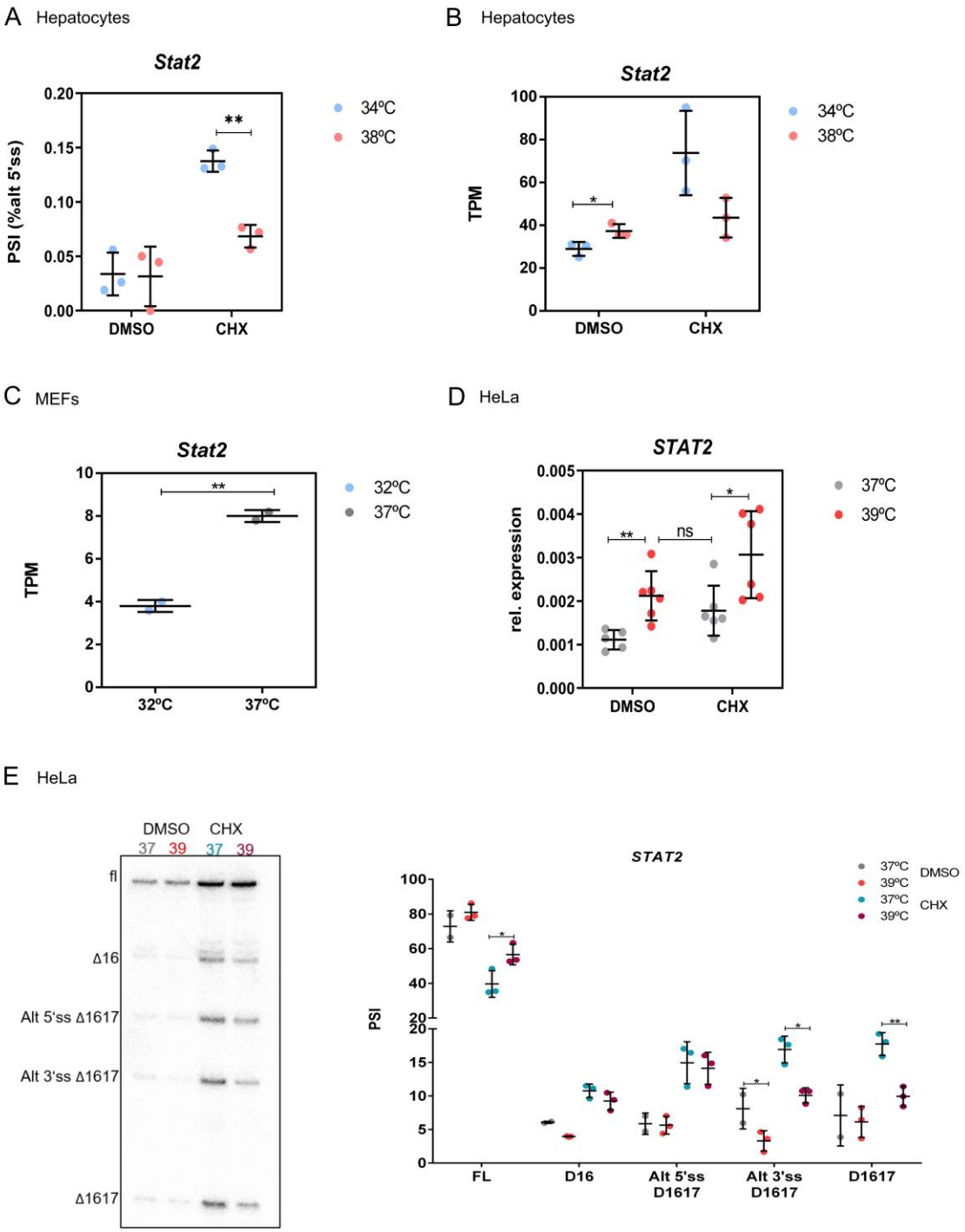

Figure 3.10. *Stat2* alternative splicing coupled to NMD in different cell lines.
(A) PSI values of the alternative NMD-inducing 5' splice site in *Stat2* exon 11 in primary mouse hepatocytes treated with CHX. Data were retrieved from (Neumann *et al.*, 2020). **(B)** *Stat2* mRNA levels in transcript per million (TPM) in primary mouse hepatocytes treated with CHX. DMSO was used as a control. Data was retrieved from (Neumann *et al.*, 2020). **(C)** *Stat2* mRNA in TPM in mouse

embryonic fibroblasts (MEFs). Data was retrieved from (Liu *et al.*, 2013). **(D)** *STAT2* mRNA levels in HeLa cells. HeLa cells were incubated at the indicated temperature for 8h, then treated with ± CHX for 4h. DMSO was used as a control. Gene expression was analyzed by RT-qPCR. C_T values of *STAT2* were normalized to the mean of *GAPDH* C_T values (n = 6, mean ± SD). **(E)** Representative image of a denaturing urea-PAGE gel showing alternative NMD-inducing *STAT2* isoforms in HeLa cells (left). fl = full length, Δ16 = exclusion of exon 16, Alt 5'ss Δ16,17 = alternative 5' splice site leading to the exclusion of exons 16 and 17, Alt 3'ss Δ16,17 = alternative 3' splice site leading to the exclusion of exons 16 and 17, Δ16,17 = exclusion of exons 16 and 17. Quantification of the radioactive splice-sensitive PCR shown in percent spliced in (PSI) (right, n = 3, mean ± SD; for DMSO 37°C, n = 2). Samples as in (D) were used. Statistical significance was determined by unpaired t-tests and is indicated by asterisks *p < 0.05, **p < 0.01. Adapted from Los *et al.*, 2022.

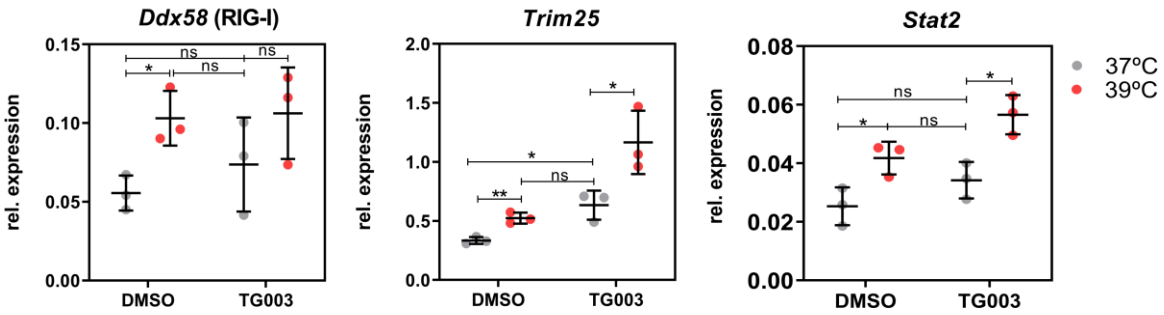

Figure 3.11. Effect of CLK inhibition on the expression of antiviral genes.
RAW 264.7 cells were incubated ± TG003 (CLK inhibitor) for 6 h at 37°C, then for 12h at the indicated temperature. DMSO was used as a control. Gene expression was analyzed by RT-qPCR. C_T values of target genes were normalized to the mean of *Hprt* C_T values (n = 3, mean ± SD). Statistical significance was determined by unpaired t-tests and is indicated by asterisks, *p<0.05, **p<0.01, ns = not significant. Adapted from Los *et al.*, 2022.

3.5. Temperature-controlled *Stat2* pre-mRNA processing can induce transcription of antiviral genes

To validate the influence of the alternative 5' splice site of exon 11 in *Stat2* on the expression of antiviral genes, we used antisense oligonucleotides (ASO) that allow direct manipulation of *Stat2* AS by blocking the usage of the alternative 5' splice site. For this experiment, we used 3T3 and N2a cells, which showed a reasonable transfection efficiency with the ASOs. Cells transfected with two different ASOs, targeting the alternative NMD-inducing 5' splice site, showed a significant reduction in the usage of this splice site (**Figure 3.12. A-B**). RT-qPCR analysis showed an increased expression of *Stat2* and other ISGs in the ASO-treated cells (**Figure 3.12. C-D**). Similarly to RAW 264.7 cells, 3T3 cells showed increased expression of antiviral genes at 39°C when compared to 37°C (**Figure 3.13.**) and a corresponding decreased usage of the alternative 5' splice site at 39°C (**Figure 3.12. A**). To

independently validate the observed effect, we generated a CRISPR/Cas9-edited N2a cell line lacking the alternative NMD-inducing 5' splice site. Either homozygous or heterozygous removal of the respective target sequence was confirmed by radioactive RT-PCR at the RNA level (**Figure 3.14. A**). As expected, we observed higher *Stat2* expression in the homozygous cell line when compared with a non-edited control and a small but significant increase in the heterozygous cell line (**Figure 3.14. B**). We then addressed the impact of the depletion of the alternative 5' splice site on the expression of other antiviral genes. The expression of *Ddx58* was significantly increased in both cell lines and the expression of *Oasl2* and *Ifit3* was significantly increased in the homozygous cell line, compared to the non-edited control (**Figure 3.14. B**). In conclusion, these data show that alternative splicing coupled to NMD regulates temperature dependent *Stat2* expression and can induce the transcription of antiviral genes. Furthermore, we addressed whether SR proteins would be responsible for regulating the usage of the alternative NMD-inducing 5' splice site. N2a cells were transfected with siRNAs against Srsf1 to Srsf12 (**Figure 3.15. A**). We observed a potential decrease in the usage of the alternative 5' splice site in cells transfected with siSrsf1 and an increase in the usage of the alternative 5' splice site in cells transfected with siSrsf7. To independently confirm this, N2a cells were transfected with siRNAs against Srsf1 and Srsf7 (**Figure 3.15. B**). Srsf1 knockdown significantly decreased the usage of the alternative 5' splice site, while Srsf7 knockdown did not further increase the usage of this splice site (**Figure 3.15. C**). Additionally, gene expression analysis showed that the expression of *Stat2*, *Trim25*, and *Oasl2* was increased upon Srsf1 knockdown supporting our previous findings (**Figure 3.15. D**). Together, this data indicates that Srsf1 is responsible for regulating the usage of the alternative NMD-inducing 5' splice site in *Stat2*.

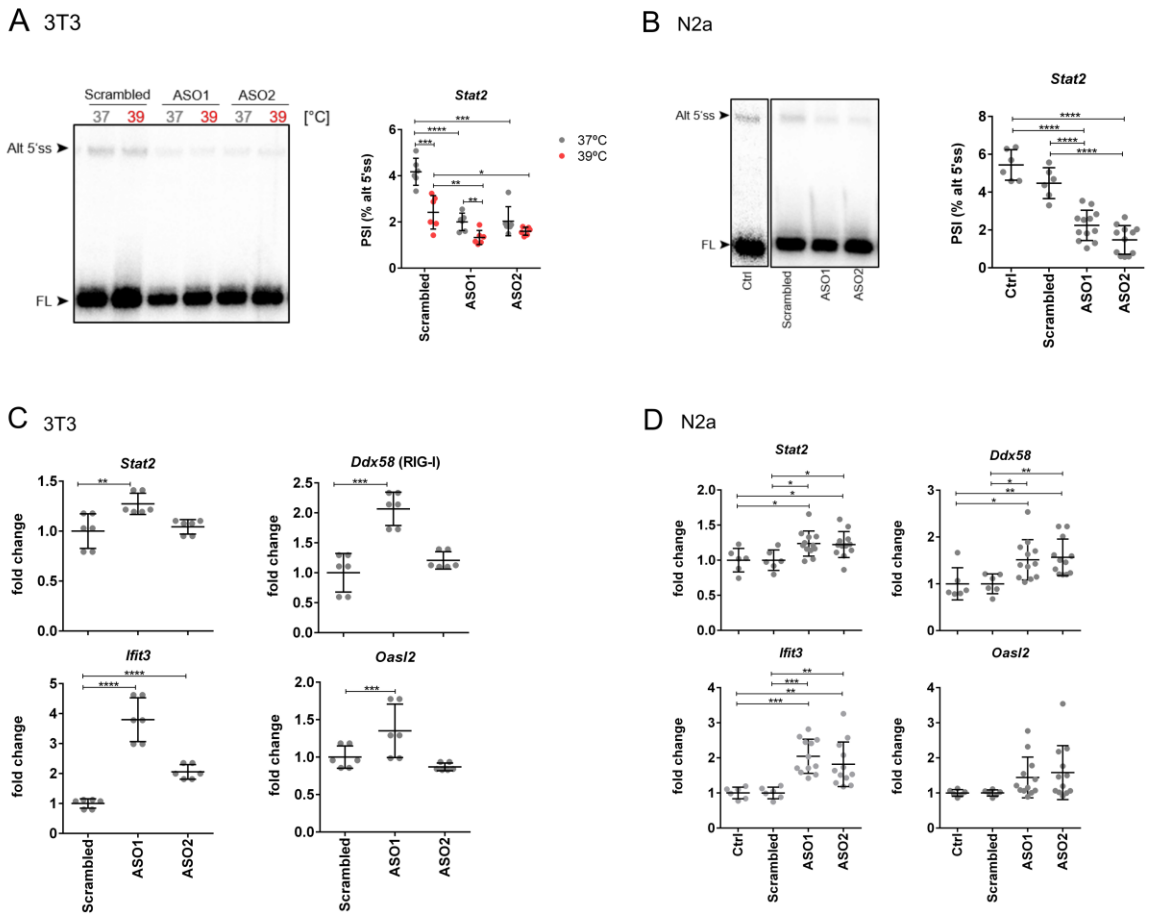

Figure 3.12. Reduced usage of the alternative 5' splice site of exon 11 in *Stat2* increases the expression of antiviral genes.
(A) 3T3 cells were transfected with two different ASOs targeting the alternative 5' splice site in *Stat2* exon 11. 32h post-transfection, cells were incubated for 16h at 37°C or 39°C. A scrambled ASO was used as a control. Representative image of a denaturing urea-PAGE gel showing the alternative NMD-inducing 5' splice site in *Stat2* (left). FL = full length. Alt 5'ss = alternative 5' splice site. Quantification of the radioactive splice-sensitive PCR shown in percent spliced in (PSI) (right, n = 6, mean ± SD). **(B)** N2a cells were transfected with two different ASOs targeting the alternative 5' splice site in Stat2 exon 11. 48h post-transfection, cells were harvested, and RNA was isolated. Empty transfection (Ctrl) and a scrambled ASO were used as control. Representative image of a denaturing urea-PAGE gel showing the alternative NMD-inducing 5' splice site in *Stat2* (left). Quantification of the radioactive splice-sensitive PCR shown in percent spliced in (PSI) (right, mean ± SD; ctrl and scrambled ASO = 6; ASOs = 12). **(C)** Gene expression analysis of antiviral genes by RT-qPCR upon ASO treatment in 3T3 cells. mRNAs are normalized to scrambled ASO at 37°C (n = 6, mean ± SD). **(D)** Same as in (C) for N2a cells (mean ± SD; ctrl and scrambled ASO = 6; ASOs = 12). Adapted from Los *et al.*, 2022.

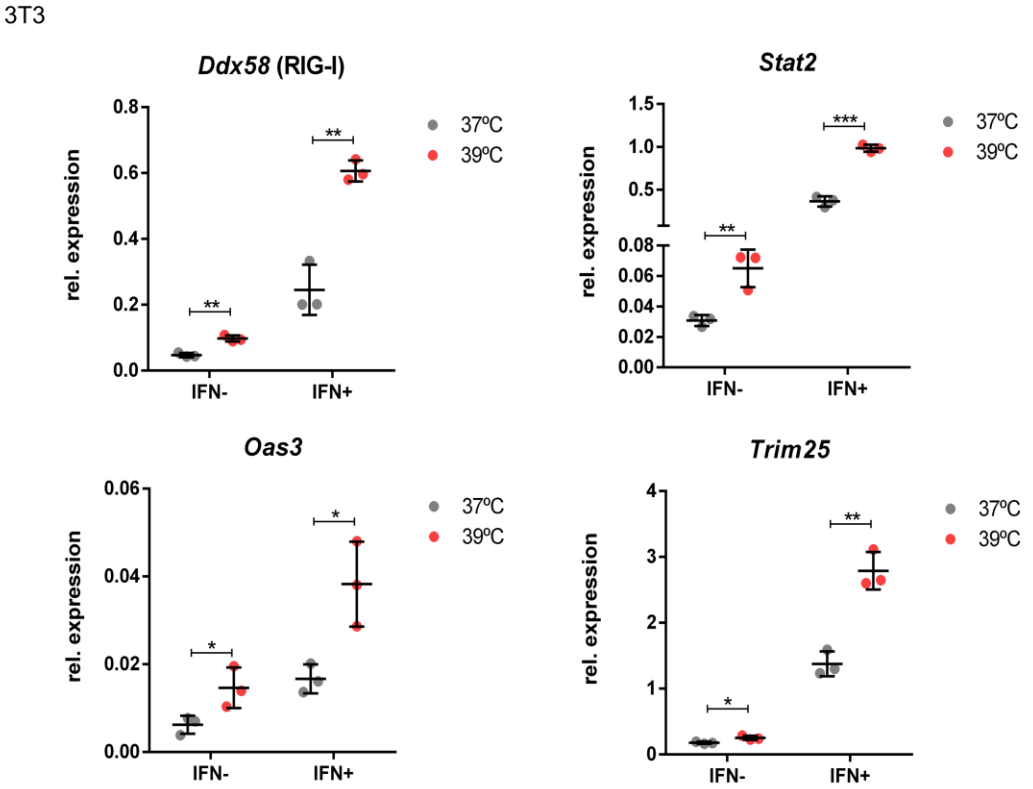

Figure 3.13. Expression of antiviral genes in 3T3 cells.
3T3 cells were incubated for 12 h at the indicated temperatures, then ± IFN (100U/mL). Gene expression was analyzed using RT-qPCR. C_T values from target genes were normalized to the mean of *Hprt* C_T values. (n = 3, mean ± SD). Statistical significance was determined by unpaired t-tests and is indicated by asterisks, *p<0.05; **p<0.01; ***p<0.001. Adapted from Los *et al.*, 2022.

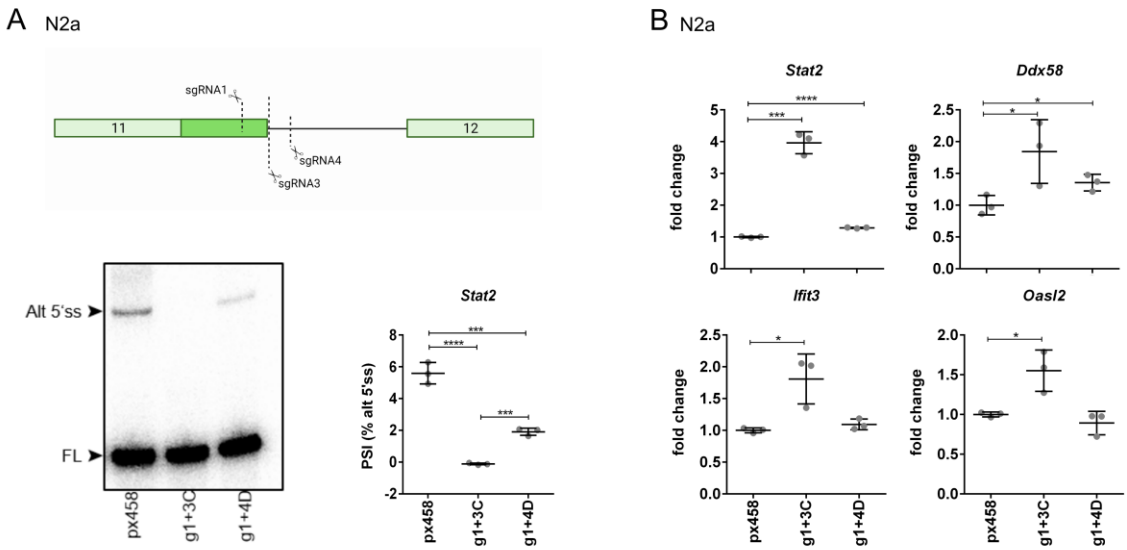

Figure 3.14. Deletion of the alternative 5' splice site of exon 11 in *Stat2* increases the expression of antiviral genes.

(A) Depletion of the alternative 5' splice site of exon 11 using CRISPR/Cas9 in N2a cells (top: position of the sgRNAs. Created with BioRender.com), below a representative image of a denaturing urea-PAGE gel showing *Stat2* isoforms in a homozygous clone (g1+3C) and a heterozygous clone (g1+4D). Quantification of the radioactive splice-sensitive PCR shown in percent spliced in (PSI) (right, n = 3, mean ± SD). **(B)** Increased expression of *Stat2* and other antiviral genes in cells lacking the alternative 5' splice site. Gene expression was investigated by RT-qPCR. mRNAs are normalized to px458 as non-edited control (n = 3, mean ± SD). Statistical significance was determined by unpaired t-tests and is indicated by asterisks, **P* < 0.05; ** *P* < 0.01; *** *P* < 0.001; **** *P* < 0.0001. Adapted from Los *et al.*, 2022.

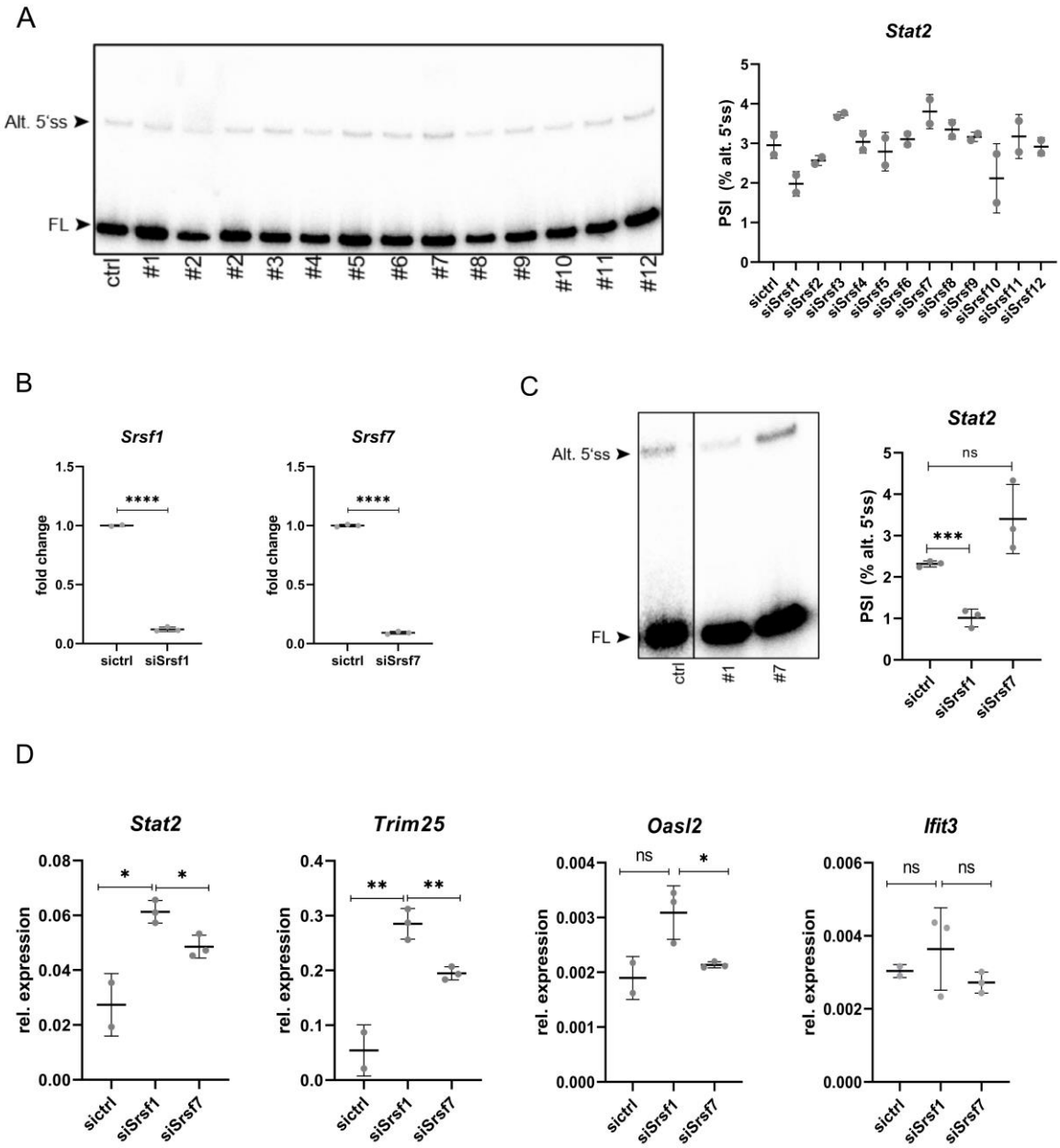

Figure 3.15. Srsf1 regulates the usage of the alternative 5' splice site of exon 11 in *Stat2*.

(A) SR proteins knockdown in N2a cells. N2a cells were transfected with siRNA against SR proteins. 48h post-transfection, cells were harvested and RNA was isolated. Representative image of a denaturing urea-PAGE gel showing *Stat2* isoforms in transfected N2A cells (left). Quantification of the radioactive splice-sensitive PCR shown in percent spliced in (PSI) (right, n = 2, mean ± SD). Ctrl = siAllstar; #1 = siSrsf1; #2 = siSrsf2; #3 = siSrsf3; #4 = siSrsf4; #5 = siSrsf5; #6 = siSrsf6; #7 = siSrsf7; #8 = siSrsf8; #9 = siSrsf9; #10 = siSrsf10; #11 = siSrsf11; #12 = siSrsf12. The RNA samples from N2a cells transfected with the different siRNAs were provided by Marco Preußner. **(B)** N2a cells transfected with siSrsf1 and siSrsf7. siAllstar was used as a control. Gene expression analysis was performed by RT-qPCR (right, n = 3, mean ± SD). **(C)** Samples as in B were used for radioactive splicing RT-PCR. Representative image of a denaturing urea-PAGE gel showing *Stat2* isoforms in transfected N2A cells (left). Quantification of the radioactive splice-sensitive RT-PCR shown in percent spliced in (PSI) (right, n = 3, mean ± SD). **(D)** Increased expression of *Stat2* and other antiviral genes in Srsf1 knockdown samples. Gene expression was investigated by RT-qPCR. C_T values of target genes were normalized to the mean of *Hprt* C_T values (n = 3, mean ± SD). Statistical significance was determined by unpaired t-tests and is indicated by asterisks, **P* < 0.05; ***P* < 0.01; ****P* < 0.001; *****P* < 0.0001.

3.6. SARS-CoV-2 infection is less efficient at higher temperatures in cell culture

To investigate the impact of temperature-controlled antiviral immunity during virus infection, we used SARS-CoV-2 as a model system. We first analyzed published data that identified 65 cellular factors that restrict SARS-CoV-2 infection (Martin-Sancho *et al.*, 2021). Nine of these factors showed a significant (P^{adj} < 0.001) and higher (log2FC > 0.8) expression at 38°C when compared to 37°C in our RNA-seq data (**Figure 3.16. A**), while no SARS-CoV-2 restriction factor showed higher expression at lower temperature (37°C). This result suggests that increasing the temperature from 37°C to 38°C creates a condition that limits SARS-CoV-2 infection. This could be especially relevant during aging, as children have a higher body temperature than adults and older individuals. This correlates with higher susceptibility for severe SARS-CoV-2 infections in seniors (with reduced body temperature) than is observed for children (with higher body temperature) (Garg *et al.*, 2020; O'Driscoll *et al.*, 2021; Sun *et al.*, 2021). To connect the expression of antiviral genes with aging we used a single-cell RNA-seq dataset from different mouse tissues sequenced at one month and 30 months of age, corresponding to early childhood and 100 years of age in humans (Almanzar *et al.*, 2020). We then analyzed the expression of antiviral genes in all tissues and cell types available in the dataset. In line with our hypothesis, several antiviral genes that are warm-induced in our RNA-seq data showed increased expression in younger animals (**Figure 3.16. B**). Although we could only observe a slight increase in the expression of the target genes, we hypothesize that the combined effect of these small changes in the same pathway can influence the antiviral immunity response. Notably, two known cold-induced genes: *Rbm3* and the cold-induced RNA binding protein (*Cirbp*) showed higher expression in

older animals (**Figure 3.16. B**), indicating reduced body temperature. To confirm the impact of temperature on SARS-CoV-2 infection, Calu-3, and Caco-2 cells were used. Cells were pre-incubated at 37°C or 39°C for 16h, as this was the timeframe required to induce antiviral genes, then infected with SARS-CoV-2 and incubation was continued at 37°C for 24h and 48h. Calu-3 and Caco-2 cells showed increased expression of *STAT2* and *DDX58* after 16h pre-incubation at 39°C when compared with 37°C (**Figure 3.17. A-B**). Further stimulation with IFN-I increased the expression of other antiviral genes, such as *OAS1* and *TRIM25* at 39°C (**Figure 3.17. A-B**). These data support the idea that an increase in *STAT2* expression can induce the antiviral cascade and lead to a primed state, which can then be triggered by an additional stimulus for full activation. We then determined the viral titer 24h and 48h post-infection. Higher viral loads were observed in cells that were incubated the whole time at 37°C when compared with the cells that were pre-incubated at 39°C (**Figure 3.17. C-D**). This experiment confirms that a slightly increased temperature before infection can slightly but significantly limit viral replication and suggests that body temperature at the time point of infection can determine how well the body can handle a viral infection.

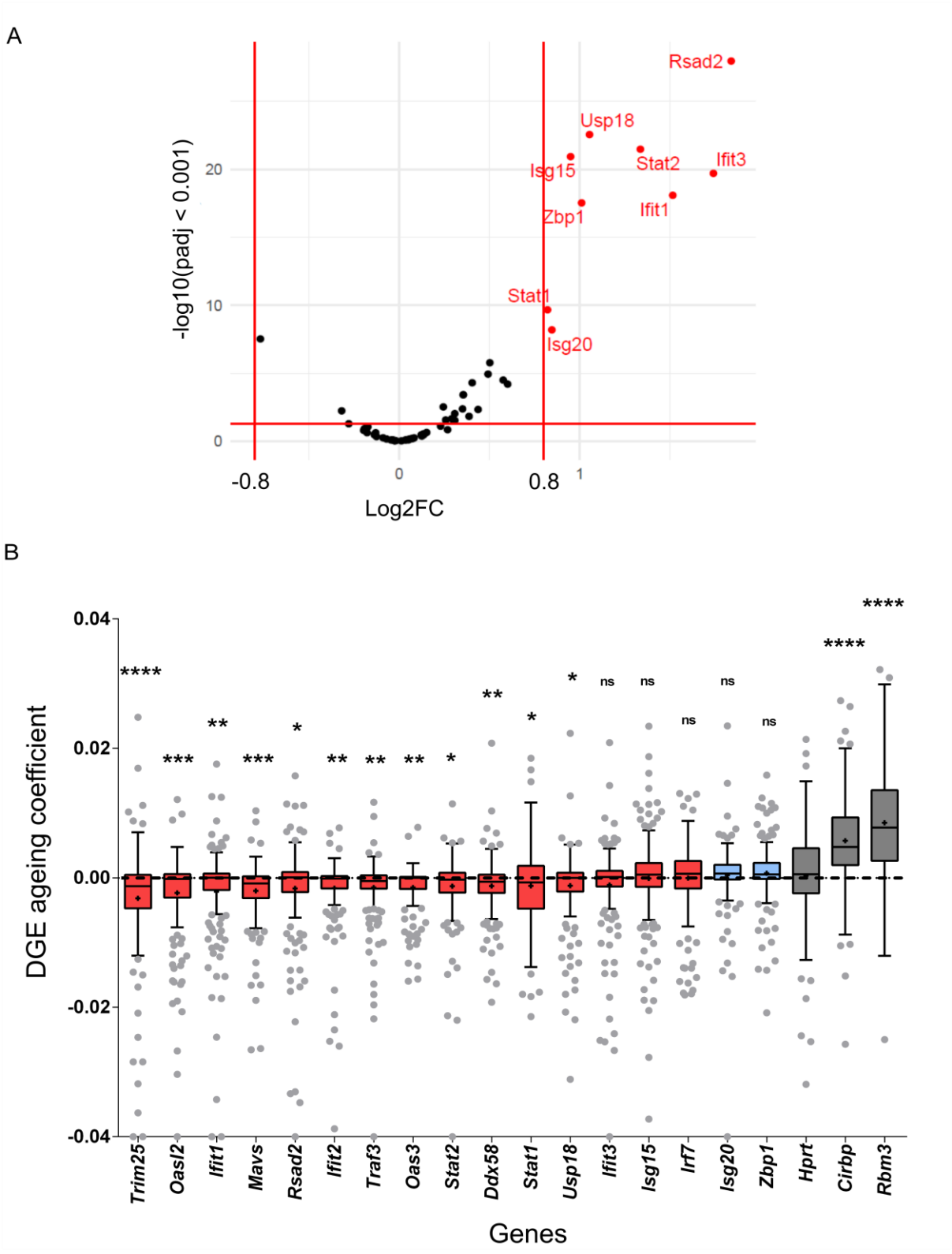

Figure 3.16. Gene expression analysis of SARS-CoV-2 restriction factors at different temperatures.

(A) The expression of 65 SARS-CoV-2 restriction factors from (Martin-Sancho *et al.*, 2021) was analyzed in our RNA-Seq data from RAW 264.7 cells and compared between 37°C and 38°C. In the volcano plot, log2FC was plotted against P^{adj} < 0.001, fold changes were considered significant if log2FC > 0.8 (or < -0.8). Genes up-regulated at 38ºC are shown in red. **(B)** Warm-induced antiviral

genes and SARS-CoV-2 restriction factors show decreased expression with increasing age. Differential gene expression (DGE) data for the stated genes in 24 tissues (193 cell types) from one-month and 30-month-old mice are compared. Indicated is the 'aging coefficient' as defined by (Almanzar *et al.*, 2020). The ageing coefficient is shown for all analyzed tissues. The box plot shows the interquartile range (IQR) divided by the median, and Tukey-style whiskers extend to a maximum of 1.5 × IQR beyond the box, mean values are indicated by (+). Values were sorted by the mean (red = negative mean values, corresponding to reduced expression in old individuals, blue = positive mean values). The cold-induced RNA binding proteins *Rbm3* and *Cirbp* serve as control; their increased expression in old individuals indicates reduced body temperature with aging. Each gene was compared to *Hprt* DGE and statistical significance was determined by unpaired *t*-tests and is indicated by asterisks, *P <0.05; ** P < 0.01; ***P < 0.001; **** P < 0.0001; ns = not significant. Adapted from Los *et al.*, 2022.

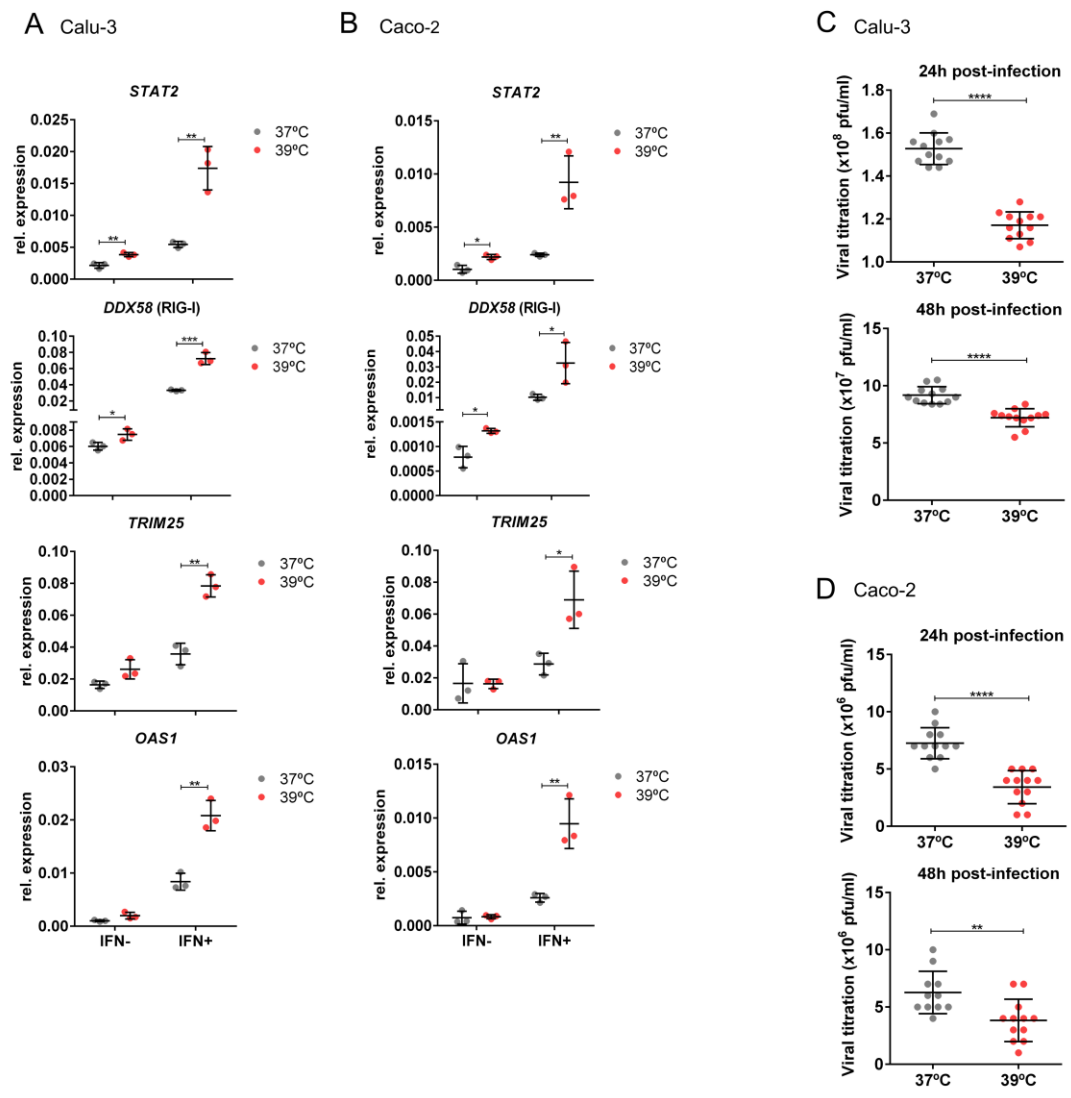

Figure 3.17. SARS-CoV-2 replication is reduced by pre-incubation at warmer temperatures in cell culture.

(A) Calu-3 cells show increased expression of antiviral genes at 39°C. Cells were incubated at the indicated temperature for 12h, then for 4h ± IFN (100U/mL). RNA was isolated and analyzed by RT-qPCR. C_T values of target genes were normalized to the mean of *GAPDH* C_T values (n = 3, mean ± SD). **(B)** Same as in (A) for Caco-2 cells. **(C)** Pre-incubation at 39°C for 16h reduced viral replication. Calu-3 cells were pre-incubated at 37°C or 39°C for 16h and then infected with SARS-CoV-2, following incubation at 37°C for 24h and 48h. The viral titer as determined by plaque assay is reduced in cells that were pre-incubated at 39°C (n = 12, mean ± SD). **(D)** Same as in (C) for Caco-2 cells. Statistical significance was determined by unpaired *t*-tests and is indicated by asterisks, **P* < 0.05; ***P* < 0.01; ****P* < 0.001; *****P* < 0.0001. Experiments C and D were performed by Jakob Trimpert, Kathrin Eschke, Ricardo Martin Vidal, Azza Abdelgawad from the Institute of Virology - Freie Universität Berlin. Adapted from Los *et al.*, 2022.

4. DISCUSSION

In the present study, we addressed the impact of the variation in the healthy human core body temperature in controlling antiviral gene expression and described a mechanism responsible for triggering these changes.

Previous studies have demonstrated that hyperthermia together with inflammatory stimuli enhances the production of pyrogenic cytokines (*e.g.* IL-6 and TNF) (Jiang *et al.*, 1999; Lee *et al.*, 2012). Extracellular HSP70 and other HSPs were also shown to be responsible for releasing NO, IL-1β, IL-6, and IL-12 (Evans, Repasky and Fisher, 2015). Hence suggesting that hyperthermia confers a survival advantage for the host following infection. However, thermally sensitive mechanisms by which physiological temperature changes regulate cellular functions are still not fully understood.

Here, we showed that the expression of antiviral genes is increased when body temperature rises above 37°C and reaches its maximum increase at 38°C, thus suggesting that individual and age-dependent body temperature variations can already control the expression of the antiviral genes. Accordingly, some antiviral genes, including *Ddx58*, *Stat2*, and *Irf7*, were already increased at 37.5°C compared to 36.5°C.

Additionally, we observed increased protein and phosphorylation levels of Stat2 and higher phosphorylation of Stat3 at elevated temperatures, suggesting an activation of the JAK/STAT pathway. Inhibition of JAK1/2 with Ruxolitinib completely prevented the temperature-controlled increase in all antiviral genes tested, indicating that JAK is responsible for the temperature-controlled expression of antiviral genes. The JAK family is composed of four members, JAK1, JAK2, JAK3, and TYK2, which are differentially activated in response to cytokines and can either act alone or in a combination with other JAK members (Rawlings, Rosler and Harrison, 2004; Ghoreschi, Laurence and O'Shea, 2009). The STAT family mediates signals derived from cytokine receptors and has seven members: STAT1, STAT2, STAT3, STAT4, STAT5a, STAT5b, and STAT6 (Rawlings, Rosler and Harrison, 2004; Ghoreschi, Laurence and O'Shea, 2009). Some members of the JAK/STAT pathway were reported to respond to temperature. For instance, Stat3 activation (higher phosphorylation) was observed at mild heat shock (42°C) (Matozaki *et al.*, 2019). In contrast, fever range temperature (40°C) was reported to aggregate JAK2, reducing its function. The same study showed lower protein levels of STAT5b at 40°C (Nespital and Strous, 2012).

As mentioned above, febrile temperatures induce the expression of pyrogenic cytokines. However, this also leads to the expression of antipyretic cytokines, such as IL-10 that acts as endogenous fever regulators by inhibiting the production of IL-6 (Leon *et al.*, 1999). Although febrile temperatures confer survival advantages during an infection, a

prolongated fever can be harmful, and therefore, need to be tightly regulated (Evans, Repasky and Fisher, 2015). Here we showed an upregulation of IFN-I and ISGs at elevated temperatures. IFN-I mainly activates the JAK1/TYK2 kinases, followed by the phosphorylation of STAT1, STAT2, and the IRF family of proteins that will lead to the transcription of ISGs (Kotenko and Pestka, 2000). This indicates that at elevated temperatures the IFN-I and ISGs are activated to assure better control of infection, while other mechanisms, such as the ones mediated by JAK2 and STAT5b, are reduced to avoid overactivation of the cytokine signaling and ensure a balanced response.

The expression of antiviral genes at elevated temperatures is only significantly increased after 12 hours of incubation. This temperature profile suggests that a short-term increase in core body temperature (*e.g.* during physical exercise) is insufficient to induce antiviral immunity, and potentially acts as a safety mechanism to avoid unnecessary and harmful activation of the IFN-I response and NO production. Interestingly, the increased expression of antiviral genes observed only after 12 hours (and decreasing after around 12 hours when shifted back to 37°C) corresponds to the rhythmicity of body temperature with approximately 12 hours of active period (higher body temperature) and 12 hours resting phase (lower body temperature) (Refinetti, 2020). The upregulation of antiviral genes at elevated temperatures probably occurs to defend the host against peaks of pathogens encounter that occur mostly during the behavioral active period (Wang *et al.*, 2022). Consistently, higher antiviral effects mediated by IFN were observed during the active phase compared to the resting phase in mice (Takane *et al.*, 2002). Mice infected during the active phase were also shown to respond better to virus infection than mice infected during the resting phase (Edgar *et al.*, 2016). Likewise, female mice have been reported to better control viral infections when treated with progesterone at concentrations that mimic the luteal phase of the hormone cycle, which is also the phase with higher body temperature (Hall *et al.*, 2016). Increased levels of type-1 inflammatory cytokines (IL-1β, IL-6, IL-8, MCP-1, TNFα, and IFNγ) were also observed during the luteal phase in pig-tailed macaques (Swaims-Kohlmeier *et al.*, 2021). Additionally, previous studies observed a higher induction of the proinflammatory response in mice challenged with LPS or infected with influenza during the active phase compared to the resting phase. However, this enhanced inflammation was associated with a worse outcome (Gibbs *et al.*, 2014; Curtis *et al.*, 2015; Sengupta *et al.*, 2019). As mentioned above, a more robust immune response during the active period probably acts as an anticipatory protection against potential threats that are more likely to happen during this period. Hence, the circadian clock has an important role in balancing pathogen resistance and host tolerance (Sengupta *et al.*, 2019). The different outcomes based on the time of virus inoculation are in accordance with vaccination trials that showed that vaccination response is time-of-day dependent (Wang *et al.*, 2022).

Moreover, the IFN-I and the JAK/STAT pathway are also responsible for the full transcriptional induction of *Nos2*, the gene encoding inducible nitric oxide synthetase, and NO production (Farlik *et al.*, 2010). NO production has a positive antiviral effect on respiratory viruses, and NO-based therapies were suggested as a treatment for COVID-19 (Lisi, Zelikin and Chandrawati, 2021). Our data showed higher expression of *Nos2* and higher production of NO at elevated temperatures (39°C) in LPS-induced RAW 264.7 cells and primary macrophages. Consistently, NO production and inducible nitric oxide synthase were shown to be enhanced in LPS-induced macrophages exposed to hyperthermia (39.5°C). However, hyperthermia alone did not affect NO production or nitric oxide synthetase expression (Pritchard, Li and Repasky, 2005). We also observed that temperature alone was insufficient to induce the expression of antiviral genes in some cell types, such as primary macrophages and Jurkat cells, which needed a further stimulus to show higher antiviral gene expression at higher temperatures. These data suggested that elevated temperature primes the innate immune system for a stronger activation and may function to lower the activation threshold needed to produce IFN-I and NO.

We then investigated the mechanism behind the observed delayed response in the expression of antiviral genes at elevated temperatures. Around 30% of rhythmic changes in mRNAs are due to changes in the level of transcription, while the remaining are probably controlled by post-transcriptional modifications, such as translation and splicing (Koike *et al.*, 2012; Menet *et al.*, 2012). Therefore, we investigated changes in *de novo* transcription, mRNA stability, and splicing. When comparing the expression pattern of antiviral genes between different temperatures in chromatin-associated pre-mRNA and total mRNA, we observed that *Stat2* and *Irf7* showed similar transcriptional rhythms, with higher expression levels in chromatin-associated pre-mRNA coinciding with the peak of the respective mRNA. Thus, suggesting that the transcription of antiviral genes is partially controlled via *de novo* transcription. Likewise, the expression of several inflammatory cytokines and antiviral genes was shown to be dependent on *de novo* recruitment of Pol II (Haas *et al.*, 2018). In addition, IRF3 was shown to drive *de novo* Pol II recruitment at transcriptional target sites, stimulating the expression of IFN-I genes during virus infection (Freaney *et al.*, 2013). The *de novo* recruitment of Pol II can potentially prevent unnecessary activation of signaling pathways and biological responses in the absence of a stimulus (Freaney *et al.*, 2013). Moreover, we did not observe changes in mRNA stability, indicating that mRNA stability is not responsible for the temperature-controlled expression of antiviral genes.

Lastly, we investigate changes in alternative splicing, especially of members of the JAK/STAT pathway, as this pathway is responsible for the induction of antiviral genes at elevated temperatures. We identified an alternative 5’ splice site in *Stat2*, which is used more frequently at colder temperatures, and its usage leads to a frameshift and inclusion of

a PTC. Stat2 is a key component of the JAK/STAT pathway and it is responsible for inducing the expression of several ISGs, which are important for controlling viral replication (Park *et al.*, 2000; McNab *et al.*, 2015). For example, Stat2 was shown to be necessary for suppressing viral replication and restricting the dissemination of SARS-CoV-2 in hamsters (Boudewijns *et al.*, 2020). Therefore, Stat2 expression must be tightly controlled to maintain immune homeostasis. PTC-containing mRNAs are usually recognized and degraded by the NMD pathway, and recent work showed that AS coupled to mRNA degradation is sufficient to generate temperature-dependent GE changes (Hug, Longman and Cáceres, 2016; Neumann *et al.*, 2020). Moreover, the NMD pathway has been shown to play a role in the regulation of the immune response by degrading cytokines mRNAs (Mino *et al.*, 2015). Consistently, we observed an increased *Stat2* expression at colder temperatures (35 and 37°C) when blocking NMD with CHX, suggesting that AS coupled to NMD is the main mechanism controlling *Stat2* expression. However, as CHX inhibits other mRNA decay pathways coupled to translation, a more specific inhibitor (*e.g.* Calbiochem or NMDI14) or knockdown of NMD factors, such as UPF1, could be used to confirm that this AS event is coupled to NMD. Recently, a study showed that STAT3 can bind to SMG1 promoter, and can induce a stronger NMD activity upon stimulation with the pyrogenic cytokine IL-6 (Meraviglia-Crivelli *et al.*, 2022). STAT3 can also be induced by IFN-I (Tsai, Pai and Lee, 2019). Interestingly, we also observed reduced usage of the *Stat2* alternative 5' splice site in IFN-I-stimulated cells (**Figure S2**), thus suggesting a potential increase in NMD activity upon IFN-I stimulation.

We then hypothesize that the delayed response in the expression of antiviral genes is not directly coupled to temperature changes but linked through this intermediate step of *Stat2* pre-mRNA processing. In agreement with this hypothesis, we showed that the expression of *Stat2* and other antiviral genes increases upon depletion or decreased usage of the alternative 5' splice site of *Stat2*. Amongst the genes that were increased, *Ddx58* is an important PPRs, and *Ifit3* and *Oasl2* are responsible for reducing viral replication (Ivashkiv and Donlin, 2014; McNab *et al.*, 2015; Schultze and Aschenbrenner, 2021). For example, Ifit3 was reported to reduce more than 50% of SARS-CoV-2 RNA levels (Martin-Sancho *et al.*, 2021). Alternative splicing has also been shown to regulate the expression of other antiviral genes. For example, *Oas1* has an alternative 5' splice coupled to NMD. The removal of this alternative 5' splice site leads to increased expression of *Oas1* and better control of virus infection (Frankiw *et al.*, 2020). However, the removal of the 5' splice site also increased the number of apoptotic cells, suggesting that this splice site exists to balance the antiviral benefits and collateral damage associated with Oas1 activity (Frankiw *et al.*, 2020). In addition, human genetic variants were shown to decrease *OAS1* expression via allele-specific regulation of splicing and NMD (Banday *et al.*, 2022). The NMD-coupled

isoforms decreased the expression of *OAS1* and were associated with impaired viral clearance and severe COVID-19 (Banday *et al.*, 2022). Thus, providing further evidence that an early and robust IFN response is important to prevent a severe outcome of the COVID-19 disease.

Similarly to the CHX treatment, we observed increased expression of *Stat2* and other antiviral genes, including *Ddx58* and *Trim25*, at 37°C when blocking CLKs using TG003. Noteworthy, CLK1 inhibition and knockdown were shown to reduce influenza A virus replication *in vitro* (Karlas *et al.*, 2010; Artarini *et al.*, 2019). Inhibition of CLKs at 37°C mimics the effect of warmer temperatures. However, the temperature profile (between 36.5°C and 38°C) that controls the expression of antiviral genes is different from the temperature-dependent change in CLK activity observed *in vitro* (Haltenhof *et al.*, 2020). Therefore, the further increased in the expression of antiviral genes at 39°C in TG003-treated cells is probably not mediated by CLKs. Conversely to CLKs, the protein phosphatase 2A (PP2A) was shown to be more active at higher temperatures, and inhibition of PP1/PP2A with okadaic acid (OA) impacted temperature-controlled AS and GE (unpublished data from AG Heyd). However, inhibition of PP1/PP2A with OA did not strongly alter the expression of antiviral genes at different temperatures (**Figure S3**). Therefore, it is likely that an additional mechanism, yet unknown, contributes to the regulation of antiviral genes to achieve remarkable temperature sensitivity.

Furthermore, we showed that the usage of the alternative 5' splice site in *Stat2* is controlled by Srsf1. Srsf1 knockdown led to the decreased expression of *Stat2*, *Trim25*, and *Oasl2* mRNA levels. Interestingly, a negative correlation between ISGs and SRSF1 expression has been reported (Sertznig *et al.*, 2022). These data are in line with the fact that CLKs are more active at lower temperatures and that this higher activity will lead to more Srsf1 phosphorylation, and consequently, promoting the recognition and usage of the alternative 5' splice site by the spliceosome (Haltenhof *et al.*, 2020).

The rhythmic changes in antiviral expression may also be associated with changes in chromatin architecture. STAT proteins are global regulators of active enhancer landscapes (Vahedi *et al.*, 2012). For example, STAT1 was reported to generate enhancers during T-cell differentiation and to activate latent enhancers in macrophages (Vahedi *et al.*, 2012; Ostuni *et al.*, 2013; Qiao *et al.*, 2013). Therefore, STATs not only transiently induce gene expression, but can also initiate chromatin remodeling and alter epigenetic states upon stimulation (Qiao *et al.*, 2013). Although *Stat1* expression is temperature-controlled, temperature-driven changes in the epigenetic landscape still need to be examined.

Ultimately, we addressed the functional impact of elevated temperature during virus infection using SARS-CoV-2 as a model system. Recently, a study performed a gain-of-function screen to uncover the cellular antiviral response to SARS-CoV-2 and identified 65

SARS-CoV-2 restriction factors (Martin-Sancho *et al.*, 2021). Nine of these factors, including *Stat1, Stat2, Ifit1,* and *Ifit3*, were increased at 38°C in our RNA-seq dataset. This data suggested that body temperature could create a condition that limits SARS-CoV-2 replication. Additionally, we showed that both IFN-I response and NO production are controlled by temperature, suggesting that fluctuations in the core body temperature can have an impact on the outcome of viral infections.

Elderly individuals have significantly higher COVID-19 severity and mortality rates, as compared with children and adults, indicating an absence of long-lasting pre-existing adaptive immunity (O'Driscoll *et al.*, 2021; Schultze and Aschenbrenner, 2021). In this scenario, the control of SARS-CoV-2 infection requires an early and highly coordinated innate antiviral immunity (Schultze and Aschenbrenner, 2021). Accordingly, the innate immune response to SARS-CoV-2 infection was reported to determine the disease outcome, whereas a more efficient IFN-I contributes to a milder course of the disease, and an impaired IFN-I response favors a more severe outcome (Arunachalam *et al.*, 2020; Hadjadj *et al.*, 2020). It has extensively been reported that body temperature decreases with aging (Waalen and Buxbaum, 2011; Geneva *et al.*, 2019). Overall, younger adults and children exhibit a higher body temperature when compared to healthy elderly people (Waalen and Buxbaum, 2011; Geneva *et al.*, 2019). In addition, elderly people usually fail to reach the fever temperature range. Hence are frequently incapable of mounting a robust inflammatory response to infection and disease (Geneva *et al.*, 2019). Interestingly, we found that several antiviral genes that are warm-induced in our dataset are more expressed in younger animals. Also, two known cold-induced genes, *Rbm3* and *Cirbp*, were more expressed in older animals, which could suggest colder body temperature (Liu *et al.*, 2013). These results are in accordance with our assumption that individual and age-dependent body temperature variation controls the expression of antiviral genes and SARS-CoV-2 replication. However, this correlation needs further experimental validation, for example, by manipulating the body temperature of aged mice and investigating the impact on antiviral gene expression. Also, aging is a multifactorial process and body temperature is likely only one of the factors that impact the expression of antiviral genes in the elderly population. Nevertheless, age-dependent differences during SARS-CoV-2 infection were examined in animal models and humans (Osterrieder *et al.*, 2020; Loske *et al.*, 2021; Oishi *et al.*, 2022). For example, aged golden hamsters (27 weeks old) showed lower innate and repair responses following SARS-CoV-2 infection as compared with young hamsters (6–10 weeks old) (Oishi *et al.*, 2022). Additionally, children showed an enhanced antiviral capacity upon SARS-CoV-2 infection, leading to increased early production of interferons in the infected upper airways (Loske *et al.*, 2021). This enhanced innate antiviral capacity likely contributes to the better protection of children against a severe course of COVID-19 and their lower susceptibility to SARS-CoV-2

infection (Garg *et al.*, 2020; O'Driscoll *et al.*, 2021; Sun *et al.*, 2021). Further, the expression of several genes that are temperature controlled in our study, for example, *DDX58* (RIG-I), *IFIT1, IFIT2, IFIT3*, *OAS1, OAS3*, *OASL,* are reduced in >60 years old versus <60 years old SARS-CoV-2 positive subjects (Lieberman *et al.*, 2020).

Finally, our cell culture experiments with Calu-3 and Caco-2 infected cells showed that 16 h preincubation at higher temperature reduced SARS-CoV-2 replication. These data further support our idea that an increased body temperature at the point of infection is important for reducing virus replication. Similarly, another study showed lower SARS-CoV-2 replication at 40°C compared to 37°C in a respiratory tissue model (Herder, Dee, Joanna K. Wojtus, *et al.*, 2021). Pseudoviruses containing the SARS-CoV-2 S protein and the HCoV-229E S protein were also more infectious at 33°C than at 37°C (Laporte *et al.*, 2021). Lower viral replication at higher temperatures was also observed for other viruses (Foxman *et al.*, 2015; Lane *et al.*, 2018). For example, the human rhinovirus, the most frequent cause of the common cold, was found to replicate better at colder temperatures in the upper respiratory tract (33°C) than at warmer temperatures in the lung (37°C), which is probably due to a less robust IFN and ISG response at colder temperatures (Foxman *et al.*, 2015). A similar pattern was observed for chikungunya arbovirus, which showed lower viral replication and stronger IFN response at 39°C when compared to lower temperatures (30 and 37°C) (Lane *et al.*, 2018). Furthermore, it has long been hypothesized that exposure to cold air decreases the temperature of the nasal respiratory epithelium, and this leads to a decrease in virus clearance (Eccles, 2002). Besides the same study has suggested that prewarming breathing air in winter, for example by using a scarf or a face mask, could reduce viral infections (Eccles, 2002). Accordingly, the effectiveness of face masks during the COVID-19 pandemic was considered to be partly due to increased temperature in the upper respiratory tract (Gupta, 2020). Also, decreasing body temperature during a viral infection using antipyretic medicaments to diminish fever correlates with increased mortality in human populations and animal models (Kurosawa *et al.*, 1987; Earn, Andrews and Bolker, 2014). Therefore, the benefits of increasing the temperature of the upper respiratory tract during winter; and allowing a normal febrile response could be related to the mechanism described in this thesis.

Our results could also have translational potential, as a temporary or rhythmic increase in core body temperature could be used as a protective measure against viral infections. For example, hyperthermia treatment (20 min at 45°C) in HeLa cells six hours post-infection with rhinovirus reduced more than 90% of virus yield related to control (Conti *et al.*, 1999). Additionally, several viruses, such as chikungunya, affect limbs and extremities in humans, which are usually cooler than the core body temperature, resulting in reduced IFN-mediated antiviral responses (Prow *et al.*, 2017). Therefore, local hyperthermia could be

used in these cases to induce antiviral responses (Zhu *et al.*, 2010; Prow *et al.*, 2017). However, hyperthermia is not suitable as a treatment for all viruses. HIV-infected cell lines at 39.5°C showed increased HIV-1 replication compared to 37°C (Roesch *et al.*, 2012). Nonetheless, *in vitro* studies showed that SARS-CoV-2 is sensitive to IFN treatment, and therefore, local hyperthermia that would lead to increased IFN-I response could potentially be beneficial for patients during the early stages of mild-to-moderate COVID-19 (Lokugamage *et al.*, 2020; Mancilla-Galindo and Galindo-Sevilla, 2021).

Other therapeutical approaches, such as nucleic acid-based therapies could also be effective against viral infections. Recently, a study has shown that ASOs targeting SARS-CoV-2 or host entry factors, such as *ACE2*, decreased SARS-CoV-2 infection in different cell lines (Qiao *et al.*, 2023). Here, we showed that an ASO flacking the alternative 5' splice site of *Stat2* increases the expression of *Stat2* and other antiviral genes in mice cell lines. Although cells treated with this ASO could potentially show a more robust antiviral response, studies addressing the effect of this ASO in inducing virus clearance are still necessary. Besides, as humans have different *STAT2* NMD-coupled isoforms, different ASOs would have to be designed and tested.

In summary, we showed that alternative splicing coupled with NMD decreases the expression of *Stat2* at lower temperatures. The upregulation of *Stat2* at higher temperatures in conjunction with JAK1 activity induces the expression of antiviral genes, which mounts a successful antiviral response, leading to lower viral replication (**Figure 4.1.**). Taken together, our data may contribute to a mechanistic explanation of why children are better able to control SARS-CoV-2 infection, while a reduced body temperature in the elderly population favors a more severe outcome of the COVID-19 disease.

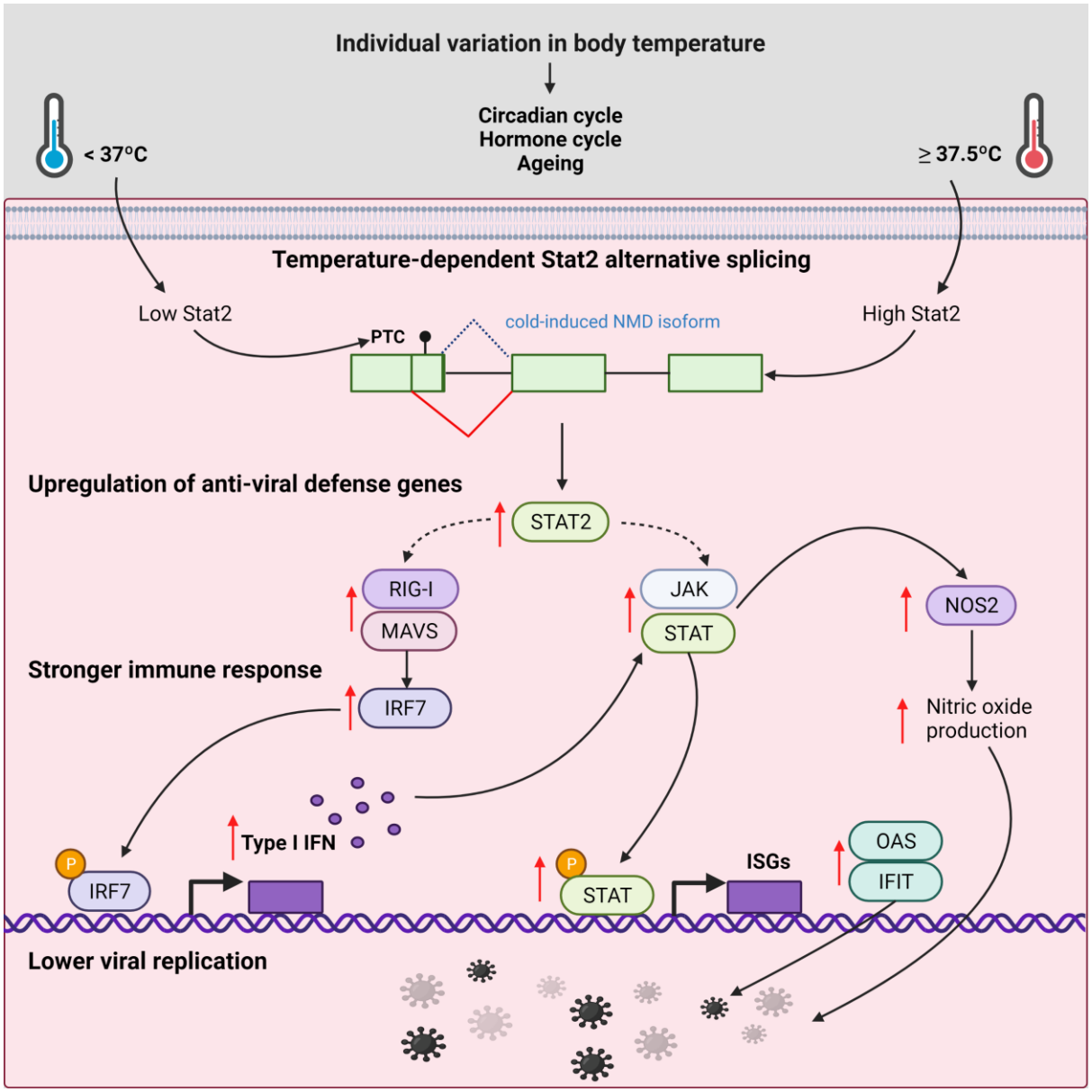

Figure 4.1. Schematic representation of the impact of *Stat2* on the expression of antiviral genes at higher temperatures.
Alternative splicing coupled with NMD decreases *Stat2* expression in colder temperatures. *Stat2* upregulation at higher temperatures in conjunction with JAK activity will induce the expression of antiviral genes. The upregulation of antiviral genes will lead to a stronger antiviral immune response and, therefore, to a lower viral replication. Created with BioRender.com. Adapted from Los *et al.*, 2022.

5. REFERENCES

Almanzar, N. *et al.* (2020) 'A single-cell transcriptomic atlas characterizes ageing tissues in the mouse', *Nature*, 583(7817), pp. 590–595. doi: 10.1038/s41586-020-2496-1.

Artarini, A. *et al.* (2019) 'Regulation of influenza A virus mRNA splicing by CLK1.', *Antiviral research*, 168, pp. 187–196. doi: 10.1016/j.antiviral.2019.06.003.

Arunachalam, P. S. *et al.* (2020) 'Systems biological assessment of immunity to mild versus severe COVID-19 infection in humans.', *Science (New York, N.Y.)*, 369(6508), pp. 1210–1220. doi: 10.1126/science.abc6261.

Banday, A. R. *et al.* (2022) 'Genetic regulation of OAS1 nonsense-mediated decay underlies association with COVID-19 hospitalization in patients of European and African ancestries', *Nature Genetics*, 54(8), pp. 1103–1116. doi: 10.1038/s41588-022-01113-z.

Banerjee, A. K. *et al.* (2020) 'SARS-CoV-2 Disrupts Splicing, Translation, and Protein Trafficking to Suppress Host Defenses.', *Cell*, 183(5), pp. 1325-1339.e21. doi: 10.1016/j.cell.2020.10.004.

Blanco-Melo, D. *et al.* (2020) 'Imbalanced Host Response to SARS-CoV-2 Drives Development of COVID-19.', *Cell*, 181(5), pp. 1036-1045.e9. doi: 10.1016/j.cell.2020.04.026.

Boehm, V. *et al.* (2021) 'SMG5-SMG7 authorize nonsense-mediated mRNA decay by enabling SMG6 endonucleolytic activity.', *Nature communications*, 12(1), p. 3965. doi: 10.1038/s41467-021-24046-3.

Boudewijns, R. *et al.* (2020) 'STAT2 signaling restricts viral dissemination but drives severe pneumonia in SARS-CoV-2 infected hamsters.', *Nature communications*, 11(1), p. 5838. doi: 10.1038/s41467-020-19684-y.

Boulant, J. A. (2000) 'Role of the preoptic-anterior hypothalamus in thermoregulation and fever.', *Clinical infectious diseases : an official publication of the Infectious Diseases Society of America*, 31 Suppl 5, pp. S157-61. doi: 10.1086/317521.

Brogna, S. and Wen, J. (2009) 'Nonsense-mediated mRNA decay (NMD) mechanisms', *Nature Structural and Molecular Biology*, 16(2), pp. 107–113. doi: 10.1038/nsmb.1550.

Busch, A. and Hertel, K. J. (2012) 'Evolution of SR protein and hnRNP splicing regulatory factors.', *Wiley interdisciplinary reviews. RNA*, 3(1), pp. 1–12. doi: 10.1002/wrna.100.

Chakrabarti, S. *et al.* (2014) 'Phospho-dependent and phospho-independent interactions of the helicase UPF1 with the NMD factors SMG5-SMG7 and SMG6.', *Nucleic acids research*, 42(14), pp. 9447–9460. doi: 10.1093/nar/gku578.

Chamieh, H. *et al.* (2008) 'NMD factors UPF2 and UPF3 bridge UPF1 to the exon junction complex and stimulate its RNA helicase activity.', *Nature structural & molecular biology*, 15(1), pp. 85–93. doi: 10.1038/nsmb1330.

Chen, M. and Manley, J. L. (2009) 'Mechanisms of alternative splicing regulation: insights from molecular and genomics approaches.', *Nature reviews. Molecular cell biology*, 10(11), pp. 741–754. doi: 10.1038/nrm2777.

Conti, C. *et al.* (1999) 'Antiviral effect of hyperthermic treatment in rhinovirus infection.', *Antimicrobial agents and chemotherapy*, 43(4), pp. 822–829. doi: 10.1128/AAC.43.4.822.

Crick, F. and Watson, J. (1953) 'Molecular structure of nucleic acids', *Nature*, 171, pp. 737–738.

Curtis, A. M. *et al.* (2015) 'Circadian control of innate immunity in macrophages by miR-155 targeting Bmal1.', *Proceedings of the National Academy of Sciences of the United States of America*, 112(23), pp. 7231–7236. doi: 10.1073/pnas.1501327112.

Diallo, A. B. *et al.* (2021) 'Daytime variation in SARS-CoV-2 infection and cytokine production.', *Microbial pathogenesis*, 158, p. 105067. doi: 10.1016/j.micpath.2021.105067.

Dupuis, S. *et al.* (2003) 'Impaired response to interferon-alpha/beta and lethal viral disease in human STAT1 deficiency.', *Nature genetics*, 33(3), pp. 388–391. doi: 10.1038/ng1097.

Durbin, J. E. *et al.* (1996) 'Targeted disruption of the mouse Stat1 gene results in compromised innate immunity to viral disease.', *Cell*, 84(3), pp. 443–450. doi: 10.1016/s0092-8674(00)81289-1.

Earn, D. J. D., Andrews, P. W. and Bolker, B. M. (2014) 'Population-level effects of suppressing fever.', *Proceedings. Biological sciences*, 281(1778), p. 20132570. doi: 10.1098/rspb.2013.2570.

Eberle, A. B. *et al.* (2009) 'SMG6 promotes endonucleolytic cleavage of nonsense mRNA in human cells.', *Nature structural & molecular biology*, 16(1), pp. 49–55. doi: 10.1038/nsmb.1530.

Eccles, R. (2002) 'An explanation for the seasonality of acute upper respiratory tract viral

infections', *Acta Oto-Laryngologica*, 122(2), pp. 183–191. doi: 10.1080/00016480252814207.

Edgar, R. S. *et al.* (2016) 'Cell autonomous regulation of herpes and influenza virus infection by the circadian clock', *Proceedings of the National Academy of Sciences of the United States of America*, 113(36), pp. 10085–10090. doi: 10.1073/pnas.1601895113.

Eskildsen, S. *et al.* (2003) 'Characterization of the 2'-5'-oligoadenylate synthetase ubiquitin-like family.', *Nucleic acids research*, 31(12), pp. 3166–3173. doi: 10.1093/nar/gkg427.

Evans, S. S., Repasky, E. A. and Fisher, D. T. (2015) 'Fever and the thermal regulation of immunity: The immune system feels the heat', *Nature Reviews Immunology*. Nature Publishing Group, pp. 335–349. doi: 10.1038/nri3843.

Farlik, M. *et al.* (2010) 'Nonconventional initiation complex assembly by STAT and NF-κB transcription factors regulates nitric oxide synthase expression', *Immunity*, 33(1), pp. 25–34. doi: 10.1016/j.immuni.2010.07.001.

Felgenhauer, U. *et al.* (2020) 'Inhibition of SARS-CoV-2 by type I and type III interferons.', *The Journal of biological chemistry*, 295(41), pp. 13958–13964. doi: 10.1074/jbc.AC120.013788.

Finkel, Y. *et al.* (2021) 'The coding capacity of SARS-CoV-2.', *Nature*, 589(7840), pp. 125–130. doi: 10.1038/s41586-020-2739-1.

Foxman, E. F. *et al.* (2015) 'Temperature-dependent innate defense against the common cold virus limits viral replication at warm temperature in mouse airway cells', *Proceedings of the National Academy of Sciences of the United States of America*, 112(3), pp. 827–832. doi: 10.1073/pnas.1411030112.

Frankiw, L. *et al.* (2020) 'Alternative splicing coupled with transcript degradation modulates OAS1g antiviral activity.', *RNA (New York, N.Y.)*, 26(2), pp. 126–136. doi: 10.1261/rna.073825.119.

Freaney, J. E. *et al.* (2013) 'Extensive cooperation of immune master regulators IRF3 and NFκB in RNA Pol II recruitment and pause release in human innate antiviral transcription.', *Cell reports*, 4(5), pp. 959–973. doi: 10.1016/j.celrep.2013.07.043.

Fu, X.-D. and Ares, M. J. (2014) 'Context-dependent control of alternative splicing by RNA-binding proteins.', *Nature reviews. Genetics*, 15(10), pp. 689–701. doi: 10.1038/nrg3778.

Gack, M. U. *et al.* (2008) 'Roles of RIG-I N-terminal tandem CARD and splice variant in TRIM25-mediated antiviral signal transduction.', *Proceedings of the National Academy of Sciences of the United States of America*, 105(43), pp. 16743–16748. doi: 10.1073/pnas.0804947105.

Garg, S. *et al.* (2020) 'Hospitalization Rates and Characteristics of Patients Hospitalized with', *Morbidity and Mortality Weekly Report, US Department of Health and Human Services/Centers for Disease Control and Prevention*, 69(15), pp. 458–464. Available at: https://www.cdc.gov/mmwr/volumes/69/wr/mm6915e3.htm.

Geneva, I. I. *et al.* (2019) 'Normal body temperature: A systematic review', *Open Forum Infectious Diseases*, 6(4). doi: 10.1093/ofid/ofz032.

Georgakopoulos-Soares, I., Parada, G. E. and Hemberg, M. (2022) 'Secondary structures in RNA synthesis, splicing and translation', *Computational and Structural Biotechnology Journal*, 20, pp. 2871–2884. doi: 10.1016/j.csbj.2022.05.041.

Gerber, A. *et al.* (2015) 'The systemic control of circadian gene expression.', *Diabetes, obesity & metabolism*, 17 Suppl 1, pp. 23–32. doi: 10.1111/dom.12512.

Ghoreschi, K., Laurence, A. and O'Shea, J. J. (2009) 'Janus kinases in immune cell signaling.', *Immunological reviews*, 228(1), pp. 273–287. doi: 10.1111/j.1600-065X.2008.00754.x.

Gibbs, J. *et al.* (2014) 'An epithelial circadian clock controls pulmonary inflammation and glucocorticoid action.', *Nature medicine*, 20(8), pp. 919–926. doi: 10.1038/nm.3599.

Gupta, D. (2020) '"Therapeutic" facemasks.', *Medical hypotheses*. United States, p. 109855. doi: 10.1016/j.mehy.2020.109855.

Haas, D. A. *et al.* (2018) 'Viral targeting of TFIIB impairs de novo polymerase II recruitment and affects antiviral immunity.', *PLoS pathogens*, 14(4), p. e1006980. doi: 10.1371/journal.ppat.1006980.

Hadjadj, J. *et al.* (2020) 'Impaired type I interferon activity and inflammatory responses in severe COVID-19 patients', *Science*, 369(August), pp. 718–724.

Hall, O. J. *et al.* (2016) 'Progesterone-Based Therapy Protects Against Influenza by Promoting Lung Repair and Recovery in Females', *PLoS Pathogens*, 12(9). doi: 10.1371/journal.ppat.1005840.

Haltenhof, T. *et al.* (2020) 'A Conserved Kinase-Based Body-Temperature Sensor Globally Controls Alternative Splicing and Gene Expression', *Molecular Cell*, 78(1), pp. 57-69.e4. doi: 10.1016/j.molcel.2020.01.028.

Hatzfeld-Charbonnier, A. S. *et al.* (2007) 'Influence of heat stress on human monocyte-derived dendritic cell functions with immunotherapeutic potential for antitumor vaccines.', *Journal of leukocyte biology*, 81(5), pp. 1179–1187. doi: 10.1189/jlb.0506347.

Herder, V., Dee, K., Wojtus, Joanna K, *et al.* (2021) 'Elevated temperature inhibits SARS-CoV-2 replication in respiratory epithelium independently of IFN-mediated innate immune defenses.', *PLoS biology*, 19(12), p. e3001065. doi: 10.1371/journal.pbio.3001065.

Herder, V., Dee, K., Wojtus, Joanna K., *et al.* (2021) 'Elevated temperature inhibits SARS-CoV-2 replication in respiratory epithelium independently of IFN-mediated innate immune defenses', *PLoS Biology*, 19(12), pp. 1–27. doi: 10.1371/journal.pbio.3001065.

Le Hir, H. *et al.* (2000) 'The spliceosome deposits multiple proteins 20-24 nucleotides upstream of mRNA exon-exon junctions.', *The EMBO journal*, 19(24), pp. 6860–6869. doi: 10.1093/emboj/19.24.6860.

Le Hir, H., Saulière, J. and Wang, Z. (2016) 'The exon junction complex as a node of post-transcriptional networks.', *Nature reviews. Molecular cell biology*, 17(1), pp. 41–54. doi: 10.1038/nrm.2015.7.

Hoek, T. A. *et al.* (2019) 'Single-Molecule Imaging Uncovers Rules Governing Nonsense-Mediated mRNA Decay', *Molecular Cell*, 75(2), pp. 324-339.e11. doi: 10.1016/j.molcel.2019.05.008.

Hoffmann, M. *et al.* (2020) 'SARS-CoV-2 Cell Entry Depends on ACE2 and TMPRSS2 and Is Blocked by a Clinically Proven Protease Inhibitor.', *Cell*, 181(2), pp. 271-280.e8. doi: 10.1016/j.cell.2020.02.052.

Hu, B. *et al.* (2021) 'Characteristics of SARS-CoV-2 and COVID-19.', *Nature reviews. Microbiology*, 19(3), pp. 141–154. doi: 10.1038/s41579-020-00459-7.

Hua, Y. *et al.* (2010) 'Antisense correction of SMN2 splicing in the CNS rescues necrosis in a type III SMA mouse model.', *Genes & development*, 24(15), pp. 1634–1644. doi: 10.1101/gad.1941310.

Huang, C. *et al.* (2020) 'Clinical features of patients infected with 2019 novel coronavirus in

Wuhan, China.', *Lancet (London, England)*, 395(10223), pp. 497–506. doi: 10.1016/S0140-6736(20)30183-5.

Hug, N., Longman, D. and Cáceres, J. F. (2016) 'Mechanism and regulation of the nonsense-mediated decay pathway.', *Nucleic acids research*, 44(4), pp. 1483–1495. doi: 10.1093/nar/gkw010.

Hurt, J. A., Robertson, A. D. and Burge, C. B. (2013) 'Global analyses of UPF1 binding and function reveal expanded scope of nonsense-mediated mRNA decay.', *Genome research*, 23(10), pp. 1636–1650. doi: 10.1101/gr.157354.113.

Ivashkiv, L. B. and Donlin, L. T. (2014) 'Regulation of type I interferon responses.', *Nature reviews. Immunology*, 14(1), pp. 36–49. doi: 10.1038/nri3581.

Jackson, L. J. (1991) 'A reappraisal of non-consensus mRNA splice sites', *Nucleic Acids Research*, 19(14), pp. 3795–3798. doi: 10.1093/nar/19.14.3795.

Jiang, Q. *et al.* (1999) 'Exposure to febrile temperature upregulates expression of pyrogenic cytokines in endotoxin-challenged mice.', *The American journal of physiology*, 276(6), pp. R1653-60. doi: 10.1152/ajpregu.1999.276.6.R1653.

Karlas, A. *et al.* (2010) 'Genome-wide RNAi screen identifies human host factors crucial for influenza virus replication.', *Nature*, 463(7282), pp. 818–822. doi: 10.1038/nature08760.

Kashima, I. *et al.* (2006) 'Binding of a novel SMG-1-Upf1-eRF1-eRF3 complex (SURF) to the exon junction complex triggers Upf1 phosphorylation and nonsense-mediated mRNA decay.', *Genes & development*, 20(3), pp. 355–367. doi: 10.1101/gad.1389006.

Kelemen, O. *et al.* (2013) 'Function of alternative splicing', *Gene*, 514(1), pp. 1–30. doi: 10.1016/j.gene.2012.07.083.

Knippertz, I. *et al.* (2011) 'Mild hyperthermia enhances human monocyte-derived dendritic cell functions and offers potential for applications in vaccination strategies.', *International journal of hyperthermia : the official journal of European Society for Hyperthermic Oncology, North American Hyperthermia Group*, 27(6), pp. 591–603. doi: 10.3109/02656736.2011.589234.

Koike, N. *et al.* (2012) 'Transcriptional architecture and chromatin landscape of the core circadian clock in mammals.', *Science (New York, N.Y.)*, 338(6105), pp. 349–354. doi: 10.1126/science.1226339.

Kojima, S. and Green, C. B. (2015) ‘Circadian genomics reveal a role for post-transcriptional regulation in mammals.’, *Biochemistry*, 54(2), pp. 124–133. doi: 10.1021/bi500707c.

Koop, A. *et al.* (2011) ‘Novel splice variants of human IKKε negatively regulate IKKε-induced IRF3 and NF-kB activation.’, *European journal of immunology*, 41(1), pp. 224–234. doi: 10.1002/eji.201040814.

Kotenko, S. V and Pestka, S. (2000) ‘Jak-Stat signal transduction pathway through the eyes of cytokine class II receptor complexes.’, *Oncogene*, 19(21), pp. 2557–2565. doi: 10.1038/sj.onc.1203524.

Kurosawa, S. *et al.* (1987) ‘Effects of antipyretics in rinderpest virus infection in rabbits.’, *The Journal of infectious diseases*, 155(5), pp. 991–997. doi: 10.1093/infdis/155.5.991.

de la Mata, M. and Kornblihtt, A. R. (2006) ‘RNA polymerase II C-terminal domain mediates regulation of alternative splicing by SRp20.’, *Nature structural & molecular biology*, 13(11), pp. 973–980. doi: 10.1038/nsmb1155.

Lane, W. C. *et al.* (2018) ‘The efficacy of the interferon alpha/beta response versus arboviruses is temperature dependent’, *mBio*, 9(2). doi: 10.1128/mBio.00535-18.

Laporte, M. *et al.* (2021) ‘The SARS-CoV-2 and other human coronavirus spike proteins are fine-tuned towards temperature and proteases of the human airways’, *PLoS Pathogens*, 17(4), pp. 1–29. doi: 10.1371/journal.ppat.1009500.

Lee, C. T. *et al.* (2012) ‘Elevation in body temperature to fever range enhances and prolongs subsequent responsiveness of macrophages to endotoxin challenge’, *PLoS ONE*, 7(1). doi: 10.1371/journal.pone.0030077.

Leon, L. R. *et al.* (1999) ‘An antipyretic role for interleukin-10 in LPS fever in mice.’, *The American journal of physiology*, 276(1), pp. R81-9. doi: 10.1152/ajpregu.1999.276.1.R81.

Lieberman, N. A. P. *et al.* (2020) ‘In vivo antiviral host transcriptional response to SARS-CoV-2 by viral load, sex, and age’, *PLoS Biology*, 18(9). doi: 10.1371/JOURNAL.PBIO.3000849.

Lim, C. and Allada, R. (2013) ‘Emerging roles for post-transcriptional regulation in circadian clocks.’, *Nature neuroscience*, 16(11), pp. 1544–1550. doi: 10.1038/nn.3543.

Lim, K. H. *et al.* (2020) ‘Antisense oligonucleotide modulation of non-productive alternative splicing upregulates gene expression.’, *Nature communications*, 11(1), p. 3501. doi:

10.1038/s41467-020-17093-9.

Lisi, F., Zelikin, A. N. and Chandrawati, R. (2021) 'Nitric Oxide to Fight Viral Infections', *Advanced Science*, 8(7), pp. 1–9. doi: 10.1002/advs.202003895.

Liu, Y. *et al.* (2013) 'Cold-induced RNA-binding proteins regulate circadian gene expression by controlling alternative polyadenylation', *Scientific Reports*, 3. doi: 10.1038/srep02054.

Loh, B., Jonas, S. and Izaurralde, E. (2013) 'The SMG5-SMG7 heterodimer directly recruits the CCR4-NOT deadenylase complex to mRNAs containing nonsense codons via interaction with POP2.', *Genes & development*, 27(19), pp. 2125–2138. doi: 10.1101/gad.226951.113.

Lokugamage, K. G. *et al.* (2020) 'Type I Interferon Susceptibility Distinguishes SARS-CoV-2 from SARS-CoV.', *Journal of virology*, 94(23). doi: 10.1128/JVI.01410-20.

Los, B. *et al.* (2022) 'Body temperature variation controls pre-mRNA processing and transcription of antiviral genes and SARS-CoV-2 replication.', *Nucleic acids research*, 50(12), pp. 6769–6785. doi: 10.1093/nar/gkac513.

Loske, J. *et al.* (2021) 'Pre-activated antiviral innate immunity in the upper airways controls early SARS-CoV-2 infection in children', *Nature Biotechnology*. doi: 10.1038/s41587-021-01037-9.

Lu, R. *et al.* (2020) 'Genomic characterisation and epidemiology of 2019 novel coronavirus: implications for virus origins and receptor binding', *The Lancet*, 395(10224), pp. 565–574. doi: 10.1016/S0140-6736(20)30251-8.

Lykke-Andersen, S. and Jensen, T. H. (2015) 'Nonsense-mediated mRNA decay: an intricate machinery that shapes transcriptomes.', *Nature reviews. Molecular cell biology*, 16(11), pp. 665–677. doi: 10.1038/nrm4063.

Man, K., Loudon, A. and Chawla, A. (2016) 'Immunity around the clock.', *Science (New York, N.Y.)*, 354(6315), pp. 999–1003. doi: 10.1126/science.aah4966.

Mancilla-Galindo, J. and Galindo-Sevilla, N. (2021) 'Exploring the rationale for thermotherapy in COVID-19.', *International journal of hyperthermia : the official journal of European Society for Hyperthermic Oncology, North American Hyperthermia Group*, 38(1), pp. 202–212. doi: 10.1080/02656736.2021.1883127.

Maniatis, T. and Tasic, B. (2002) 'Alternative pre-mRNA splicing and proteome expansion in

metazoans', *Nature*, 418(6894), pp. 236–243. doi: 10.1038/418236a.

Martin-Sancho, L. *et al.* (2021) 'Functional landscape of SARS-CoV-2 cellular restriction', *Molecular Cell*, 81(12), pp. 2656-2668.e8. doi: 10.1016/j.molcel.2021.04.008.

Matozaki, M. *et al.* (2019) 'Involvement of Stat3 phosphorylation in mild heat shock-induced thermotolerance.', *Experimental cell research*, 377(1–2), pp. 67–74. doi: 10.1016/j.yexcr.2019.02.011.

McGlincy, N. J. and Smith, C. W. J. (2008) 'Alternative splicing resulting in nonsense-mediated mRNA decay: what is the meaning of nonsense?', *Trends in Biochemical Sciences*, 33(8), pp. 385–393. doi: 10.1016/j.tibs.2008.06.001.

McNab, F. *et al.* (2015) 'Type I interferons in infectious disease', *Nature Reviews Immunology*. Nature Publishing Group, pp. 87–103. doi: 10.1038/nri3787.

Menet, J. S. *et al.* (2012) 'Nascent-Seq reveals novel features of mouse circadian transcriptional regulation.', *eLife*, 1, p. e00011. doi: 10.7554/eLife.00011.

Meraviglia-Crivelli, D. *et al.* (2022) 'IL-6/STAT3 signaling in tumor cells restricts the expression of frameshift-derived neoantigens by SMG1 induction.', *Molecular cancer*, 21(1), p. 211. doi: 10.1186/s12943-022-01679-6.

Merkin, J. *et al.* (2012) 'Evolutionary Dynamics of Gene and Isoform Regulation in Mammalian Tissues', *Science*, 338, pp. 1593–1599. doi: doi:10.1126/science.1228186.

Minchin, S. and Lodge, J. (2019) 'Understanding biochemistry: Structure and function of nucleic acids', *Essays in Biochemistry*, 63(4), pp. 433–456. doi: 10.1042/EBC20180038.

Mino, T. *et al.* (2015) 'Regnase-1 and Roquin Regulate a Common Element in Inflammatory mRNAs by Spatiotemporally Distinct Mechanisms.', *Cell*, 161(5), pp. 1058–1073. doi: 10.1016/j.cell.2015.04.029.

Mockenhaupt, S. and Makeyev, E. V (2015) 'Non-coding functions of alternative pre-mRNA splicing in development.', *Seminars in cell & developmental biology*, 47–48, pp. 32–39. doi: 10.1016/j.semcdb.2015.10.018.

Müller-Mcnicoll, M. *et al.* (2019) 'Auto-regulatory feedback by RNA-binding proteins', *Journal of Molecular Cell Biology*, 11(10), pp. 930–939. doi: 10.1093/jmcb/mjz043.

Naftelberg, S. *et al.* (2015) 'Regulation of alternative splicing through coupling with

transcription and chromatin structure.', *Annual review of biochemistry*, 84, pp. 165–198. doi: 10.1146/annurev-biochem-060614-034242.

Nespital, T. and Strous, G. J. (2012) 'The Jak/STAT signaling pathway is downregulated at febrile temperatures.', *PloS one*, 7(11), p. e49374. doi: 10.1371/journal.pone.0049374.

Neumann, A. *et al.* (2020) 'Alternative splicing coupled mRNA decay shapes the temperature-dependent transcriptome', *EMBO reports*, 21(12). doi: 10.15252/embr.202051369.

Nilsen, T. W. and Graveley, B. R. (2010) 'Expansion of the eukaryotic proteome by alternative splicing', *Nature*, 463(7280), pp. 457–463. doi: 10.1038/nature08909.

O'Driscoll, M. *et al.* (2021) 'Age-specific mortality and immunity patterns of SARS-CoV-2', *Nature*, 590(7844), pp. 140–145. doi: 10.1038/s41586-020-2918-0.

Oishi, K. *et al.* (2022) 'A diminished immune response underlies age-related SARS-CoV-2 pathologies.', *Cell reports*, 39(13), p. 111002. doi: 10.1016/j.celrep.2022.111002.

OSAWA, E. and MUSCHEL, L. H. (1964) 'STUDIES RELATING TO THE SERUM RESISTANCE OF CERTAIN GRAM-NEGATIVE BACTERIA.', *The Journal of experimental medicine*, 119(1), pp. 41–51. doi: 10.1084/jem.119.1.41.

Ostberg, J. R. *et al.* (2001) 'Regulatory potential of fever-range whole body hyperthermia on Langerhans cells and lymphocytes in an antigen-dependent cellular immune response.', *Journal of immunology (Baltimore, Md.: 1950)*, 167(5), pp. 2666–2670. doi: 10.4049/jimmunol.167.5.2666.

Osterrieder, N. *et al.* (2020) 'Age-Dependent Progression of SARS-CoV-2 Infection', *Viruses*, 12(779), pp. 1–11.

Ostuni, R. *et al.* (2013) 'Latent enhancers activated by stimulation in differentiated cells.', *Cell*, 152(1–2), pp. 157–171. doi: 10.1016/j.cell.2012.12.018.

Pan, Q. *et al.* (2008) 'Deep surveying of alternative splicing complexity in the human transcriptome by high-throughput sequencing', *Nature Genetics*, 40(12), pp. 1413–1415. doi: 10.1038/ng.259.

Park, A. and Iwasaki, A. (2020) 'Type I and Type III Interferons – Induction, Signaling, Evasion, and Application to Combat COVID-19', *Cell Host and Microbe*, 27(6), pp. 870–878. doi: 10.1016/j.chom.2020.05.008.

Park, C. *et al.* (2000) 'Immune response in Stat2 knockout mice.', *Immunity*, 13(6), pp. 795–804. doi: 10.1016/s1074-7613(00)00077-7.

Patel, A. A. and Steitz, J. A. (2003) 'Splicing double: Insights from the second spliceosome', *Nature Reviews Molecular Cell Biology*, 4(12), pp. 960–970. doi: 10.1038/nrm1259.

Preußner, M. *et al.* (2014) 'Rhythmic U2af26 alternative splicing controls PERIOD1 stability and the circadian clock in mice.', *Molecular cell*, 54(4), pp. 651–662. doi: 10.1016/j.molcel.2014.04.015.

Preußner, M. *et al.* (2017) 'Body Temperature Cycles Control Rhythmic Alternative Splicing in Mammals', *Molecular Cell*, 67(3), pp. 433-446.e4. doi: 10.1016/j.molcel.2017.06.006.

Pritchard, M. T., Li, Z. and Repasky, E. A. (2005) 'Nitric oxide production is regulated by fever-range thermal stimulation of murine macrophages.', *Journal of leukocyte biology*, 78(3), pp. 630–638. doi: 10.1189/jlb.0404220.

Prow, N. A. *et al.* (2017) 'Lower temperatures reduce type I interferon activity and promote alphaviral arthritis.', *PLoS pathogens*, 13(12), p. e1006788. doi: 10.1371/journal.ppat.1006788.

Qiao, Y. *et al.* (2013) 'Synergistic activation of inflammatory cytokine genes by interferon-γ-induced chromatin remodeling and toll-like receptor signaling.', *Immunity*, 39(3), pp. 454–469. doi: 10.1016/j.immuni.2013.08.009.

Qiao, Y. *et al.* (2023) 'Antisense oligonucleotides to therapeutically target SARS-CoV-2 infection.', *PloS one*, 18(2), p. e0281281. doi: 10.1371/journal.pone.0281281.

Rawlings, J. S., Rosler, K. M. and Harrison, D. A. (2004) 'The JAK/STAT signaling pathway.', *Journal of cell science*, 117(Pt 8), pp. 1281–1283. doi: 10.1242/jcs.00963.

Refinetti, R. (2020) 'Circadian rhythmicity of body temperature and metabolism', *Temperature*, 7(4), pp. 321–362. doi: 10.1080/23328940.2020.1743605.

Roesch, F. *et al.* (2012) 'Hyperthermia stimulates HIV-1 replication.', *PLoS pathogens*, 8(7), p. e1002792. doi: 10.1371/journal.ppat.1002792.

Rogalska, M. E., Vivori, C. and Valcárcel, J. (2022) 'Regulation of pre-mRNA splicing: roles in physiology and disease, and therapeutic prospects', *Nature Reviews Genetics*. doi: 10.1038/s41576-022-00556-8.

Ruf, T. and Geiser, F. (2015) ‘Daily torpor and hibernation in birds and mammals.’, *Biological reviews of the Cambridge Philosophical Society*, 90(3), pp. 891–926. doi: 10.1111/brv.12137.

Sa Ribero, M. *et al.* (2020) ‘Interplay between SARS-CoV-2 and the type I interferon response.’, *PLoS pathogens*, 16(7), p. e1008737. doi: 10.1371/journal.ppat.1008737.

Sato, N. *et al.* (2003) ‘Involvement of heat-shock protein 90 in the interleukin-6-mediated signaling pathway through STAT3.’, *Biochemical and biophysical research communications*, 300(4), pp. 847–852. doi: 10.1016/s0006-291x(02)02941-8.

Schultze, J. L. and Aschenbrenner, A. C. (2021) ‘COVID-19 and the human innate immune system’, *Cell*. Elsevier B.V., pp. 1671–1692. doi: 10.1016/j.cell.2021.02.029.

Sengupta, S. *et al.* (2019) ‘Circadian control of lung inflammation in influenza infection.’, *Nature communications*, 10(1), p. 4107. doi: 10.1038/s41467-019-11400-9.

Sertznig, H. *et al.* (2022) ‘SRSF1 acts as an IFN-I-regulated cellular dependency factor decisively affecting HIV-1 post-integration steps’, *Frontiers in Immunology*, 13(November), pp. 1–28. doi: 10.3389/fimmu.2022.935800.

Shang, J. *et al.* (2020) ‘Cell entry mechanisms of SARS-CoV-2.’, *Proceedings of the National Academy of Sciences of the United States of America*, 117(21), pp. 11727–11734. doi: 10.1073/pnas.2003138117.

Shoemaker, C. J. and Green, R. (2012) ‘Translation drives mRNA quality control.’, *Nature structural & molecular biology*, 19(6), pp. 594–601. doi: 10.1038/nsmb.2301.

Singh, R., Valcárcel, J. and Green, M. R. (1995) ‘Distinct binding specificities and functions of higher eukaryotic polypyrimidine tract-binding proteins’, *Science*, 268(5214), pp. 1173–1176. doi: 10.1126/science.7761834.

Sinitcyn, P. *et al.* (2023) ‘Global detection of human variants and isoforms by deep proteome sequencing.’, *Nature biotechnology*. doi: 10.1038/s41587-023-01714-x.

Song, K. *et al.* (2016) ‘The TRPM2 channel is a hypothalamic heat sensor that limits fever and can drive hypothermia.’, *Science (New York, N.Y.)*, 353(6306), pp. 1393–1398. doi: 10.1126/science.aaf7537.

Sun, K. *et al.* (2021) ‘Transmission heterogeneities, kinetics, and controllability of SARS-CoV-2’, *Science*, 371(6526). doi: 10.1126/science.abe2424.

Swaims-Kohlmeier, A. *et al.* (2021) 'Proinflammatory oscillations over the menstrual cycle drives bystander CD4 T cell recruitment and SHIV susceptibility from vaginal challenge.', *EBioMedicine*, 69, p. 103472. doi: 10.1016/j.ebiom.2021.103472.

Takahashi, J. S. (2017) 'Transcriptional architecture of the mammalian circadian clock.', *Nature reviews. Genetics*, 18(3), pp. 164–179. doi: 10.1038/nrg.2016.150.

Takane, H. *et al.* (2002) 'Relationship between 24-hour rhythm in antiviral effect of interferon-beta and interferon-alpha/beta receptor expression in mice.', *Japanese journal of pharmacology*, 90(4), pp. 304–312. doi: 10.1254/jjp.90.304.

Tazi, J., Bakkour, N. and Stamm, S. (2009) 'Alternative splicing and disease.', *Biochimica et biophysica acta*, 1792(1), pp. 14–26. doi: 10.1016/j.bbadis.2008.09.017.

Thoms, M. *et al.* (2020) 'Structural basis for translational shutdown and immune evasion by the Nsp1 protein of SARS-CoV-2.', *Science (New York, N.Y.)*, 369(6508), pp. 1249–1255. doi: 10.1126/science.abc8665.

Tsai, M.-H., Pai, L.-M. and Lee, C.-K. (2019) 'Fine-Tuning of Type I Interferon Response by STAT3.', *Frontiers in immunology*, 10, p. 1448. doi: 10.3389/fimmu.2019.01448.

Tsan, M.-F. and Gao, B. (2004) 'Cytokine function of heat shock proteins.', *American journal of physiology. Cell physiology*, 286(4), pp. C739-44. doi: 10.1152/ajpcell.00364.2003.

Turunen, J. J. *et al.* (2013) 'The significant other: Splicing by the minor spliceosome', *Wiley Interdisciplinary Reviews: RNA*, 4(1), pp. 61–76. doi: 10.1002/wrna.1141.

Vahedi, G. *et al.* (2012) 'STATs shape the active enhancer landscape of T cell populations.', *Cell*, 151(5), pp. 981–993. doi: 10.1016/j.cell.2012.09.044.

Vardam, T. D. *et al.* (2007) 'Regulation of a lymphocyte-endothelial-IL-6 trans-signaling axis by fever-range thermal stress: hot spot of immune surveillance.', *Cytokine*, 39(1), pp. 84–96. doi: 10.1016/j.cyto.2007.07.184.

Waalen, J. and Buxbaum, J. N. (2011) 'Is older colder or colder older? The association of age with body temperature in 18,630 individuals', *Journals of Gerontology - Series A Biological Sciences and Medical Sciences*, 66 A(5), pp. 487–492. doi: 10.1093/gerona/glr001.

Wahl, M. C., Will, C. L. and Lührmann, R. (2009) 'The Spliceosome: Design Principles of a Dynamic RNP Machine', *Cell*, 136(4), pp. 701–718. doi: 10.1016/j.cell.2009.02.009.

Wang, C. *et al.* (2022) 'The circadian immune system.', *Science immunology*, 7(72), p. eabm2465. doi: 10.1126/sciimmunol.abm2465.

Wang, E. T. *et al.* (2008) 'Alternative isoform regulation in human tissue transcriptomes', *Nature*, 456(7221), pp. 470–476. doi: 10.1038/nature07509.

Wetsel, W. C. (2011) 'Sensing hot and cold with TRP channels', *International Journal of Hyperthermia*, 27(4), pp. 388–398. doi: 10.3109/02656736.2011.554337.

Will, C. L. and Lührmann, R. (2011) 'Spliceosome structure and function', *Cold Spring Harbor Perspectives in Biology*, 3(7), pp. 1–2. doi: 10.1101/cshperspect.a003707.

Wyler, E. *et al.* (2021) 'Transcriptomic profiling of SARS-CoV-2 infected human cell lines identifies HSP90 as target for COVID-19 therapy.', *iScience*, 24(3), p. 102151. doi: 10.1016/j.isci.2021.102151.

Yan, N. and Chen, Z. J. (2012) 'Intrinsic antiviral immunity.', *Nature immunology*, 13(3), pp. 214–222. doi: 10.1038/ni.2229.

Zarnack, K. *et al.* (2013) 'Direct competition between hnRNP C and U2AF65 protects the transcriptome from the exonization of Alu elements', *Cell*, 152(3), pp. 453–466. doi: 10.1016/j.cell.2012.12.023.

Zhang, R. *et al.* (2014) 'A circadian gene expression atlas in mammals: implications for biology and medicine.', *Proceedings of the National Academy of Sciences of the United States of America*, 111(45), pp. 16219–16224. doi: 10.1073/pnas.1408886111.

Zhang, Z. and Krainer, A. R. (2004) 'Involvement of SR proteins in mRNA surveillance', *Molecular Cell*, 16(4), pp. 597–607. doi: 10.1016/j.molcel.2004.10.031.

Zhu, L. *et al.* (2010) 'Local hyperthermia could induce antiviral activity by endogenous interferon-dependent pathway in condyloma acuminata.', *Antiviral research*, 88(2), pp. 187–192. doi: 10.1016/j.antiviral.2010.08.012.

Zhuang, X. *et al.* (2021) 'The circadian clock component BMAL1 regulates SARS-CoV-2 entry and replication in lung epithelial cells.', *iScience*, 24(10), p. 103144. doi: 10.1016/j.isci.2021.103144.

6. APPENDIX

6.1. Contributions

The following experiments were performed partially or entirely by other researchers. Marco Preußner and Didrik Olofsson performed RNA-seq analysis (Figure 3.1, Figure 3.2, Figure 3.9 A). Sandra Keiper performed initial RT-qPCR experiments (Figure 3.3, Figures 3.8 A, C). Stefan Meinke helped with FACS experiments (Figures 3.6 B-C, E-F). Marco Preußner assisted with the evaluation of other RNA-seq datasets (Figures 3.10 A-C), and provided the RNA samples used in Figure 3.15 A. Margarida Paulo-Pedro assisted with the antisense oligonucleotides and CRISPR/Cas9 experiments (Figure 3.12, Figure 3.14). The SARS-CoV-2 infection experiments were performed by Jakob Trimpert, Kathrin Eschke, Ricardo Martin Vidal, Azza Abdelgawad from the Institute of Virology - Freie Universität Berlin (Figures 3.17 C-D). The abstract was translated into German by Felix Ostwaldt.

6.2. List of publications

I. **Bruna Los**, Marco Preußner, Kathrin Eschke, Ricardo Martin Vidal, Azza Abdelgawad, Didrik Olofsson, Sandra Keiper, Margarida Paulo-Pedro, Alica Grindel, Stefan Meinke, Jakob Trimpert, Florian Heyd. Body temperature variation controls pre-mRNA processing and transcription of antiviral genes and SARS-CoV-2 replication. Nucleic Acids Res. 2022 Jun 17;50(12):6769-6785.doi: 10.1093/nar/gkac513.

This work was published during the time in the AG Heyd, but it is not part of the monograph:

II. Felix Ostwaldt, **Bruna Los**, Florian Heyd. *In silico* analysis of alternative splicing events implicated in intracellular trafficking during B-lymphocyte differentiation. Front Immunol. 2022 Nov 10;13:1030409. doi: 10.3389/fimmu.2022.1030409. eCollection 2022.

6.3. Supplement

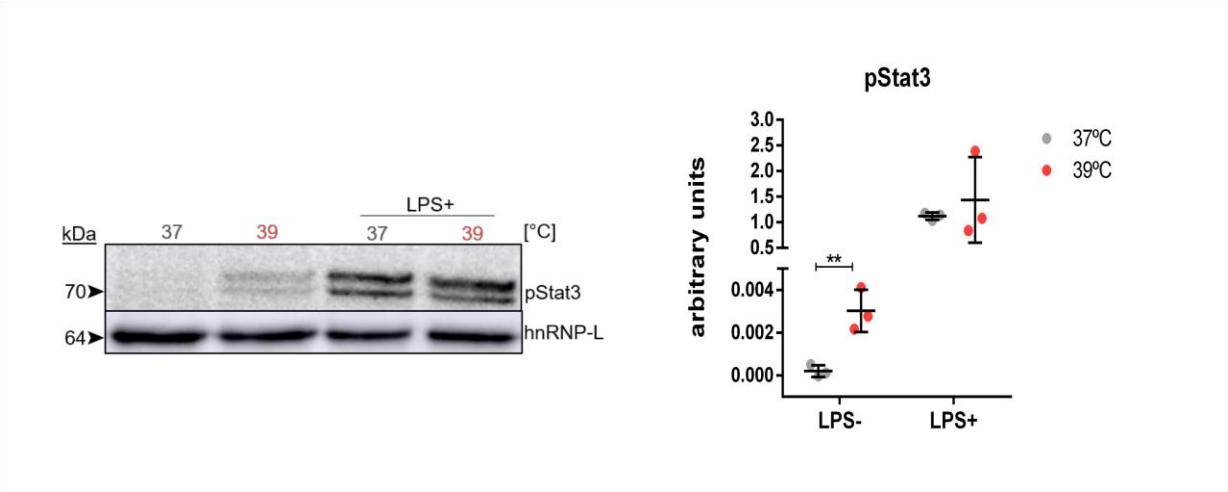

Figure S1. Elevated temperature induces activation of Stat3.
RAW 264.7 cells were incubated at the indicated temperature for 12h and phosphorylation (activation) of Stat3 was analyzed by Western blot. As a positive control, cells were incubated for 16h with LPS (2.25 µg/mL). A representative blot and quantification of three independent experiments are shown. hnRNP-L served as a loading control. Statistical significance was determined by unpaired *t*-tests and is indicated by asterisks, ***P*<0.01. Adapted from Los *et al.*, 2022.

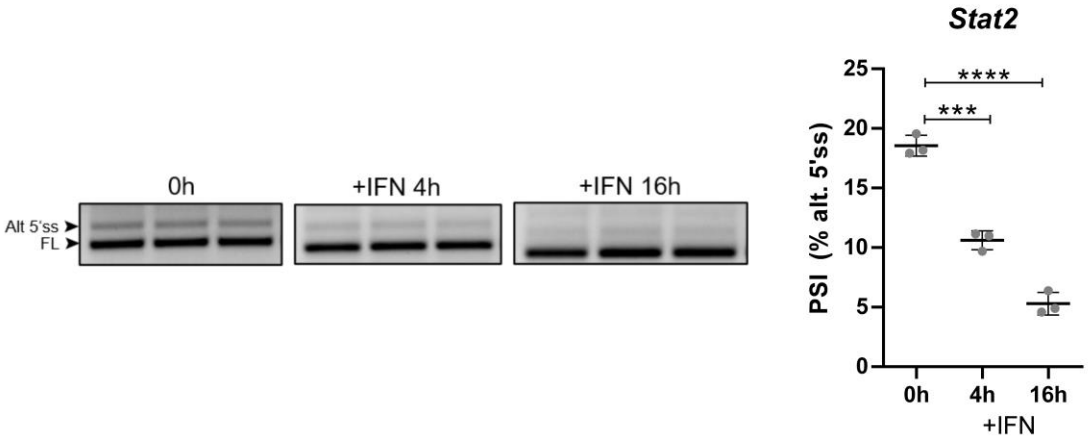

Figure S2. Reduced usage of the alternative 5' splice site of exon 11 in *Stat2* in IFN-I treated cells.
N2a cells were treated with ± IFN (100U/mL) for 4 and 16h. Representative image of a 2% agarose gel showing the alternative NMD-inducing 5' splice site in *Stat2* (left). FL = full length. Alt 5'ss = alternative 5' splice site. Quantification of the splicing RT-PCR shown in percent spliced in (PSI) (right, n = 3, mean ± SD). Statistical significance was determined by unpaired t-tests and is indicated by asterisks, ****P*<0.001, *****P*<0.0001.

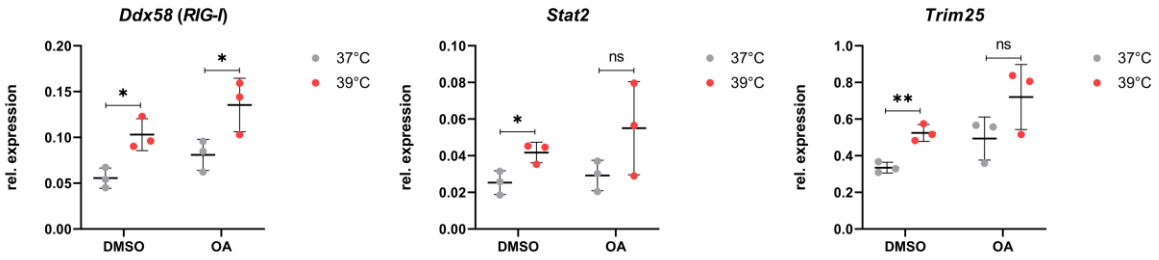

Figure S3. Effect of PP1/PP2A inhibition on the expression of antiviral genes.
RAW 264.7 cells were incubated ± 50 nM okadaic acid - OA (PP1/PP2A inhibitor) for 6 h at 37°C, then for 12h at the indicated temperature. DMSO was used as a control. Gene expression was analyzed by RT-qPCR. C_T values of target genes were normalized to the mean of *Hprt* C_T values (n = 3, mean ± SD). Statistical significance was determined by unpaired *t*-tests and is indicated by asterisks, **P*<0.05, ***P*<0.01, ns = not significant.

6.4. List of abbreviations

%	Percent
°C	Degree Celsius
2'-MOE	2‘-O-(2-Methoxyethyl)-oligoribonucleotides
3’ss	3‘splice site
3T3	Fibroblast cell line that was isolated from a mouse NIH/Swiss embryo
5’ss	5‘splice site
ACE2	Angiotensin-converting enzyme 2
ActD	Actinomycin D
Alt 3’ss	Alternative 3‘ splice site
Alt 5’ss	Alternative 5‘ splice site
APS	Ammonium peroxodisulfate
AS	Alternative splicing
ASO	Antisense oligonucleotides
BCA	Bicinchoninic acid
bp	Base pair
BP	Branch point
BSA	Bovine serum albumin
Caco-2	Cancer coli-2
Calu-3	Cultured human airway epithelial cells
Cas9	CRISPR-associated endonuclease
cDNA	Complementary DNA
CHX	Cycloheximide
Cirbp	Cold-induced RNA binding protein
CLK	Cdc2-like kinases
CO_2	Carbon dioxide
COVID-19	Coronavirus disease 2019
CRISPR	Clustered regularly interspaced short palindromic repeats
C_T	Cycle threshold
ctrl	Control
DGE	Differential gene expression
DMEM	Dulbecco's modified eagle's medium
DMSO	Dimethyl sulfoxide
DNA	Desoxyribonucleic acid

DNase	Deoxyribonuclease
dNTPs	Deoxyribonucleotide triphosphate
DTT	Dithiothreitol
E. coli	*Escherichia coli*
ECL	Enhanced chemiluminescence
EDTA	Ethylendiamintetraacetate
EJC	Exon junction complex
ESE	Exonic splicing enhancer
ESS	Exonic splicing silencer
et al.	*Et alii*
F	Forward
FACS	Fluorescence-activated cell sorting
FBS	Fetal bovine serum
FC	Fold change
FDR	False discovery rate
FL	Full length
g	Gram / centrifugal force
GE	Gene expression
GO	Gene ontology
h	Hour
H_2O	Water
HCl	Hydrochloric acid
HeLa	Henrietta Lacks
HEPES	N-2-Hydroxyethylpiperazin-N-2-ethansulfonic acid
hnRNP	Heterogeneous nuclear ribonucleoproteins
HS	High salt
HSP	Heat-shock protein
IFN	Interferon
IFNAR	Interferon alpha and beta receptor
IFN-I	Type I IFN
IFIT	Interferon-induced proteins with tetratricopeptide repeats
IKKε	Inhibitor of nuclear factor κB kinase-ε
IL	Interleukin
IRF	Interferon regulatory factor
ISE	Intronic splicing enhancer

ISG	Interferon-stimulated gene
ISGF3	IFN-α-Stimulated Gene Factor 3
ISRE	Interferon-stimulated response elements
ISS	Intronic splicing silencer
IκB	Inhibitor of nuclear factor κb
JAK	Janus kinase
Jurkat/JSL1	Immortalized line of human T lymphocyte cells
kb	Kilo bases
KCL	Potassium chloride
kDa	Kilodalton
L	Liter
LB	Luria Bertani
LPS	Lipopolysaccharides
LS	Low salt
M	Molar/million
m	Milli
m7G	7-methylguanosine residue
mA	Milliampere
MAVS	Mitochondrial antiviral signaling protein
MDA5	Melanoma differentiation-associated gene 5
MEM	Minimal essential medium
$MgCl_2$	Magnesium chloride
min	Minutes
MOI	Multiplicity of infection
mRNA	Messenger RNA
n	Nano
N2a	Neuro2a cells
NaCl	Sodium chloride
NaOH	Sodium hydroxide
NMD	Nonsense-mediated decay
NO	Nitric oxide
Nos2	Nitric oxide synthase 2
NP-40	Nonoxynol-40
NSP	Nonstructural protein
nt	Nucleotide

Oas	2'-5'-oligoadenylate synthetases
ORF	Open reading frame
P^{adj}	Benjamini-Hochberg adjusted *P*-value
PAGE	Polyacrylamide gel-electrophoresis
PBS	Phosphate buffered saline
PCI	Phenol-chloroform-isoamyl alcohol
PCR	Polymerase chain reaction
PGE2	Secrete prostaglandin E2
pH	Preponderance of hydrogen ions
PMA	Phorbol myristate acetate
PPT	Polypyrimidine tract
Pre-mRNA	Precursor-mRNA
PRR	Pathogen recognition receptor
PSI	Percent spliced in
PTC	Premature termination codon
R	Reverse
RAW 264.7	Macrophage-like, Abelson leukemia virus-transformed cell line derived from BALB/c mice
RBM3	RNA binding protein 3
RBP	RNA-binding protein
RIG-I	RNA helicases retinoic acid-inducible gene I
RNA	Ribonucleic acid
RNA-Seq	RNA-sequencing
rpm	Revolutions per minute
RPMI	Roswell Park Memorial Institute Medium
RT	Reverse transcription
RT-PCR	Reverse transcription polymerase chain reaction
S	Spike
SARS-CoV-2	Severe acute respiratory syndrome coronavirus 2
SCN	Suprachiasmatic nucleus
SD	Standard deviation
SDS	Sodium dodecyl sulfate
SF1	Splicing factor 1
sgRNA	Single guide RNA
siRNA	Small interfering RNA

snRNP	Small nuclear ribonucleoparticles
SOCS	Suppressor of cytokine signaling
SR	Serine arginine-rich
ss	Splice site
STAT	Signal transducer and activator of transcription
TBK1	TANK-binding kinase 1
TBST	Tris-buffered saline with Tween-20
TEMED	Tetramethylethylenediamine
TF	Transcription factor
TNF	Tumor necrosis factor
Tris	Tris-(hydroxymethyl)-aminomethane
TRP	Transient receptor potential
Tween-20	Polysorbate 20
TYK2	Tyrosine kinase 2
U	Unit
U2AF	U2 auxiliary factor
USP18	Ubiquitin specific peptidase 18
UV	Ultraviolet
V	Volt
v/v	Volume per volume
w/v	Weight per volume
WT	Wild type
Δ	Skipping
µ	Micro

6.5. List of Figures

6.6. List of Tables